Vaporization and autoignition characteristics of ethanol and 1-propanol droplets : influence of water

Sanisah Binti Saharin

SPIM

Thèse de Doctorat

école doctorale sciences pour l'ingénieur et microtechniques

UNIVERSITÉ DE BOURGOGNE

Vaporization and Autoignition Characteristics of Ethanol and 1-propanol Droplets: Influence of Water

SANISAH BINTI SAHARIN

THESIS

to obtain the grade of

DOCTOR OF THE UNIVERSITY BURGUNDY

Speciality : Mechanic and energetic

Presented by

Sanisah BINTI SAHARIN

4 February 2013

Vaporization and autoignition characteristics of ethanol and 1-propanol droplets: influence of water

Jury Members:

Roger PRUD'HOMME, Emeritus CNRS Research Director, Université Pierre et Marie Curie: Head of Jury

José-Vicente PASTOR, Professor, Universidad Politecnica de Valencia: Reviewer

Pascal HIGELIN, Professor, Université d'Orleans: Reviewer

Céline MORIN, Professor, Université de Valenciennes: Examiner

Raed KAFAFY, Associate Professor, Int. Islamic University Malaysia: Examiner

Benoîte LEFORT, Associate Professor, ISAT- University Burgundy: Examiner

Luis LE MOYNE, Professor, ISAT-University Burgundy: Director of Thesis

ACKNOWLEDGMENTS

I would like to thank Prof. Luis Le Moyne, the Director of ISAT as well as my supportive Supervisor. He has always been enthusiastic and provided calm friendly guidance. I am deeply grateful to Benoîte Lefort for her constant guidance, support and help during my three and half years in ISAT. She is a good mentor and a great friend: I am extremely thankful.

The experimental aspect of this work could not have been performed without immense help of Christian Chauveau who generously sharing his experimental set-up in CNRS with me. Thank you for your precious knowledge and time. To Céline Morin, I sincerely thank you for your constant assistance and direction.

To Alan Kéromnès, without you, the RCM experimental work would be definitely impossible. I would like also to thank the C3-NUIG team under direction of Dr. Henry Curran for the use of RCM. To Dr. Raed Kafafy, thank you for your guidance, thoughts and doa.

To all the juries; Prof. Pastor, Prof. Higelin and Prof. Prud'homme, thank you for accepting the request for being the juries of my work. Your comments and your feedbacks are highly appreciated.

I would like to thank my friends and colleagues, for the laughter, and the good tears.

Financial support over the course of my Ph.D. studies was provided by Ministry of Higher Education Malaysia and is gratefully appreciated.

I would like to thank my family: Mom, Dad and my far away brothers and sisters for all their supports.

Last but not the least: to my caring husband and my little angels. Thank you for being extremely patient by my side through good and bad. None of this would have been possible without them.

ABSTRACT

The study of the gasification of a droplet via vaporization, which involves heat, mass and momentum transfer processes in gas and liquid phases, and their coupling at the droplet interface, is necessary for better understanding and modeling of complex spray and mixture formation issues. The study of chemistry of fuel oxidation through autoignition is also a key to improve efficiency of internal combustion engines generally. Both vaporization and autoignition are needed to characterize a fuel and to develop efficient design of injection systems for internal combustion engine, propulsion and power generation.

Detailed investigation of the vaporization of an isolated of ethanol and 1-propanol droplet was carried out in this experimental study. The experimental set-up consists of a heated chamber with a cross quartz fibers configuration as droplet support. An alcohol droplet is located at the intersection of the cross quartz fibre with a controlled initial diameter (300 - 600µm). Ambient temperature is varied from 298 to 973 K at atmospheric pressure. The quasi-steady theory has been used to compare and to explain all experimental results. The results show that the d^2-law is obeyed and an average vaporization rate is achieved in the case of 1-propanol vaporization. The real impact of the water concentration on the vaporization rate of an ethanol droplet in a large range of temperature is also examined, where two 'quasi-steady' periods are observed on the d^2-curves, clearly showing that the vaporization of an ethanol droplet is accompanied by the simultaneous condensation of water vapour on the droplet surface and thus the temporal evolution of the droplet squared diameter exhibits an unsteady behaviour. The histories of the instantaneous vaporization rates calculated from the d^2 (t) curves of both 1-propanol and ethanol droplets confirm this phenomenon.

The autoignition experimental study of ethanol, 1-propanol and blends of ethanol and water have been carried out in a rapid compression machine (RCM) at a compressed pressure of 30 bar over a temperature range of 750-860 K for stoichiometric mixture of fuel and air. The

thermodynamic conditions are relevant to those encountered in internal combustion engines. The experiments have been performed in the twin piston at NUIG RCM. The compressed gas temperature was changed by adjusting the initial temperature. Fuel-oxidiser mixtures were prepared manometrically in stainless steel tanks. All gases and reactants used for the experiments had a purity of 99.9 % or higher. The ignition delay times recorded show a significant decrease with increasing temperature. 1-propanol is more reactive than ethanol which results in shorter ignition delay times. However, water addition to ethanol increases the reactivity of the mixture and results in a shorter ignition delay times than 1-propanol. Ethanol and 1-propanol auto-ignition process results in the same level of peak pressure but water addition to ethanol reduces the peak pressure due to absorption by water of the part of the heat released. Moreover, the heat release rate of ethanol is higher than 1-propanol but is reduced when water is added to ethanol.

Keywords: Droplet, vaporization, alcohols, d^2-law, water vapour, average and instantaneous vaporization rate, autoignition delay time, kinetics mechanism

TABLE OF CONTENTS

LIST OF TABLES

LIST OF FIGURES

NOMENCLATURE

A: frequency factor, $cm^3mol^{-1}s^{-1}$

B: Spalding transfer number

B_M: mass transfer number

B_T: thermal transfer number

C_p: specific heat per unit mass, J/Kg

D: binary diffusion coefficient, mm^2/s

d_0: initial droplet diameter, μm

d: droplet diameter, μm

E_A: activation energy, cal mol^{-1}

k: Boltzmann constant

K: average vaporization rate, mm^2/s

K_{inst}: instantaneous vaporization rate, mm^2/s

K_i: average vaporization rate at first linear part of d^2-curve of ethanol, mm^2/s

K_f: average vaporization rate at second linear part of d^2-curve of ethanol, mm^2/s

K_{th}: theoretical average vaporization rate, mm^2/s

L_v: enthalpy of vaporization, J/mol

$\dot{m}$: fuel vaporization rate, mm2/s

M: molecular weight, g/mol

P_c: compressed pressure, bar

P_∞: ambient pressure, MPa

P_{sat}: vapour saturated pressure, MPa

R: universal gas constant

S: surface area, (mm^2)

t: time, s

T_b: boiling temperature, K

T_c: after compressed temperature, K

T_r: reference temperature, K

$T_{s:}$ droplet surface temperature, K

T_∞: ambient gas temperature, K

Y: mass fraction

ΔH: latent heat of vaporization, kJ/mol

Symbols

Ω_D: collision integral

λ: thermal conductivity, W/m.K

ε: characteristic energy of Lennard-Jones (J)

ν: kinematic viscosity, m^2/s

μ: dynamic viscosity, mPa.s

ψ: intermolecular energy

ρ: density, kg/m^3

σ: characteristic length of Lennard –Jones, Å or sensitivity coefficient

τ: ignition delay time, ms

Indices

F: fuel

g: gaseous

l: liquid

O: oxidant

r: radial, reference

s: value at droplet surface

th: theoretical value

1 INTRODUCTION

1.1 General introduction

For ages, population of the world has depended on the fossil fuels as the main resources of energy for many industries including the automotive. The reality that the fossil fuels will become extinct in near future has developed significant and extensive researches for alternative fuels. Environmental concerns also have led to the increased interest in the future use of these alternative fuels. This is where biofuels came into the picture; they have potential as they are derived from renewable sources, they are environmental friendly as in reducing the pollutant emissions and rather inexpensive means in terms of reducing the dependency on fossil fuels. The term biofuels is usually defined and used to refer to that of alternative and substitutes for petrol, diesel or aircraft fuels that are based from fossil.

There are so many reasons for biofuels to have imminently been alternative to fossil fuels. The biofuels that are manufactured from biomass are identified to be renewable, biodegrable, oxygenated and significantly produce much less pollutant emissions such as particulate matter (PM), unburned hydrocarbon (HC) and carbon monoxide (CO). They are also having prospective to reduce the production of carbon dioxide (CO_2). This is primarily based on the fact that plants which are used for biofuels production absorb CO_2 during their growth which is then released during the biofuels combustion.

Nonetheless, the study of the gasification of a biofuel droplet via vaporization is still needed and necessary to give better understanding and modelling of complex spray and mixture formation issues. The behaviour of biofuel droplets especially in atomization and spray is still unknown and unpredictable. The proper characterization of this behaviour is necessary as

it involves heat, mass and momentum transfer processes in gas and liquid phase and their coupling at the droplet interface.

1.2 Objectives of study

The main objective of this study is to investigate the vaporization behaviour of an isolated droplet and its characteristics which affects the atomization of sprays in conventional internal combustion engines. A detailed description of the vaporization of an isolated droplet has been realized in this experimental study aimed at investigating the low molecular weight alcohols; ethanol and 1-propanol and the effects of their miscibility with water property will be further examined. The characterization of the vaporization phenomenon is necessary for this liquid fuel to design efficient injection systems for internal combustion engines, for propulsion and power generation. An extensive theoretical calculation and evaluation is also carried out to validate experimental results. Experimental studies of autoignition behaviour of alcohols at various initial temperatures and at atmospheric pressure are also accomplished using a Rapid Compression Machine (RCM), courtesy of Centre of Combustion Chemistry, National University of Ireland, Galway. To better assess the effect of the presence of oxygenated compound in alcohol fuels especially on the engine efficiency and the pollutants formation, it is very imperative to well validate a developed kinetic models for the combustion and oxidation of the oxygenated component of biofuels. Well-known detailed kinetics combustion analysis from literature is carried out to predict and validate the experimental results. The effects of different molecular weight alcohol on autoignition behaviour have been thoroughly studied and the impact of water addition to ethanol oxidation has been assessed by sensitivity analysis.

1.3 Challenges

The biggest challenge in this study is to overcome all the unworthiness of utilisation of alcohols as a reliable alternative fuel especially in automotive transportation. Many researchers found that alcohols are still unpractical to be explored as the definite alternative fuel to replace the current conventional fossil fuels such as gasoline and diesel. However for many decades, researches are trying to keep on working in detailing and improving the goodness and reliability of alcohols properties. The unpredictable and volatile behaviours of alcohols made the whole studies even much more challenging.

1.4 Thesis Layout

This thesis has been divided into seven chapters. After a brief overview of background and introduction in chapter 1, chapter 2 mainly consists of literature review and bibliography analysis related to biofuels generally and alcohols particularly. The development of isolated droplet vaporization experimental works on alcohols particularly is also included in this chapter. In addition, a description of the background history of autoignition characteristics of alcohols is also incorporated in this chapter. Chapter 3 gives the insights of the experimental set-up for isolated droplet vaporization study on ethanol and 1-propanol. The properties of ethanol and 1-propanol are provided and all parameters and variables are defined. The post-processing details are included to give crystal clear view on the overall processes. Autoignition experimental set-up is also discussed and explained in great details. Chapter 4 describes in greater length the theoretical calculation of droplet vaporization that includes all related physical and thermodynamic properties. Chapter 5 reports the results of the experimental works for the isolated droplet of ethanol and 1-propanol vaporization at various ambient temperature ranges from 293K to 973K, which is necessary to gain both some physical insights and to give accessible range for theoretical evaluation while the furnace pressure is main-

tained atmospheric. Meanwhile in Chapter 6, detailed kinetic model from literature to predict the autoignition behaviour of ethanol and 1-propanol is further exploited. Autoignition experimental results from Rapid Compression Machine (RCM) of ethanol, 1-propanol and ethanol/water mixture are presented. Sensitivity analysis that consisted a set of reactions of potential species is also carried out for both alcohols and ethanol/water mixture to discuss for further comprehension on the kinetic impact of water on ethanol oxidation. Conclusions, imperative findings and further works available in these studies are given in Chapter 7.

2 LITERATURE REVIEW

2.1 Biofuels and Alcohols in general

Recent growing alarm on declination of conventional petroleum based fuels particularly in global automotive industry has caused significant interest in biofuels research. Biofuels such as pure vegetable oils, biodiesel based on cross transesterification of vegetable oils or animal fats and alcohols based on biochemical processes are currently readily available. These biofuels issued from the biomasses which are known to be renewable, biodegradable, oxygenated and produce fewer pollutants (Agarwal, 2007) than conventional fuels require further and more extensive investigations especially in terms of fundamental characteristics such as vaporization and oxidation behaviours.

Biofuels are usually referred to liquid, gas and solid fuels predominantly for transport produced from biomass. A variety of fuels can be produced from biomass such as ethanol, methanol, biodiesel, Fischer-Tropsch diesel, hydrogen and methane. They could be pure biofuels or blend fuels in such a proportion that they can substitute conventional motor fuels without or minimized altering of the car performance. Figure 2.1 (adopted from Tran *et al.* (2012)) shows variety of oxygenated fuels can be obtained through wide range of processes involving fermentation and catalytic reactions. From this figure, alcohols as the main interest biofuels in this study are generally derived from the fermentation process of starch and sugar. The lower molecular weight alcohols such as methanol and ethanol could be also produced through gasification process from lignocelluloses sources such as crop and forest waste.

Figure 2.1: Summary of fuel components derived from biomass (Adopted from Tran *et al.* (2012)).

Nigam and Singh (2011) have generally classified the biofuels into two major categories (Figure 2.2). Primary biofuels referred to as natural and unprocessed biomass such as fire-wood, wood chips and pellets, and are mainly those where the organic material is utilised essentially in its natural and non-modified chemical form. Primary fuels are directly combusted, usually to supply cooking fuel, heating or electricity production. Meanwhile the secondary biofuels are adapted primary fuels, which have been processed and produced in the form of solids (e.g. charcoal), or liquids (e.g. ethanol, biodiesel and bio-oil), or gases (e.g. biogas, synthesis gas and hydrogen). Secondary fuels can be used for multiple ranges of applications, including transport and high temperature industrial processes. The secondary biofuels are further classified to first, second and third generation biofuels based on their raw material and technology used for their production.

Figure 2.2: Classification of biofuels (Nigam and Singh (2010)).

2.1.1 The physical and chemical properties of alcohols-Ethanol and 1-propanol

Alcohols is an interesting alternative fuel for transportation purposes as they have properties that allow its use in existing internal combustion engines without or with minor hardware modifications. Comparisons of typical fuel physical properties have been made between alcohols such as ethanol (C_2H_5OH) and 1-propanol (C_3H_7OH) as the main subjects in this current study and gasoline as summarized in Table 2-1.

Table 2.1: Common physical properties[a] of Ethanol, 1-propanol and Gasoline

	Ethanol	1-Propanol	Gasoline
Molar Mass (g/mol)	46.07[b]	60.1[b]	102.5
C (wt. %)	52.2	59.96	86.5
H (wt. %)	13.1	13.42	13.5
O (wt. %)	34.7	26.62	0
Density (kg/mm^3)	790[c]	803[c]	735-760
Boiling Temperature (K)	351.6[b]	370.3[b]	303-473[c]
Autoignition Temperature (K)	763[c]	753[c]	723[c]
Latent Heat of Vaporization (kJ/kg)	854	689	289
Lower Heating Value (MJ/kg)	26.8[c]	30.9 [c]	42.7 [c]
Stoichiometric Ratio	8.95	10.28	14.4
Research Octane Number (RON)	109[d]	112[c]	91-99[d]

[a] All data from Jeuland *et al.* (2004) unless stated otherwise. [b] data from Reid *et al.* (1987), [c] data from Tran *et al.* (2012) and [d] data from Anderson *et al.* (2010).

A number of observations can be made from Table 2.1 regarding the properties of alcohols as an alternative fuel or addictive to gasoline. Ethanol and 1-propanol have a very high octane number, which induces a strong resistance to knock and consequently the ability to optimize

the engine, thus allows for use at higher compression ratios and significantly improves the engine performance. A fuel with a higher octane number can endure higher compression ratios before engine starts knocking, thus giving engine an ability to deliver more power efficiently and economically. They also have a density close to the gasoline which is suitable to the existing internal engines without any further adjustment. In the meantime the presence of oxygen in the formula of alcohols, can provide a more homogeneous fuel/air mixing and consequently a decrease in unburned or partially burned molecule emissions (HC and CO) resulting in cleaner environment due to less pollutants.. A high latent heat of vaporization enabling a "cooling effect" of air and consequently can enhance the volumetric efficiency.

However, the existence of oxygen included in the molecule (~30% wt) of alcohols can induce an increase in the fuel volumetric consumption. Meanwhile the high latent heat of vaporization can tempt running difficulties in cold conditions, especially cold start. To lower this phenomenon, some technical solutions may be applied. The most frequently used solution is to use E85 (85% ethanol) instead of pure ethanol. The addition of 15% light hydrocarbon fraction in ethanol induces a strong increase in volatility and consequently an easier engine start. Ethanol is more and more largely used in spark ignition (SI) engines as pure fuel or "flex-fuel" blends up to 85 % in gasoline in Europe. With this high percentage, ethanol vaporization as fundamental process in combustion phenomenon must be correctly characterized. When compared to gasoline, with a higher latent heat of vaporization, ethanol can cause difficulties at start-up in cold conditions. With a lower heat value, it is necessary to ignite richer mixtures that are unfavourable for pollutant emissions. The introduction of engines that can be fuelled by gasoline, ethanol or a blend of both at any appropriate proportion are frequently called ''flex-fuel", and became attractive because car owners do no longer depend on ethanol price and market availability. Ethanol also leads to azeotropes with light hydrocarbon fractions and can lead to volatility issues. Ethanol and 1-propanol are also miscible with wa-

ter, which can cause demixing issues when blended with hydrocarbons. The high oxygen content in alcohols and its ability to oxidize into acetic acid provoke compatibility issues with some materials used in the engine, such as metals or polymers. Alcohol, especially 1-propanol combustion in engines encourages formation of aldehydes emissions, which can have a negative impact on health (Koshland, (1994)). Aldehydes also play an important role in formation of photochemical smog.

2.1.2 The historical background of alcohols in internal combustion engines

Alcohols particularly ethanol has been known as a fuel for many years. In fact, when Henry Ford designed the Model T in early 19th century, his expectation was that ethanol; made from renewable biological materials would be the most important fuel for automobile. Nevertheless, gasoline emerged as the dominant transportation fuel in the early twentieth century because of two main factors; ease of operation of gasoline engines with the materials then available for engine construction, and a rising supply of cheaper petroleum from oil field discoveries all around the world. Nevertheless gasoline had many drawbacks and less attractive properties as an automotive fuel. It had a lower octane rating than ethanol, was much more toxic (particularly when blended with tetra-ethyl lead and other compounds to enhance octane rating), and emitted harmful air pollutants. Gasoline was more likely to explode and burn accidentally; gum would form on storage surfaces, and carbon deposits would form in combustion chamber. Petroleum was much more physically and chemically varied than ethanol, requiring intricate refining procedures to ensure the manufacture of a consistent ‘‘gasoline’’ product. Because of its lower octane rating relative to ethanol, the use of gasoline meant the use of lower compression engines and larger cooling systems. Diesel engine technology, which developed soon after the emergence of gasoline as the dominant transportation fuel, also resulted in the generation of large quantities of pollutants. However, despite these envi-

ronmental flaws, fuels made from petroleum have dominated automobile transportation for the past three-quarters of a century. According to Agarwal, (2007), there are two key reasons: first, cost per kilometre of travel has been virtually the sole selection criteria. Second, the large investments made by the oil and auto industries in physical capital, human skills and technology make the entry of a new cost-competitive industry difficult. Until very recently, environmental concerns have been hardly considerable.

In accordance with the report produced by United Nation Environment Programme, UNEP (Assessing Biofuels, 2008), world ethanol production for transport fuel has tripled from 17 billion to more than 52 billion litres between 2000 and 2007, while biodiesel expanded eleven-fold from less than 1 billion to almost 11 billion litres. This production resulted in liquid biofuels providing a total share of 1.8% of the world's transport fuel by energy value in 2007. A recent estimate for 2008 arrives at 64.5 billion litres ethanol and 11.8 billion litres biodiesel, up 22% from 2007 (by energy content). From 2005-2007 (average) to 2008, the share of ethanol in global gasoline type fuel use was estimated to increase from 3.78% to 5.46%, and the share of biodiesel in global diesel type fuel use from 0.93% to 1.5%.

Policies have essentially triggered the development of biofuel demand by targets and blending quotas. Mandates for blending biofuels into vehicle fuels had been enacted in at least 36 states/provinces and 17 countries at the national level by 2006. Most mandates require blending 10–15% ethanol with gasoline or blending 2–5% biodiesel with diesel fuel. In addition, recent targets define higher levels of envisaged biofuel use in various countries.

For decades, regulations have been made and implemented to provide a 'greener' and 'cleaner' environment towards the usage of conventional fossil fuels. Engine requires certain minimum levels of octane to run smoothly and to resist knocking. Aromatics and alcohols have been the most popular choices. Aromatic compounds, such as benzene and toluene are known to have higher octane levels, but the presence of these compounds produces more

smoke, smog, as well as benzene (Surisetty *et al.* (2011). The US Environmental Protection Agency, EPA has approved using several alcohols and ethers in unleaded gasoline. For years, ethanol and methyl tertiary butyl ethers (MTBE) are the two most popular additives. According to Rasskazchikova *et al*. (2004), the use of ethanol as high octane additive has been justified despite its higher cost due to its low toxicity, reduced environmental pressure when burning ethanol-containing fuel and a fact that it was produced from renewable sources.

Due to the phase out of lead in all gasoline grades and the adverse health and environmental effects of MTBE, the synthesis of higher alcohols, from synthesis gas has attracted considerable interest. Low molecular weight alcohols such as ethanol have replaced other additives as octane boosters in automotive fuels. Adding alcohols to petroleum products permits the fuel to combust more completely due to the presence of oxygen, which increases the combustion efficiency and reduces air pollution. However, the presence of alcohols in fuel can cause corrosion to metallic fuel system components. In order to make the best use of alcohols as alternative fuels; the engine or the vehicle can be redesigned; one or more additives to ethanol or methanol can be blended to improve its characteristics.

Using ethanol as a fuel additive to unleaded gasoline causes an improvement in engine performance and exhaust emissions (Al Hassan, (2003); Al-Farayedhi *et al*., (2004)). Ethanol addition resulted in an improvement in brake power, brake thermal efficiency, volumetric efficiency and fuel consumption; however the brake specific fuel consumption and equivalence air–fuel ratio decreased because of lower calorific value of the gasoline-alcohol fuel blends. Using an ethanol–unleaded gasoline blend leads to a significant reduction in exhaust emissions of CO and HC for all engine speeds. Ethanol diesel blends up to 20% can very well be used in present day constant speed compressed ignition engines without any hardware modification (Meiring *et al*. (1983); Mouloungui *et al*. (2001)). Hsieh *et al.* (2002) have experimentally investigated the engine performance and pollutant emissions of commercial spark

ignition (SI) engine using ethanol-diesel blends at various blended rates. Results showed that with increasing the ethanol content, the heating value of the blended fuels is decreased, while the octane number of the blended fuels increases. They also found that with increasing the ethanol content, the Reid vapour pressure of the blended fuels initially increases to a maximum at 10% ethanol addition, and then decreases. Results of the engine test indicated that using ethanol–gasoline blended fuels, torque output and fuel consumption of the engine slightly increase; CO and HC emissions decrease dramatically as a result of the leaning effect caused by the ethanol addition; and CO_2 emission increases because of the improved combustion whereas NO_x emission depends on the engine operating condition rather than the ethanol content. Exhaust gas temperatures and lubricating oil temperatures were lower for ethanol diesel blends than mineral diesel. The engine could be started normally both hot and cold. Costa and Sodre (2004) have studied the comparison of performance and emissions from a four-stroke engine fuelled with hydrous ethanol or 78% gasoline-22% ethanol blend. The results showed that torque and brake mean effective pressure were higher when gasoline-ethanol blend was used at low engine speeds. However, higher torque and brake mean effective pressure were achieved when hydrous ethanol was used at high engine speeds.

Alcohols such as methanol and ethanol have been studied extensively and they are used currently either as gasoline additives or pure fuel. Both alcohols however, have low energy densities, relatively high vapour pressures, and they are notably *hygroscopic*. On the other hand, saturated C_3 alcohols, namely n-propanol and iso-propanol have a better energy density and lower affinity for water compared to methanol and ethanol. Though both propanol isomers can be produced commercially via fermentation, currently they are produced largely from petrochemical feedstocks. Recently, Shen and Liao (2008) and Atsumi and Liao (2008) demonstrated techniques to produce n-propanol from glucose using bacteria Escherichia coli.

As such, there is growing interest in C_3 (saturated) alcohols as potential alternatives to lower molecular weight alcohols.

2.2 Isolated Liquid Fuel Droplet Vaporization

2.2.1 Liquid fuel droplet vaporization

Liquid fuel droplet vaporization is fundamental mechanism in spray combustion for various applications such as internal combustion (IC) engines, aerospace-propulsion engines and industrial burners. In these systems, fuel is injected into combustion chamber as a spray or jet. This spray or jet breaks down into droplets that evaporate due to the surrounding atmosphere forming a combustible mixture that ignites once appropriate conditions are achieved. Numerous works on investigating the major spray characteristics (spray macroscopic and microscopic characteristics) have been carried on conventional fuels such as gasoline and diesel (Hiroyasu and Arai (1990); Zhao et al. (1997); Zhao et al. (1999); Kong et al. (1999); Desantes et al. (1999); Payri et al. (2005); Desantes et al. (2005); Taşkiran and Ergeneman (2011)) as they influence the combustion efficiency and exhaust emissions. The evaporation process controls the combustion process that is eventually controls the design of combustion chamber and performance of engine. However it is highly necessary also to study the vaporization of a single droplet before completely characterizing spray vaporization and combustion. For many years, studies have been conducted experimentally and numerically in various environments to highlight the influence of the isolated parameters.

2.2.2 Quasi-steady Theory

The so-called ‘quasi-steady’ model was established by the work of Godsave (1953) and Spalding (1953) in early 1950 and has led to the development of a theoretical model capable

of describing the gasification process of a fuel droplet. The model, renowned as 'Quasi-steady model' or else called the d^2-law, shows that during the gasification process, the droplet surface area, represented by the droplet-squared diameter, changes linearly during its lifetime. The d^2-law consists much of the crucial physics and rough approximations of droplet gasification. However, this model is based on a few vital hypotheses. The most common hypotheses are as listed below:

a. Constant and uniform droplet temperature: The mechanisms of the heating and mass transport inside the liquid phase are negligible.

b. The droplet is always symmetrically spherical: This means that both natural and forced convections are always absent and thus the droplet remains spherical during its lifetime. The consequence of this assumption is that non-radial motion in the gas-phase is absent. Hence the analysis reduces to one dimension i.e. in radial direction only.

c. The gas-phase quasi-steadiness: This assumption indicates that the gas-phase immediately adjusts itself to the local boundary conditions and droplet size at each instant of time.

d. The processes are considered as spatially isobaric; the pressure is equal to that of ambient.

e. The properties of transport in gas phase are constant. Such properties are thermal conductivity and calorific capacity. The number of Lewis must be equal to 1. That means the thermal diffusivity will always equal to the mass diffusivity.

$$Le = \frac{\alpha}{D} = \frac{\lambda}{\rho \cdot C_p \cdot D} = 1 \tag{2-1}$$

where λ is thermal conductivity, ρ density, C_p the specific heat per unit mass and D binary diffusion coefficient.

f. The change of the liquid phase: the mechanism of transport is quicker in the gas phase. At the instant time, at the surface of the droplet, there will be equilibrium between the liquid and the vapour where the saturated vapour pressure corresponds to the temperature at the surface of the droplet.

g. The effect of Soret and Dufour are negligible.

h. Absence of droplet-droplet interaction. Only an isolated droplet in an infinite oxidant ambient is considered.

i. No internal liquid motion inside the droplet.

j. Single component fuel.

By applying those hypotheses above, the problem is solved by the main three conservation equations; continuity equation, conservation of energy equation and conservation of species equation.

Continuity Equation

$$\frac{d\dot{m}}{dr} = 0 \tag{2-2}$$

$$\dot{m} = 4\dot{\cdot}\pi \cdot r^2 \cdot \rho_{Fg} \cdot v_r = constant \tag{2-3}$$

Conservation of energy equation

$$r^2 \cdot \rho_{Fg} \cdot \nu_r \cdot C_{pg} \cdot \frac{dT}{dr} = \frac{d}{dr}\left(r^2 \cdot \lambda_g \cdot \frac{dT}{dr}\right) \tag{2-4}$$

Conservation of species equation

$$\frac{d}{dr}\left[r^2 \cdot \left(\rho_{Fg} \cdot \nu_r \cdot Y_i - D \cdot \frac{dY_i}{dr}\right)\right] = 0 \tag{2-5}$$

with the boundary conditions of:

$$\text{At r = r}_s\text{: T = T}_s \text{ and } Y_F = Y_{Fs} \tag{2-6}$$

$$\text{As r} \rightarrow \infty\text{: T = T}_\infty \text{ and } Y_F = 0$$

At the interface:

$$4 \cdot \pi \cdot {r_s}^2 \cdot \lambda_g \cdot \left.\frac{dT}{dr}\right|_{r=r_s} = \dot{m} \cdot L_v \tag{2-7}$$

$$4 \cdot \pi \cdot {r_s}^2 \cdot \rho_{Fg} \cdot D \cdot \left.\frac{dY}{dr}\right|_{r=r_s} = \dot{m} \cdot (1 - Y_{Fs})$$

Therefore the solutions:

$$T = \frac{(T_s - T_{amb})}{exp\left(\frac{-\dot{m} \cdot C_{pg}}{4 \cdot \pi \cdot \lambda_g \cdot r_s}\right) - 1} \cdot \left[exp\left(\frac{-\dot{m} \cdot C_{pg}}{4 \cdot \pi \cdot \lambda_g \cdot r}\right) - 1\right] + T_{amb} \tag{2-8}$$

$$Y_F = \frac{Y_{Fs}}{exp\left(\frac{-\dot{m}}{4 \cdot \pi \cdot \rho_{Fg} \cdot D \cdot r_s}\right) - 1} \cdot \left[exp\left(\frac{-\dot{m}}{4 \cdot \pi \cdot \rho_{Fg} \cdot D \cdot r}\right) - 1\right] \tag{2-9}$$

$$\dot{m} = 4 \cdot \pi \cdot r_s \cdot \rho_{Fg} \cdot D \cdot \ln(1 + B_T) = 4 \cdot \pi \cdot r_s \cdot \rho_{Fg} \cdot D \cdot \ln(1 + B_M) \tag{2-10}$$

$$B_M = \frac{Y_{Fs}}{1 - Y_{Fs}} \qquad B_T = \frac{C_{pg}}{L_v} \cdot (T_{amb} - T_s) \tag{2-11}$$

$$B_T = B_M = B \tag{2-12}$$

With Y_{Fs} the mass fraction of the fuel in gaseous form and the Spalding transfer number B represents the ratio of the driving force for vaporization to the resistance to vaporization.

B_T and B_M are thermal transfer number and mass transfer number respectively. These numbers are equal under the condition of quasi-steadiness; i.e. $Le = 1$.

If the fuel vaporization rate at the droplet surface is equal to the consumption rate at the droplet surface, then

$$\dot{m} = \frac{d}{dt}\left(\frac{4}{3} \cdot \pi \cdot {r_s}^3 \cdot \rho_{Fl}\right) \tag{2-13}$$

Substituting Eq. 2-13 into Eq. 2.-10 and integrating gives,

$$d^2 = {d_0}^2 - K \cdot t \tag{2-14}$$

where d is the diameter of the droplet, d_0 is its initial diameter and K is the vaporization rate and t is the time. K is a constant and could be written in terms of binary diffusion coefficient as

$$K = 8 \cdot \frac{\rho_{Fg}}{\rho_{Fl}} \cdot D \cdot \ln(1 + B) \tag{2-15}$$

By utilise the hypothesis of Lewis Number equal to unity, the vaporization rate K could also be written in another form that consists mixture of thermodynamics properties,

$$K = 8 \cdot \frac{\lambda_g}{C_{pg} \cdot \rho_{Fl}} \cdot \ln(1 + B) \tag{2-16}$$

From above equations, it is shown that the evolution of the squared-diameter of the droplet against time is linear under the 'quasi-steady' assumption.

2.2.3 The limitations of the theory

Eventhough the 'quasi-steady' theory or also called the d^2-law is very successful in describing the gasification process of a fuel droplet, the hypotheses upon which the theory has been developed are subjected to several experimental and numerical analyses and also critisms due to its simplicity. The most controversial critisms which are already identified and constantly discussed are as follows:

a. Constant and uniform droplet temperature

   Based on previous studies (Chin and Lefebvre, (1983); Nomura et al., (1996), Sazhin et al., (2005)) there are a lot of evidences that show the existence of the transient heat-up period of the droplet preceeding to the occurrence of the d^2-law.

b. Unity of Lewis number

   The Lewis number is not always a unity and it keeps changing during the process of vaporization (Raghunandan and Mukunda, (1977); Udeotok, (2012)).

c. Spherical symmetry

   This assumption is used in derivation of the d^2-law, means that the convection either natural or forced is absent and therefore the droplet and the flow, temperature and species field surrounding it remain spherical during the entire droplet lifetime. This assumption facilitates the analytical development. However, the assumption is no longer valid as under practical applications, the droplet deforms during gasifica-

tion due to the pressure of natural convection or strong forced flow. Eventhough numerous experimental and numerical studies have been undertaken to verify the implications of this assumption, the results shows that the d^2-law still holds even under convective flow conditions but under the condition that the droplet reaches its thermal equilibrium first. Nonetheless, a new improved method of suspended droplet has been studied by Renaud *et al.* (2004), Mikami *et al.* (2005) and Chauveau *et al.* (2007). The findings showed that the droplet is retaining its spherical symmetry shape by improving the method of the support fibre. Instead of single suspended fibre with a droplet hanging at the end of the fibre, the new method consists of two perpendiculars of fine quartz fibres. The droplet is positioning at the intersection of these two fibres. The details of this method will further discussed and elaborated at chapter 3 under experimental set up. By comparing to the existing literature, the effects of heat transfer are significantly minimized.

There are other affects known as 'thermocapillary effects' where the spherical symmetry is not only consist of the spherical shape but also due to the temperature distribution inside the droplet. Thermocapillary effects can modify the shape of inside of the spherical symmetry. Studies showed that the theoretical results are dissimilar with the surface which is free or not (Wilson (1994); Ha and Lai (2001)).

d. Soret and Dufour effects

Soret effect describes the flow of matter caused by a temperature gradient (thermal diffusion), while Dufour effect describes the flow of heat caused by concentration gradients. The two effects occur simultaneously. Both effects are believed to be small in most cases although sometimes their contribution may be significant (Coelho and Silva, (2002); Postelnicu, (2004); Gopalakrishnan and Abraham, (2004))

e. Quasi-steadiness

Several studies have shown that the deficiency of the d^2-law is a result of the non-steadiness of the gas-phase surrounding the droplet or of the vapour accumulation near the droplet interface (Law *et al*., 1980; Waldman, 1975; Law and Faeth, 1994). However, the effects of this assumption on the d^2-law are not yet completely recognized (Faeth, 1983).

2.3 The Experimental Techniques and Methodology

There are a few known techniques or methods available in determining the liquid fuel droplet vaporization experiments. The most known techniques are as following:

a. A porous sphere with liquid fuel being fed to its interior at such rate that the surface is just wetted to support combustion;

b. A free-fall single droplet or droplet stream eventually levitating;

c. Acoustic levitation

d. A single droplet suspended at the end of a thin quartz fibre.

Each technique has been utilised for so many years and impose its own merits and limitations.

2.3.1 Porous sphere

The porous sphere experiment is an accurately steady-state and thus is the one that most closely conforms to the steady-state assumption of the d^2-law (Godsave, (1953); Williams, (1973)). In combustion experiment, it allows detailed probing of the flame structure (Canada and Faeth, (1973).The main downsides of this method are the excessively large size of drop-

let and the deterrence of observing certain transient phenomena which is inherently present in droplet combustion. In this method the diameter of the sphere made up of an inert porous material is maintained constant during combustion. Fuel is supplied to the surface of the sphere at a rate equal to the rate of its combustion which depends on the diameter of the sphere and ambient conditions. In recent years, a number of studies employing this method have been carried out on measuring burning rates of liquid fuel. Balakrishnan *et al.* (2001) have investigated quasi-steady burning of spherical fuel particles in a mixed convective environment using the porous sphere method and suggested a correlation for the variation of mass burning rate with the free stream Reynolds number. Raghavan *et al*. (2009) studied methanol combustion using the porous technique to measure the mass burning rates and suggested correlations for the same envelope and wake flame regimes. Recently, Parag and Raghavan (2009) carried out experimental study using porous sphere technique to determine the burning rates of ethanol and ethanol-blended fossil fuels. They found that the mass burning rate of fuel increases with sphere size and air velocity, and when water is added to ethanol, the mass burning rate decreases. For ethanol blended with diesel, the mass burning rate does not vary significantly. For ethanol blended with gasoline, the mass burning rate increases with increasing gasoline content due to higher volatility of gasoline.

2.3.2 Free-fall droplets

Meanwhile, free droplets experiments offer the advantages of small sizes, non-interference from suspension fibre and the capability of using volatile fuels. Nevertheless, this method provides more complex and elusive experimental methodology. Moreover, as the droplets are not stationary, more additional equipment is required to obtain detailed photography. The free fall motions also entail that the intensity of forced convection is continuously changed as the droplets size is incessantly diminished. A number of studies have employed this technique in

investigating the vaporization and combustion behaviour of hydrocarbon and alcohols droplets. One of the earliest experimental studies have been carried out by Kumagai *et al.* (1971) in developing a successful technique for achieving spherical combustion of free fuel droplets under a zero-gravity condition in a freely-falling chamber. It was followed by an improved experimental apparatus set up by Okajima and Kumagai (1975) in their further investigation of the combustion of free droplet, where the combustion of fuel droplets in weak forced convection has been studied for the first time. Wang *et al*. (1984) studied the combustion characteristics of isolated, low Reynolds number, multicomponent droplets freely falling in a hot, oxidizing gas flow. Lee and Law (1992) have experimentally studied vaporization and combustion of methanol and ethanol droplets in both dry and humid environments. Their results demonstrated that the alcohol droplets had freely absorbed water from wet environment whether the water is present in the ambient gas or is generated at the droplet flame. Stengele *et al*. (1999) conducted an experimental set-up where the evaporation of free-falling, non-interacting binary mixtures of n-pentane and n-nonane droplets was investigated. The results showed that the evaporation distance and the velocity of the droplets decreases with elevated pressures. A comparison with theoretical calculation showed an excellent agreement of the measured results.

2.3.3 Acoustic levitation

The acoustic levitation of droplets is a valuable tool for studying heat and mass transfer at the droplet surface because it allows steady droplet positioning. However, acoustic levitation results in an acoustic streaming near the droplet surface (which may affect the heat and mass transfer rate). A key element of the heat and mass transfer processes at the surface of levitated droplets is the acoustic streaming. This technique has been actively pursued by researchers especially from University of Erlangen-Nurnberg (Yarin et al. (1999) and Yarin et

al. (2002)). The acoustic levitation of single droplets is a recent development that attempts to avoid some of the errors intrinsic to the previously-used experimental methods of droplet free flight, free fall or pendant suspension on a capillary or filament.

2.3.4 Suspended droplet on support fibre

The fourth method, which is the main technique applied in this study is the suspended droplet experiment. First advantage of this method is the easiness in set up and performance. As the droplet is motionless, the detailed cine-microphotography could be taken of its evaporating or burning sequences. Most of the isolated droplet evaporation experiments have been conducted with the droplet suspended on a support fiber to avoid the experimental difficulties for free-falling droplets (Hiroyasu and Kadota (1974); Nomura *et al.* (1996); Morin *et al.* (2000); Ghasemmi *et al.* (2006)). However, due to the thickness of the suspension fibre, it is quite difficult to suspend a droplet much smaller than 1000 micrometers. This large size of droplet is much larger than the standard size of typical droplet in sprays. Recent study by Daho *et al*. (2012) on droplet vaporization of various vegetable oils and blends domestic fuel oil-cottonseed oil at different temperatures have utilized the fibre-suspended technique with diameter of 400 µm. The droplet diameters are in range between 1000 to 1420 µm. The support fibre also usually has relatively larger thickness (around 150µm) and therefore is able to increase the vaporization rate of the droplet due to the induced heat transfer from the fibre to the droplet during vaporization process. The suspension fibre also significantly distorts the droplet's spherical shape. Therefore, the assumption of spherical symmetry of the droplet is no longer valid. However, recent developments (Renaud *et al.* (2004), Mikami *et al.* (2005) and Chauveau *et al.* (2007)) have improved the suspended droplet method to provide more accurate data results by diminishing or minimizing the effect of heat transfer from the support

fibre to the droplet. This new improved technique of suspended droplet will be further elaborated in details in chapter 3.

Conclusions

Most droplet evaporation and combustion experiments have been conducted with the droplet suspended on a support fiber to avoid the experimental difficulties for free-falling droplets, such as for obtaining high-resolution droplets images. The main concern about the suspended droplet technique is the existence of the heat conduction effects from the support fibre to the evaporating droplet. The literature reports many studies appreciably improving the technique by reducing as much as possible the fiber diameter, others by taking into account in numerical models this phenomenon, then correlating their results with experimental data. It is only very recently that experimental studies could implement extremely fine suspension fibres, allowing the production of new results with improved technique (Renaud *et al.* (2004), Mikami *et al.* (2005) and Chauveau *et al*. (2007)).

2.4 Influence of different parameters

2.4.1 Influence of temperatures and pressure

In the early work for high-pressure evaporation under natural convection, Kadota and Hiroyasu (1976) have considered a mathematical model of a single droplet evaporating in high pressure and high temperature gaseous environments. The calculation covered the unsteady and steady state of droplet evaporation considering the effect of natural convection. The calculated results showed the reverse effect of ambient gas pressure on droplet lifetime; i.e. the droplet lifetime decreases with an increase in pressure at high temperatures and with a decrease in pressure at low temperatures. Hartfield and Farrell, (1993), have studied the vaporization of single refrigerant R-113 (trichlorotrifluoroethane) and n-heptane droplets experi-

mentally. They have observed that the gas temperature affected strongly droplet vaporization whereas gas pressure had a weaker effect. Stengele *et al*. (1999) conducted an experimental set up to study the evaporation of free falling, non interacting droplets in a higher pressure environments. The experiments were carried out with binary mixtures of n-pentane and n-nonane. Ghasemmi *et al.* (2006) on the vaporization of kerosene droplet experimentally investigated at high temperatures and high pressures under normal gravity. The evaporation rate increased monotonically with an increase in gas temperature. At low temperature, when the ambient pressure increased, the evaporation is also increased. However, at high temperature and higher ambient pressure, evaporation rate is increased to a maximum value around 2.0 MPa and then decreases.

2.4.2 Influence of gravity and convection

Most non-convective droplet evaporation experiments have been conducted at normal gravity. The presence of natural convection enhances the evaporation slightly for low pressure but significantly strong at high temperatures (Ristau *et al.* (1993)). However, droplet evaporation experiments at microgravity have been carried out from atmospheric pressure to supercritical pressure. These experiments are significant not only for microgravity applications but serve as comparison bases for accuracy test of evaporation models. The purpose of creating a microgravity environment condition for droplet vaporization and combustion is to remove the influence of buoyancy. The aim is to create a situation in which the evaporation induced or Stefan velocity is much larger than the relative velocity between the droplet and ambience that created either by buoyancy or a forced convection. Burning behaviour of a suspended *n*-octane droplet under both normal and microgravity fields has been studied experimentally by Sato (1990). The studies concerned the effects of natural convection at high ambient pressure levels up to four times the fuel critical pressure. Experimental results showed that the burning

rate constant increases with the increase of the ambient pressure at subcritical pressures and decreases at supercritical pressures for both microgravity and normal gravity fields. That means the natural convection increases the burning rate constant and its effect become stronger as the ambient pressure increases. Nomura *et al.* (1996) studied the evaporation of suspended *n*-heptane droplet under microgravity in a closed chamber. Microgravity conditions were used to repress the effect of natural convection in the ambient gas. They studied the effect of temperature and pressure on the evaporation rate. They also studied the effect of these parameters on the heating and evaporation time. The effects of forced and natural convection were studied in isolation by Okajima and Kumagai (1982). They used a free falling chamber provided with a wind tunnel. This was used to study the effect of forced convection without natural convection**.** Runge *et al.* (1998) and Gökalp *et al*. (1994) investigated evaporation of droplets of binary mixtures to bring in the effect of multiple components in droplet evaporation process. These experiments were done in a convective environment and at ambient pressures. Daif *et al*. (1999) reported an enhancement of the evaporation rate of a droplet in an environment without forced convection due to flow induced by natural convection in the gas phase surrounding the droplet. The natural convection could be due to thermal or solutal buoyancy. However, according to Mandal and Bakshi (2012), these effects were insignificant as they found out that the internal circulation can be induced by a small temperature variation caused by the droplet evaporation. Therefore, the internal circulation is responsible for the enhanced evaporation rate in otherwise stationary environment in a closed chamber. Their work showed that there is evaporation induced internal circulation within certain droplets while evaporating even under atmospheric conditions. This circulation enhances the evaporation rate significantly as compared to diffusion-driven evaporation. These findings seemed to agree with Hegseth *et al*. (1996) on suspended methanol droplet experiment where the results showed that when a droplet evaporates sufficiently fast, it exhibits a vigorous inte-

rior flow. This flow was driven by surface tension gradients. Chauveau *et al*. (2011) have carried out experiments of *n*-decane droplet vaporization under both normal and microgravity in stagnant hot atmospheric environment. By using the improved 'cross-fibre' suspended droplet technique, the results showed that for ambient temperature below 950 K, deviation from the d^2-law is observed during droplet vaporization in microgravity condition. However, for temperatures beyond 950 K, the experimental results demonstrate that the d^2-law holds throughout the entire lifetime. Based on their results, they concluded that microgravity condition is not necessarily guarantee that the d^2-law holds during droplet vaporization. These observations are based on their argument that once the flow radial velocity is attained beyond the critical velocity, the effect of natural convection becomes unimportant as the corresponding radial evaporation characteristic velocity becomes significantly influential.

2.4.3 Influence of external heat transfer

As our study is concerned with the vaporization of a single droplet suspended by a support fibre, therefore it is essential to discuss the effect of heat transfer conduction from the support fibre. In the early work for high pressure droplet evaporation under natural convection, Kadota and Hiroyasu (1976) have considered the effects of fibre conduction and liquid-phase radiative absorption in simplified manner. They evaluated the fibre conduction with a simple one-dimensional steady-state analysis where the radiative analysis was assumed to occur on the droplet surface. Eventhough it was only a qualitative significance, their calculations indicated enhancement on the evaporation rate. Shih and Megaridis (1995) have numerically analyzed the effect of fibre conduction on droplet evaporation under forced convection. They have observed that for a fibre parallel to the flow direction, only small enhancement of evaporation was found. Less heat input through the fibre is resulted. Avedisian and Jackson (2000) have observed the effect of support fibre on the soot patterns for droplets burning in a

stagnant ambience in reduced gravity. They have observed the nonlinearity in the variation of d^2/d_0^2 due to the influence of fibre. The soot that aggregated forming inside the flame was also found to be evolved into nonsymmetrical. The effect became more significant with thicker fibre. A study to investigate the effect of heat conduction through the support fibre on evaporation of a droplet in weakly convective flow was initiated by Yang and Wong (2002). A droplet of n-heptane or n-hexadecane was suspended at the tip of a horizontal or vertical fibre in an upward hot gas flow. In general, they found that the heat conduction through the fibre enhances the evaporation, with a stronger effect for a lower gas temperature and a thicker fibre. Also, the evaporation rate is enhanced in an oxygen-containing gas flow due to the additional heating from the oxidation around the droplet.

Conclusions

Temperature and pressure play a significant role in effecting the behaviour of vaporization of isolated droplet fuel. However, previous studies on most alkanes droplet showed that the later has less impact on the vaporization rate. Studies also showed that the natural convection is significantly noticeable at higher temperatures conditions.

In our study, all experimental works are carried out at normal gravity and ambient atmospheric pressure. Eventhough the gravitational force and ambient pressure play a significant role in influencing the vaporization rate of the droplet; it will not be covered in this study. Concerning the effect of external heat transfer from the supporting fibre, Chauveau *et al*. (2008), in their studies of the effects of heat conduction through a support fiber showed that their results obtained are important in the sense that they make it possible to clearly show that the effects of the suspension fiber can be very important and can even hide the benefit of the experiments conducted in reduced gravity if the fiber has a too important size. Taking into consideration these results, it would be thoughtful to revisit the studies carried out previously on the effect of the pressure on the droplet vaporization rates, because all these experiments

were conducted with fibers having large sizes, introducing therefore the possibility of a systematic over-estimation of the measured vaporization rates. The effect of the droplet suspending technique such as buoyancy and natural convection is eliminated by using a novel cross micro-fiber system. This technique enables to preserve the spherical shape of the droplet throughout the vaporization process in normal gravity atmosphere. As this study involved a single value of ambient pressure i.e. at normal atmospheric pressure, thus the influence of natural convection which is dependent on elevated pressures is negligible.

The heat conduction from the suspended fibre seems to play a big role in influencing the vaporization of the droplet. The 'extra' heat is used to enhance the vaporization rate; therefore the actual vaporization rate is not achievable and overestimated. Studies showed that the 'extra' heat transfer from the fibre increases with the thickness of the fibre. Fortunately, an advanced and novel technique, the 'cross-fibre' technique (Renaud *et al.* (2004), Mikami *et al*. (2005) and Chauveau *et al.* (2007)), employed in this current studies apparently reduced the said effect of the heat conduction from the suspended fibre.

2. 5 Vaporization and combustion issues and challenges of droplet alcohols

Recent concern regarding environmental issues due to hydrocarbon fuel has intensified the interest in alternative fuels such as alcohols. However, due to the latent heat of vaporization properties of alcohols that is relatively higher than conventional hydrocarbon fuels, there exist some significant worries over their vaporization efficiency and therefore the heterogeneity and uniformity of the fuel/air mixture for combustion process. Alcohols are also known to possess higher miscibility property with water. Therefore, it is our main concern in this study to properly characterize the extent of this property to the vaporization behaviour of alcohols. Alcohols droplet vaporization mechanism has been first investigated more than three decades

ago by Law and Binark (1979) through a theoretical study of spray vaporization of a monodisperse fuel spray in a cold and humid environment. The results showed that the associated condensation heat release is considerable and significantly enhance the fuel vaporization rate heterogeneously on the droplet surface. The subsequent study was carried out experimentally by Law *et al*. (1987) with the vaporization of suspended alcohols droplets such as methanol and ethanol in cold and humid environment. They observed that the condensation and subsequent dissolution of water into the alcohols droplet is significant and resulting in the deviation of diameter-squared evaluation of the droplet from the classical d^2-law. Meanwhile Choi *et al.* (1988, 1989) on the combustion of methanol droplet suggested the potential importance of surface condensation of the matter vapour produced at droplet flame. Those claims were confirmed by Choi *et al.* (1990), Lee *et al.* (1990) and Lee (1990) by experimental sampling. Lee and Law (1992) continued to study the effect of water condensation on alcohols droplet through experiments of free-falling methanol and ethanol droplets combustion in both dry and wet environments. Their results demonstrated that the alcohol droplets had freely absorbed water from wet environment whether the water is present in the ambient gas or is generated at the droplet flame. Marchese and Dryer (1996) simulated a time-dependent combustion of isolated, bicomponent liquid droplets of methanol and water using a spherosymmetric, finite element, chemically reacting flow model. The results are then compared with previously reported data from microgravity drop tower, freely falling isolated droplet and suspended droplet combustion experiments. Results suggest that droplet experiments using methanol-water mixtures should strongly characterize the magnitude of the liquid mass transport rate in a given experimental configuration. Numerical results are consistent with experiments when it is speculated that sufficient internal liquid phase motion is present to reduce the effective liquid mass Peclet number (dimensionless number used in calculations involving convective heat transfer. It is the ratio of the thermal energy transferred to the fluid by con-

vection to the thermal energy conducted within the fluid) to the order of one. Such internal motion has been noted in droplet combustion experiments and most likely arises from droplet generation/deployment techniques and/or surface tension gradients. From Mukhopadhyay and Sanyal (2001), a theoretical model for combustion of alcohol droplets has been developed by considering the quasi-steady sphericosymmetric gas phase equations. The results showed that for alcohols with boiling temperatures lower than that of water, an amount of moisture that is generated during combustion is absorbed by the droplet. It prolongs droplet lifetime and consequently reduces flame temperature**.** A study to clarify the effect of watery vapour concentration in hot ambient on droplet evaporation of a single suspended droplet of ethanol, which posses the hydrophilic property and n –hexadecane, n-heptane droplets with dehydrophile property has been carried out by Lee *et al*. (2001). The results showed that the watery vapour increases the evaporation of the ethanol droplet after entering into the droplet and it promotes evaporation velocity with occasional micro-explosion. In recent studies, Hopkins and Reid (2005) and Hopkins et al. (2006) studied multicomponent droplets of methanol/water, ethanol/water and 1-propanol/water. The results showed that the evaporation and growth of a multicomponent droplet depend on kinetic and thermodynamic parameters, including the gas and liquid-phase diffusion coefficients and the activity coefficients and vapour pressures of the constituents. Raj *et al*. (2010) have studied the evaporation of ethanol-water and methanol-water droplets by a technique measuring the surface tension concentration variation during evaporation process. The results showed evidence of rapid evaporation of more volatile component at initial phase followed by a diffusion-controlled slow evaporation towards the end of droplet lifetime. Mandal and Bakshi (2011) recently proposed the same measurement of surface concentration of an evaporating multicomponent droplet on an ethanol-water droplet under three different ambient conditions. The results showed that the decrease of surface concentration of ethanol is fastest in the case of the hot nitrogen blowing

over the surface of the droplet. Also, the slow convection at atmospheric temperature was found to enhance the rate of evaporation of ethanol eventhough the total rate of evaporation is not significantly changed.

Conclusions

Most of the experimental studies of the vaporization behaviour on the hydrogenated fuels such as alcohols are always correlated with the interference of water existence. The higher miscibility with water and the hygroscopic nature of alcohols seem to change the overall performance of alcohols fuels in terms of vaporization and combustion characteristics. Most of the observations and findings from the literature suggested that alcohols droplets have freely absorbed water from the environment and subsequently dissolved therefore changing the vaporization behaviour of ethanol vaporization. However the extent to which these water impact on actual vaporization behaviour of alcohols is still lack in literature.

Therefore, in our present study, experimental results concerning vaporization behaviour of both lower and higher molecular weight alcohols; ethanol and 1-propanol droplets respectively are presented. A new and wide range of temperatures is covered in this work. The d^2-law will be further examined and the histories of the instantaneous vaporization rates will be presented to have more comprehensible understanding on the actual vaporization behavior of alcohols. The so-called impact of water vapour on the overall alcohols droplets vaporization behavior is also investigated. To further emphasis on this issue, a quantitative measurement of water content during vaporization of alcohols is carried out. Due to the lack of experimental data in the literature, the “quasi-steady” model calculation has been used in order to compare with our experimental results.

2.6 Alcohol blends vaporization

Apart from the study on pure alcohols, blends of alcohols with diesel oil or fuel oil have been anticipated for a number of applications in engines and combustion appliances. The addition of some alcohols to a hydrocarbon fuel allows some use of energy from renewable sources without seriously changing the characteristics of the fuel and also it reduces pollutant emissions. However there are some limitations on alcohol-hydrocarbon mixtures. The limited miscibility of the components is the major constraint. Alcohols also readily absorb water, which further reduces the range of miscibility. The behaviour of evaporating or burning droplets of alcohols-hydrocarbon mixtures has been little studied. Hallet *et al*., (2010) have studied the measurements of single suspended droplet evaporation behaviour for mixtures of pure and denatured ethanol with No. 2 fuel oil (a complex combination of hydrocarbons with carbon numbers in the range C_9 and higher produced from the distillation of petroleum crude). No. 2 fuel oil is usually used for heating and is very similar to diesel fuels. The results showed that the mixtures behave identically to pure ethanol up to the point where the ethanol disappears, after which the evaporation rate becomes that of pure fuel oil. The departure from the d^2-law is due largely to the inclusion of natural convection. Burning characteristics of free-falling droplets of diesel/ethanol and biodiesel/ethanol mixtures have been experimentally studied by Botero *et al.* (2012). They observed that the diffusion-limited mechanism for multicomponent droplet burning with highly disparate boiling points was demonstrated for diesel/ethanol and biodiesel/ethanol mixtures. Three phases have been identified; steady burning with more volatile components with lower boiling points, an intermediate transient heating period as the dominant surface components transition from more volatile to less volatile and the last phase consists of steady burning by the co-gasification of both components. Ethanol micro explodes earlier during burning with stronger intensity. The addition of ethanol also reduces the yellow luminosity of the flame at early stage of droplet lifetime, indicat-

ing an overall reduction in sooting propensity. Experimental studies on Brazilian gasoline type C and hydrated ethanol mixture at various concentrations have been carried out by Delgado *et al*. (2006). The physio-chemical properties for a better comprehension of the effects caused by the flex-fuel technology have been evaluated. The results show that the mixtures of hydrated alcohol-gasoline increased the octane properties such as Motor Octane Number (MON), (RON) and Anti-Detonant-Index. The specific mass and electric conductivity also increased in values with the addition of ethanol. Parag and Raghavan (2009) carried out experimental study to determine the burning rates of ethanol and ethanol-blended fossil fuels. They found out that the fuel mass burning rate increases with sphere size and air velocity, and when water is added to ethanol, the mass burning rate decreases. For ethanol blended with diesel, the mass burning rate does not vary significantly. For ethanol blended with gasoline, the mass burning rate increases with increasing gasoline content due to higher volatility of gasoline.

Conclusions

Most commonly, alcohols are used as a pure fuel or blended with either gasoline or diesel. As our studies concern the vaporization behaviour of alcohols and the effect of water vapour during the process, the results and the data are imperative for the future works of alcohol/hydrocarbon blends especially in internal combustion engines applications.

2.7 Autoignition Studies

Autoignition process is defined as a spontantaneous process where a mixture of fuel and air undergoes a chemical reaction leading to ignition and combustion without the aid of external sources such as a flame or spark. Generally, autoignition is always associated with ignition delay time (IDT), τ and usually measured in milliseconds. Ignition delay time is a key

characteristic of a fuel which indicates its relative reactivity at given conditions. Common definition of ignition delay time is the time period between the creation of the combustible mixture (at the end of compression) and heat release (Figure 2.3). If a fuel/oxidiser mixture is compressed and heated to temperatures and pressures high enough to allow combustion to occur, ignition is not instantaneous but instead takes place after some time later. During this period, the fuel molecules decompose (initiation) and react chemically with the oxidiser to produce reactive radical species. These radicals then undergo a chain reaction with more fuel molecules producing more and more reactive radical species (propagation), resulting in the exponential growth of what is termed the "radical pool" (chain-branching). When the radical pool becomes of critical mass, the remaining fuel fraction is consumed instantaneously (chain-terminating) leading to an explosive release of energy (ignition). Ignition delay measurement is significantly important especially for the design of superior performing engines, as well as for gas turbine design and chemical kinetics research.

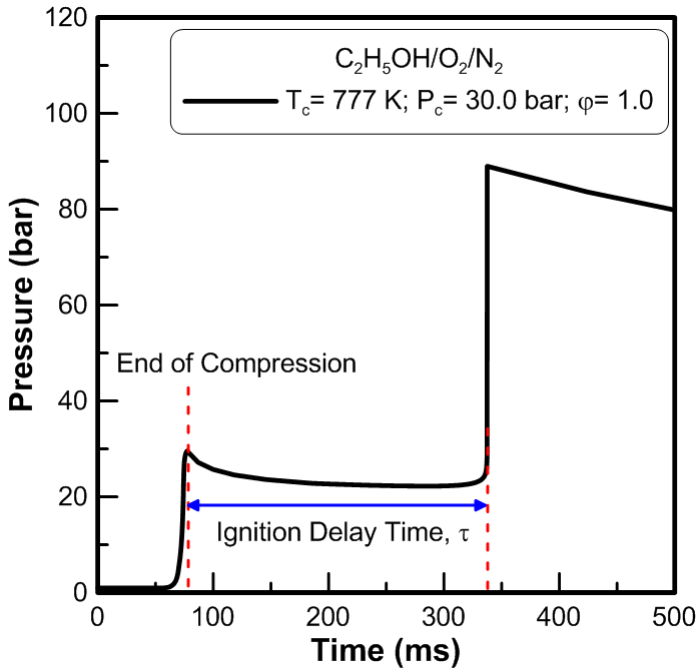

Figure 2.3: Definition of ignition delay time used in this study

2.7.1 Autoignition Experimental Devices

The main key to improve the efficiency of internal combustion engines is the understanding of the chemistry that takes place when a fuel burns. To predict the chemistry of fuel oxidation at wider range of temperatures and pressures requires a complete qualitative and quantitative characterization of these chemical reactions. Nonetheless, to study the details of fuels chemistry in an internal combustion engine is impractical, not uncomplicated and not effortless since they involve turbulent reactive flows that are complex to analyse or repeat under controllable conditions. Its environment is also plagued by varying conditions of temperature and pressure, combined with intricate fluid motions (laminar, transitional or turbulent). To overcome some of the challenges in predicting the chemistry of the fuel oxidation, some simplified experimental laboratory devices offer an alternative to complex engine environments. They eliminate some of the complexities that exist in real engines but at the same time preserve the ability to work efficiently under engine-relevant conditions.

The option of simplified experimental devices is restricted by the range of temperatures and pressures at which they can operate; and only the RCM and shock tube can reach engine-relevant temperatures and pressures rapidly enough and yet endure the high pressures that transpire after the ignition event.

Shock tube

Shock tubes are usually used at higher temperatures ($T > 1000$ K) due to their capability to rapidly bring the mixture to test conditions. In the shock tube, the premixed gas is heated by a shock wave in approximately 1 ns to pre-selected temperatures and pressures. The shock wave is usually generated by the rupturing of a diaphragm that separates two sections containing high-pressure and low-pressure gas respectively. Typically reflected shock tempera-

ture and pressure range in the tube shock are 1000-3000 K and 1-17 atm. However, the time-scale behind the shock wave is very short; normally fall between 10-1000 µs, which limits the test period, and therefore unfit for testing at lower temperatures (Crossley *et al.* (1972), Lifshitz, (2001)). According to Würmell *et al.* (2009), shock tube experiments are generally carried out with a premixed mixture of fuel, oxygen, and argon, since the shock wave behaviour is optimized in monatomic carrier gases, such as argon. Dilute fuel mixtures that contain only small proportions of fuel and oxygen in more than 90% of argon are therefore studied under the most optimal shock wave conditions, since the fraction of polyatomic gas is kept small.

Rapid Compression Machine (RCM)

Meanwhile RCMs have been widely used in the low to intermediate temperature region (700 K < T < 1100K). The RCM is a device that can rapidly compress a premixed fuel/oxygen/diluents gas mixture to a preselected temperature and pressure. It can simulate only a single stroke of the combustion engine and thus allows the study of autoignition under more favourable conditions than those in real engine. Post-compression conditions of temperature and pressure in RCM are typically in the range of 700-1200 K and 1-6 MPa. The typical test times are in the region of 1-200 ms. One shortcoming with RCMs is the inevitable loss to the walls which is due from relatively longer test times in the RCM. For years, RCMs have been utilized in autoignition and oxidation studies of alkane fuels and recently on oxygenated fuels at low to intermediate temperature range. Minetti *et al*. (1995) have studied n-heptane oxidation and autoignition in a rapid compression machine at low to intermediate temperature regimes and high pressures. N-heptane exhibits a high reactivity characterized by a relatively short ignition delay and by a relatively low ignition limit in accordance with the

octane number of this fuel. The delay times show a remarkable negative dependence upon gas temperature in the range of compressed temperature 700-860 K.

A detailed experimental study of the nine isomers of heptane has been performed in a rapid compression machine by Silke *et al*. (2005). The interest in the study lies in determining the role of molecular structure of the C_7H_{16} hydrocarbons on the rate of combustion of the various isomers. Ignition delay times were measured, and their dependence on the reaction conditions of temperature and pressure was studied, and the comparative reactivity profiles of the different isomers were obtained. The study has resulted in an RCM data for the nine isomers of heptane. In general, results showed shorter ignition delay times for isomers with low research octane number (RON) with the longest ignition delays and/or failure to ignite for isomers with high RON.

Healy *et al*. (2008) have presented an extensive range of experimental data for methane/propane mixtures in the temperature range of 740 – 1550 K at various compressed gas pressures and equivalence ratio in both shock tube and rapid compression machine.

Lee et al. (1993) have reported the autoignition characteristics of methanol, ethanol and metyl tert-butyl ether (MTBE) in a RCM at pressure range 20-40 atm and temperature within 750-1000 K.

An RCM also has been used to study the effects of fuel structure and additives on the Homogeneous Charge Compression Ignition (HCCI) of pure hydrocarbon fuels and mixtures under well determined conditions by Tanaka *et al*., (2002). The results indicated that for HCCI combustion, the ignition delay and the burn rate can be independently controlled using various fuel mixtures and additives.

Flow reactors

Another common experimental device to study the autoignition behaviour of fuels is flow reactors. Flow reactors imitate the flow conditions inside the gas turbine premixers therefore their data generally used for both gas turbine design (Spadaccini and TeVelde, (1982)) as well as chemical kinetics research (Gokulakrishnan *et al.* (2007)). Recent experimental works on flow reactors by Beerer and McDonell, (2011) on alkane autoignition at high pressures and intermediate temperatures showed a number of differences in ignition delays trend identified between high and intermediate temperatures, including overall activation energies, relative reactivity of ethane and propane and impact of small quantities of ethane or propane mixed with methane on the ignition delay time. They concluded that these contrasting trends are attributed to the different elementary reactions that control the ignition process.

Conclusions

Studies show that the choice of simplified experimental devices is limited by the range of temperatures and pressures at which they can operate. It is also observed that only the shock tube and rapid compression machine (RCM) can reach engine-relevant temperatures and pressures rapidly enough and at the same time withstand the high pressures that occur after the ignition event. The shock tube is known to be accommodating for the study of high-temperature and high-pressure reactions, while intermediate and low-temperature reactions can be studied at various ranges of pressures in rapid compression machine. Both devices provide useful data as they could present significant data on ignition delay time of reactive fuel gases.

2.7.2 Development of Autoignition Studies on Alcohols

To better assess the effect of the presence of these new molecules in fuels on the engine efficiency and the pollutants formation, it is imperative to carry out experimental investigations and to develop well validated detailed kinetics models for these oxygenated components of biofuels. Major parts of the experimental studies of oxidation and ignition of alcohols have only been performed recently. However, most of the experimental investigations of alcohols have been carried out at temperature above 770 K. This is mostly due to a lack of reactivity of these compounds at lower temperature (Tran *et al*. (2012)).

Natarajan and Bhaskaran (1981) have performed an experimental and analytical investigation of the ignition of ethanol-oxygen-argon mixtures behind reflected shock waves over the temperature range of 1300-1700 K at pressures of 1.0 and 2.0 atm. The equivalence ratio, φ is varied at 0.5, 1.0 and 2.0. The experimental ignition delay data were found to correlate with initial ethanol and oxygen concentrations and with initial temperature. A 56 steps kinetic model for ethanol oxidation in the temperature range mentioned was assembled using published rate coefficient data wherever available.

Dunphy and Simmie (1991) have studied the ignition characteristics of ethanol-oxygen mixtures behind reflected shock waves from 1080 to 1660 K in the pressure range of 1.8-4.6 bar, with equivalence ratio, φ varied from 0.25 to 2. In general, the results showed that an increase in total pressure was accompanied by a uniform decrease in the observed ignition delay for any particular reaction mixture. The results showed that the observed delay time decreases as the initial reactant concentration increases.

As a continuation from their first experimental studies on ethanol oxidation, Dunphy *et al.* (1991) have modelled a high-temperature oxidation of ethanol in a 97-steps, 30-species reaction mechanism and the results of the calculations were then compared to recent measurements of the ignition delays of mixtures of ethanol, oxygen and argon behind the reflected

shock waves in a range of 1080-1660 K at pressure of 1.8-4.6 bar with equivalence ratio of 0.25 to 2.0.

Lee *et al.* (1993) have investigated the autoignition characteristics of alcohols such as methanol and ethanol and ether (methyl-tert-butyl ether) in a rapid compression machine in the range of 20-40 atm and at low temperatures of 750-1000 K. The results showed higher autoignition temperatures than paraffins which is consistent with the high octane number of these fuels. It also confirmed the intrinsic resistance to autoignition of oxygenated fuels relative to reference fuels.

Marinov (1998) has studied a detailed chemical kinetic model for high temperature ethanol oxidation. The model has been developed and validated against a variety of experimental data. The laminar speed data obtained from a constant volume bomb and counterflow thin-flame, ignition delay data behind the reflected shock wave, ethanol oxidation product profiles from a jet-stirred and turbulent flow reactor were used for computational study. The results showed that high temperature ethanol oxidation exhibit strong sensitivity to the fall-off kinetics of ethanol decomposition.

Li *et al.* (2007) have reported the experimental profile of stable species mole fraction for ethanol oxidation in a Variable Pressure Flow Reactor (VPFR) at initial temperature range of 800 K to 950 K, constant pressure of 3 to 12 atm and various equivalence ratios from 0.3 to 1.4. A new updated ethanol mechanism has been proposed and validated against wide range set of data and showed a significant improvement of predictions. The detailed kinetics mechanism for ethanol combustion was developed, taking into consideration of a hierarchical manner of reacting system..

Yates *et al.* (2010) have carried out a detailed chemical kinetic modelling study to characterize the autoignition behaviour of full range of blends of both methanol and ethanol with a

Primary Reference Fuel (PRF) 80 base fuel. The study provided a few main observations. The cool-flame temperature rise was progressively reduced in proportion to the blend fraction and it primarily determined the characteristics of the blend autoignition chemistry.

In comparison with methanol and ethanol, studies of combustion and oxidation on higher molecular weight alcohols such as propanol and butanol were limited and only recently performed. Norton and Dryer (1991) have presented experimental results for the flow oxidation of methanol, ethanol, n-propanol, iso-propanol, tert-butyl alcohol (TBA) and methyl tert-butyl ether (MTBE) at initial temperatures of 1020-1120 K and at atmospheric pressure. The results demonstrated that in comparison with alkanes, alcohols have a more complex oxidation mechanism, which involves the production of both oxygenated and non-oxygenated intermediates directly from the fuel. According to their observations also, the primary alcohols are more inclined to dehydrogenation than to dehydration because of the weakness of the C-H bond. The direct production of aldehydes from primary alcohols causes these fuels to have much shorter reaction times than do the corresponding alkanes. Meanwhile the secondary alcohols react both by dehydration to alkanes and by dehydrogenation to ketones. Tertiary alcohols are susceptible to unimolecular dehydration.

Sinha and Thompson (2004) studied diffusion flames of C_3-oxygenated hydrocarbons and their mixtures including iso-propanol, dimethoxy methane and dimethyl carbonate. They concluded that the intermediate pools in their flames were strongly related to the fuel structural features.

Johnson *et al.* (2009) have studied the ignition characteristics of the two isomers of propanol (n-propanol and iso-propanol) in a shock tube device. Ignition delay times for propanol-oxygen-argon mixtures have been measured behind reflected shock waves at high temperatures, range of 1350-2000 K at atmospheric pressure with equivalence ratio of 0.5, 1.0 and 2.0. The experimental results illustrated that ignition times for the n-propanol mixtures are

faster than for iso-propanol in all cases. A kinetic model has been developed to describe the decomposition and ignition pathway of both n-propanol and iso-propanol isomers in this temperature range. It is based on previously validated C_3-chemistry with sub mechanisms added for the propanol isomers. The results showed that the overall trends in the data are captured fairly well by the mechanisms which include a greater level of reactivity for the n-propanol mixtures relative to iso-propanol.

Frassoldati *et al.* (2010) have developed a kinetic model to describe the combustion of n-propanol and iso-propanol. It was validated by comparing predictions made using this kinetic model with new experimental data on structures of counterflow non-premixed flames. The kinetics mechanism was made up of more than 7000 reactions among 300 species. The agreement between this kinetic model and experimental data showed satisfactory results. In general, they observed that the structures and overall combustion characteristics of n-propanol and iso-propanol flames are similar.

Veloo and Egolfopoulos (2011) have measured laminar flame speeds and extinction strain rates of *n*-propanol/air, *iso*-propanol/air and propane/air mixtures. A model was also presented which predicted experiments accurately, with deviations at rich conditions of *n*-propanol/air and propane/air flames.

Moss *et al.* (2008) have carried out the autoignition measurements of four isomers of butanol using shock tube at 1 and 4 bar pressure and higher temperature of 1200-1800 K at various equivalence ratio and fuel mole percentage. Kinetic modelling indicates that the consumption of 1-butanol and iso-butanol which are the most reactive isomers takes place primarily by H-atom abstraction resulting in the formation of radicals, the decomposition of which yields highly reactive branching agents.

Heufer *et al.* (2011) reported high pressure ignition delay results of stoichiometric n-butanol/air mixtures under the conditions behind the reflected shock of approximately 10-42 bar and temperature 770-1250 K. The results showed non-Arrhenius behaviour at temperatures lower than about 1000 K for the pressure range studied. They found that the rate of increase of ignition delay with decreasing temperature appeared to change around 1000 K.

Autoignition experiments for n-butanol have been performed by Weber *et al.* (2011) using a heated rapid compression machine at compressed pressures of 15 and 30 bar, in the low-intermediate compressed temperature range of 675-925 K. Over the conditions studied, the ignition delay decreased monotonically as temperature increased and the experimental data was performed and the reactivity in terms of the inverse of ignition delay showed nearly second order dependence on the initial oxygen mole fraction and slightly greater than first order dependence on initial fuel mole fraction and compressed pressure.

Effect of water on combustion and autoignion behaviour of alcohols

Previous studies by Christensen and Johansson (1999) have shown that water injection in an HCCI engine significantly delays combustion timing, thus increasing the required intake temperature for a specific operating point when compared to pure fuel. This method was found successful in terms of controlling the ignition timing. A later investigation by Steinhilber and Sattelmayer (2006) found that a fuel-water mixture, or an emulsion, is more effective at retarding combustion timing and reducing pressure rise rates in comparison with separate injections. A study by Megaritis *et al.* (2007) used forced induction and residual gas through negative valve overlap (NVO) to run an HCCI engine on wet ethanol containing up to 20% water, the findings suggest increased air heating can extend the operating range of ethanol-in-water mixtures beyond the limitations of their experimental set-up.

Mack *et al.* (2009) discussed the experimental results from a HCCI engine running on wet ethanol. Fuel mixtures studied range from pure ethanol to mixtures containing as high as 60% water. Stable HCCI operation was obtained for fuels containing up to 40% water. Incomplete combustion and excessive intake temperatures limited the operating range at higher water concentrations. The maximum value of the cumulative heat release profiles decreases with an increase in water concentration. Exhaust emissions data is also presented and discussed. Hydrocarbon and carbon monoxide emissions tend to increase with increasing fuel water content while NO_x levels are low, which is typical in HCCI engines.

Conclusions

The autoignition of alcohols has been studied by numerous authors either in shock tubes or rapid compression machines (RCMs). The experimental works either in shock tube or RCMs have been structured to adapt the realistic conditions in internal combustion engines. The developments of autoignition study on oxygenated fuels have attracted interests especially on alcohols. Starting with the lower molecular weight alcohols such as ethanol and methanol, the development was already extended to heavier alcohols, namely n-propanol and n-butanol. The experimental results of various mixtures have provided the data for future improvement of kinetics mechanisms. In our current work, the effect of the impact of water addition to alcohols autoignition behaviour is wholly initiated by the lack of the study concerned in the literature.

2.8 Conclusions

In the first part, the literature review underlines the important results and findings concerning the vaporization of an isolated single droplet. The key assumptions that govern the 'quasi-steady' theory have been conferred, with the lack or supports have been identified. The influ-

ences of various parameters on vaporization of alcohols have been discussed to give a clearer view on their impact to vaporization behaviour. However, our main concern in this study is the miscibility property of alcohols with water; therefore the effect of water addition to the vaporization of alcohols especially on ethanol is really significant and required further investigation. The effects of water on overall vaporization of droplet ethanol will be explored in details in terms of d^2-law compliance and the effects on instantaneous vaporization rate at various ambient temperatures.

In the second part of the review, the results and findings concerning the autoignition characteristics study have been emphasized. The common typical devices for the autoignition study; i.e. shock tube and RCMs was briefly explained. The developments of autoignition study on oxygenated fuels have been considered. Nonetheless, there is still a lack of autoignition study on the effect of the impact of water addition to alcohols. Kinetics mechanism from literature will be applied to capture the impact of water addition. Sensitivity analysis will be employed so that the actual impact of water addition in ethanol autoignition behaviour is known and discovered.

In the next chapter, a detailed interpretation of the vaporization of an isolated droplet has been carried out in this experimental study aimed at investigating ethanol and 1-propanol droplets. An alcohol droplet is located at the intersection of the cross quartz fiber with a controlled initial at various ambient temperatures and at atmospheric pressure. The real impact of the water concentration on the vaporization rate of an ethanol droplet in a wide range of temperature will be thoroughly examined.

The autoignition experiments of ethanol, 1-propanol and blends of ethanol and water have been carried out in a rapid compression machine (RCM).

3 EXPERIMENTAL STUDIES

3.1 Experimental studies of an isolated droplet of alcohol vaporization

3.1.1 Experimental Apparatus and Equipment

The main apparatus that has been utilized in this study is known as Multi User Combustion Chamber, courtesy of CNRS, Orleans, France. The MUCC has been developed in year 1988 for the purpose of combustion test. It has undergone a number of modifications since then and has been utilized for many applications. Under its actual configuration, the MUCC allows the experimental study of evaporation for various combustible fuels even in poor oxygen environment. It is possible to carry out evaporation experimental works either a single droplet or a series of several droplets (up to 9 droplets). It also permits us to carry out experiments with different criteria or parameters such as droplet size, gaseous nitrogen pressure and temperature in the chamber. Every experimental result could also be recorded in a video form. Therefore we are able to determine the time and speed of droplet evaporation at various configurations.

The experimental apparatus MUCC (see *Appendix A-1* for more details) utilised in characterising the mechanism of isolated droplet vaporization are composed of these three main elements:

a. Under-pressure chamber that consists of furnace, mobile piezo-electric injector (three motors that allow the displacement of frame in three dimensions), a moving frame, and other support equipments.

b. Programmable Logic Controller (PLC) and temperature operation panel that control the temperature, pressure, lighting and the cooling system of the furnace and its inverter.

c. A computer to permit the supervision of the experiments, post-processing data such as data collection and data analysis.

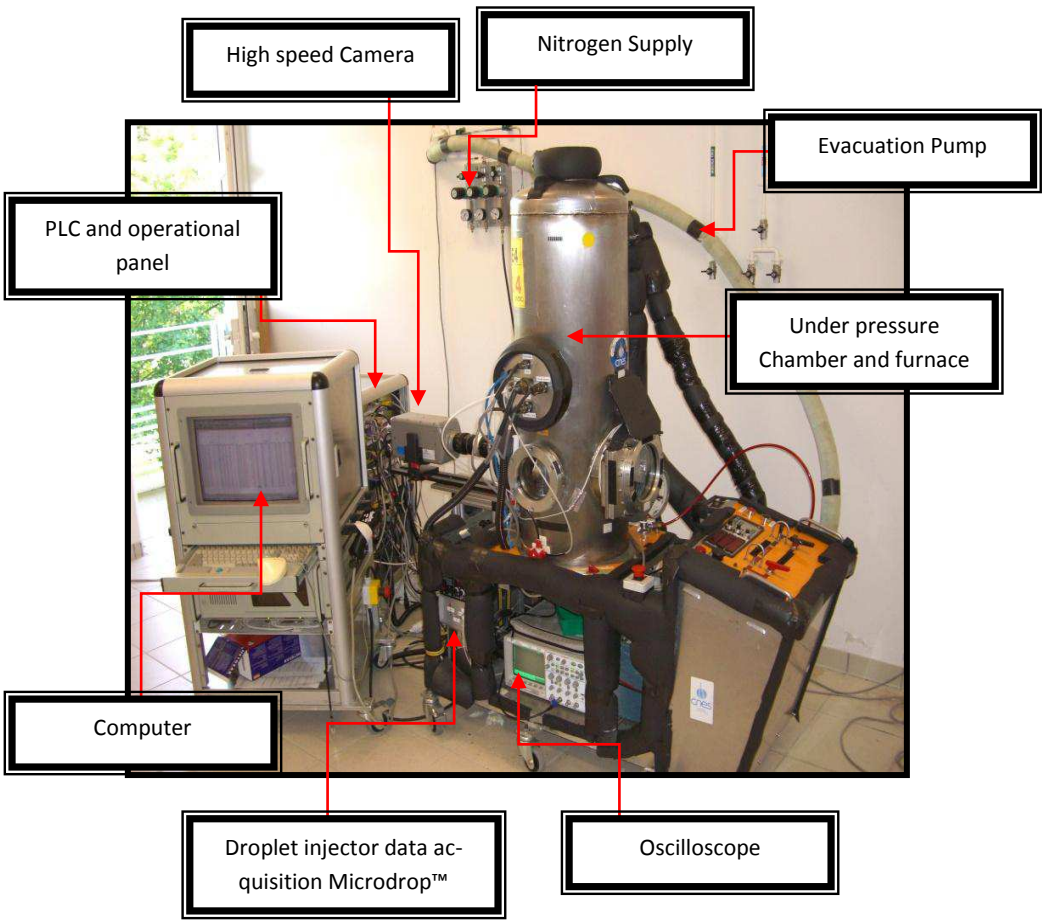

Figure 3.1: The main apparatus of Multi User Combustion Chamber (MUCC) at CNRS, Orleans, France

3.1.2 Experimental Technique

The experimental set-up is also described elsewhere by Renaud et al. (2004) and Chauveau et al. (2008) and schematically represented in Figure 3.2.

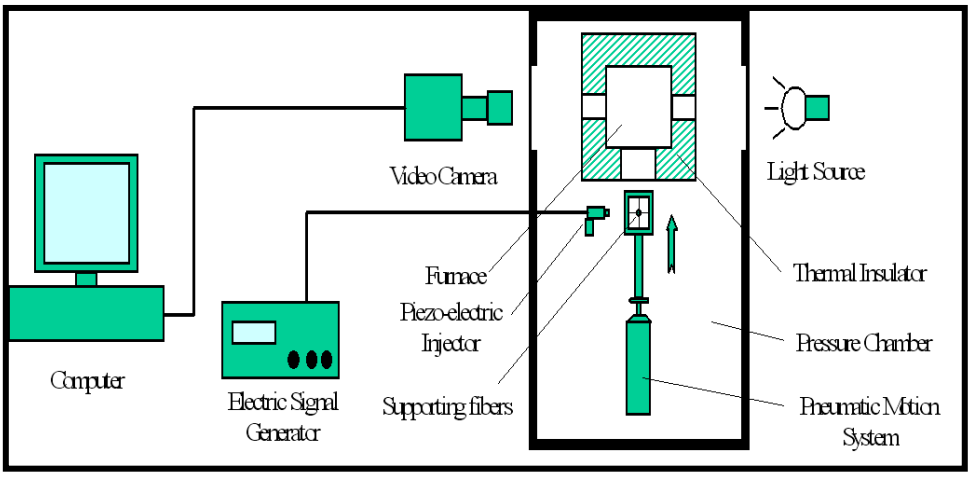

Figure 3.2: Schematic diagram of the whole experimental apparatus.

Cross Fibre Technique

The cross-fibre technique is a novel method in investigating the vaporization of an isolated droplet in a closed chamber. It is an 'improved' version of a conventional droplet suspended method (Figure 3.3). Instead of a single support fibre, it consists of two fine intersecting quartz fibre of 14 µm thickness each (Figure 3.4). The droplet under investigation will be formed at the intersecting point of the two perpendicular quartz fibres.

The droplet injection on the frame is carried out in a region of the vaporization chamber which is located at the lower part of the chamber at ambient temperature, called the 'cold zone' in order to avoid any pre-vaporization before the start of the experiment. A piezo-electric injector is utilized to generate the droplet, by supplying a monodisperse liquid jet impacting the support. Once the droplet of controlled initial diameter (300 – 600 µm) is formed on the intersection of the quartz fibres, it is then introduced into the furnace by the aid of mo-

torized displacement system. The average total transfer time measured from the lower region of the chamber into the furnace is about 700 ms. As soon as the droplet is exposed to the hot environment in the furnace; the temporal evolution is recorded using a high-speed video camera with various frame rates from 20 to 400 fps dependent on the ambient temperature.

Nitrogen (99.95% purity) fills the medium of the furnace to allow pure vaporization and to avoid any oxidation or ignition to occur particularly at elevated temperatures.

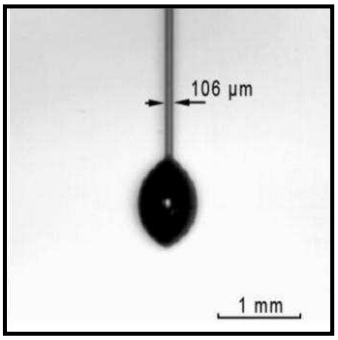

Figure 3.3: Single fibre suspended droplet technique (Chauveau et al. 2011)

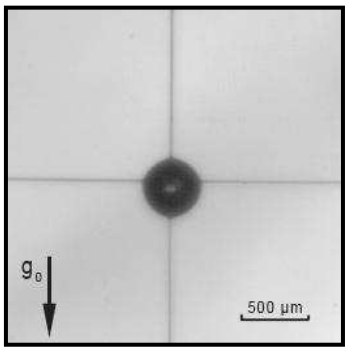

Figure 3.4: Cross-fibre supported droplet technique used in MUCC.

Purging of pressure chamber

To ensure pure vaporization and to prevent any droplet combustion to occur during experiment, a high level of pure nitrogen is essential. Therefore, it is necessary to conduct a purge to the pressure chamber. The purge is performed during heating of the furnace. In a worst case, the pressure chamber will be filled with atmospheric air. The air is commonly composed of approximately 21% of oxygen (O_2) and 78% nitrogen (N_2). However, to run the experiments only gaseous Nitrogen is needed in the system. The principle and procedure of purge is simple. It consists of depressurization and pressurization of air in the chamber.

The percentage of oxygen is reduced by half in each purge. Therefore it is possible to say that after four successive purges, the oxygen percentage will reduce to approximately 1.3%. (And indeed, in some cases, the pressure chamber is filled with nitrogen with a small proportion of tiny fuel residual injected during experiment).

$$\%\ (O_2) = \frac{2^1}{2^4} = 1.3\%$$

Materials and Fuels

Alcohols such as anhydrous ethanol with high purity GC grade (Sigma –Aldrich contain 99.6% of ethanol), and standard ethanol (in this study we refer this ethanol as ethanol 95%) that contain approximately 5 % water (Ethyl Alcohol 96.2 Re Puro by Carlo Erba) and 1-propanol (Sigma-Aldrich) are used for these experiments. Ethanol (CH_3CH_2OH) is a lower molecular weight alcohol; its molecular structure shows a polar fraction due to the hydroxyl radical and a non polar fraction in its carbon chain. Due to its short carbon chain, the properties of ethanol polar fraction overcome the non polar properties. That explains the hygroscopic nature of ethanol. Conversely, 1-propanol ($CH_3CH_2CH_2OH$) is an alcohol which is having almost equally both polar and non polar fractions in its molecules. However, the polarity frac-

tion in 1-propanol molecules is fewer comparatively to ethanol due to its longer carbon chain. 1-propanol also exhibits higher boiling temperature than ethanol.

The physical and chemical properties of ethanol and 1-propanol are presented in Table 3.1.

Table 3-1**:** Physical and chemical properties of ethanol and 1-propanol

Properties	**Ethanol**	**1-propanol**
Density, ρ (kg/m^3 @ 298K)	790	803
Dynamic viscosity, μ (mPa.s @ 298K)	1.074	1.945
Surface tension, σ (10^{-3}N.m @ 293K)	22.75	23.74
Latent heat of vaporization, L_v (kJ/mol)	42.32	47.45
Boiling temperature, T_b (K)	351.32	370.3
Molecular weight, M_w (g/mol)	46.07	60.1

3. 1.3 Experimental Operating Conditions

In all experiments, the pressure in the furnace is kept at atmospheric at P_∞= 0.1 MPa, while the ambient temperature is varied from 298 to 973 K. The homogeneity of the temperature is controlled by three thermocouples K-type placed inside the furnace. The ambient relative humidity is measured by VAISALA HMT333 Humidity and Temperature Transmitter. For each experiment set, a minimum of 700 images are captured and recorded to permit sufficient temporal resolution with at least six experiments performed for each test condition.

3.1.4 Experimental Instability

The instabilities occur during the motion of droplet from lower chamber to the furnace (Figure 3.5). This movement is accompanied by vibrations and subsequently induces oscilla-

tions. It was decided then to show the evolution of surface area of the vaporized droplet only when the droplet was stabilized.

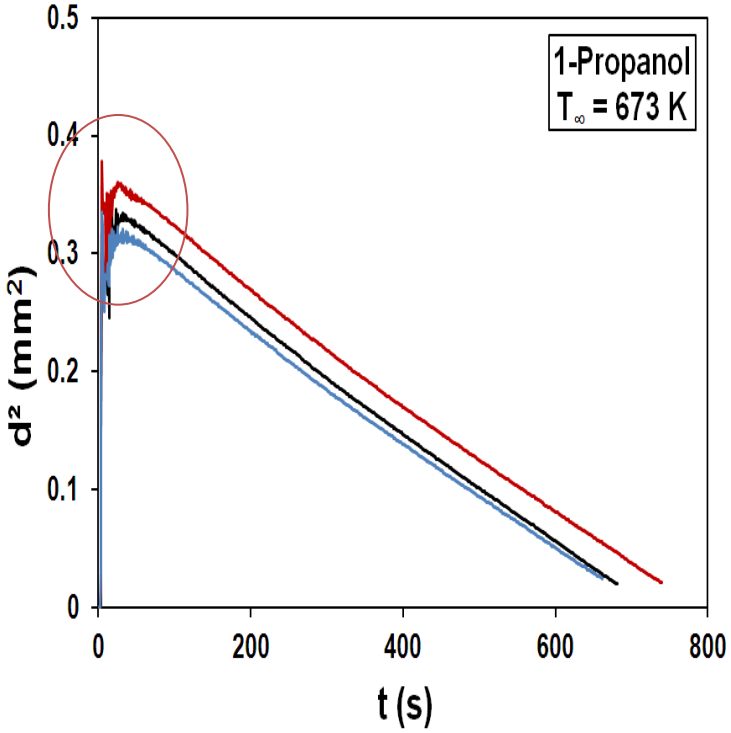

Figure 3.5: Representative set of runs showing the instabilities during the motion of the droplet from lower chamber to furnace.

3.1.5 Post-Treatment of the Data and Measurement Uncertainties Analysis

1. Computations and Post-Treatment of the Data

The images captured by the high speed video camera are transferred to a computer and analysed by post-processing to deduce the droplet instantaneous surface area and hence its diameter temporal variations.

Visualization of the vaporization phenomena is carried out using a fast video camera (Phantom v5). The vaporization sequence is first recorded in the camera memory and then transferred on the hard disk of the acquisition computer. The maximum frame rate of the

camera at full resolution of 1024 x 1024 pixels is 1200 fps.The objectives coupled to the camera allow getting a resolution of approximately 9.8μm /pixel.

The first step of the treatment is to convert the film obtained in series of consecutive images. To perform this task, the software Cine Viewer 640™ is used.

Then, we define a grey level threshold (usually at nominal value, S = 70/256) in order to "binarize" the image. These binarized pictures represent the droplet projected surface. From these pictures, we can extract an equivalent diameter for each drop. These dimensions in pixels are converted into metric sizes by knowing the resolution of the optical system, obtained by in-situ calibration.

Figure 3.6 displays the representative sequences of anhydrous ethanol droplet vaporization at T_∞ = 473 K using the cross-fibre technique and its corresponding images time respectively. Note that the cross-fibre technique allows for the formation of a nearly spherical droplet even in a normal gravity and the sequences demonstrate that the droplet spherical shape is preserved during the entire droplet lifetime.

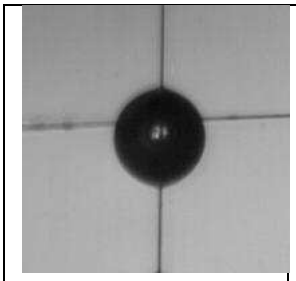	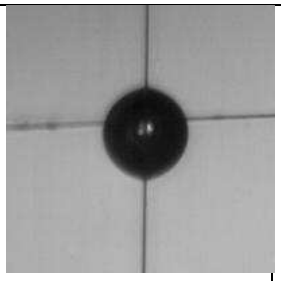	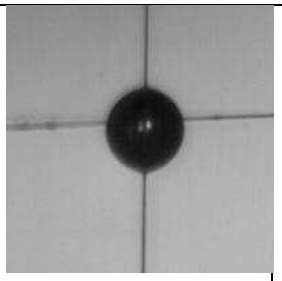	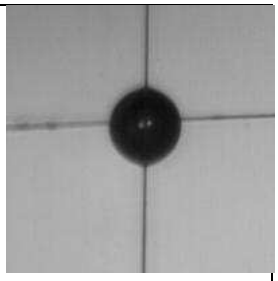
t = 1 s	t = 2 s	t = 3 s	t = 4 s
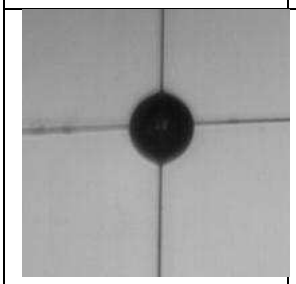	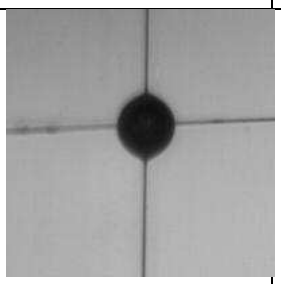	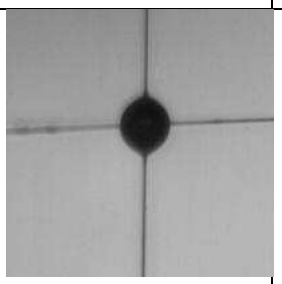	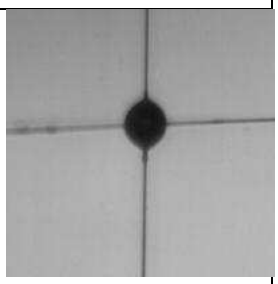
t = 5 s	t = 6 s	t = 7 s	t = 8 s
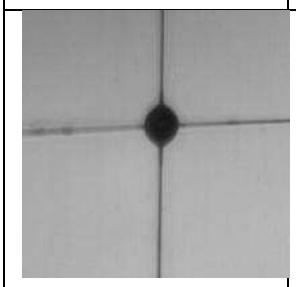	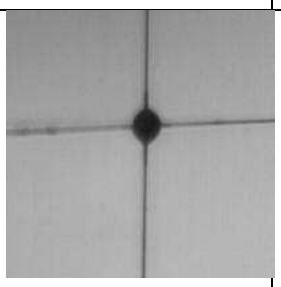	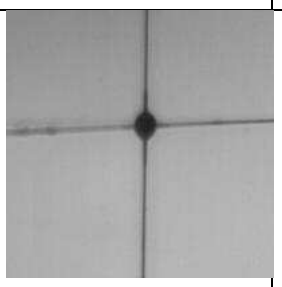	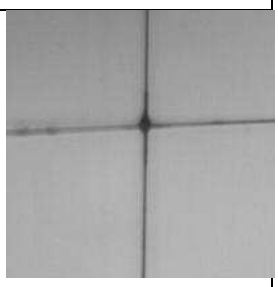
t = 9 s	t = 10 s	t = 11 s	t = 12 s

(a)

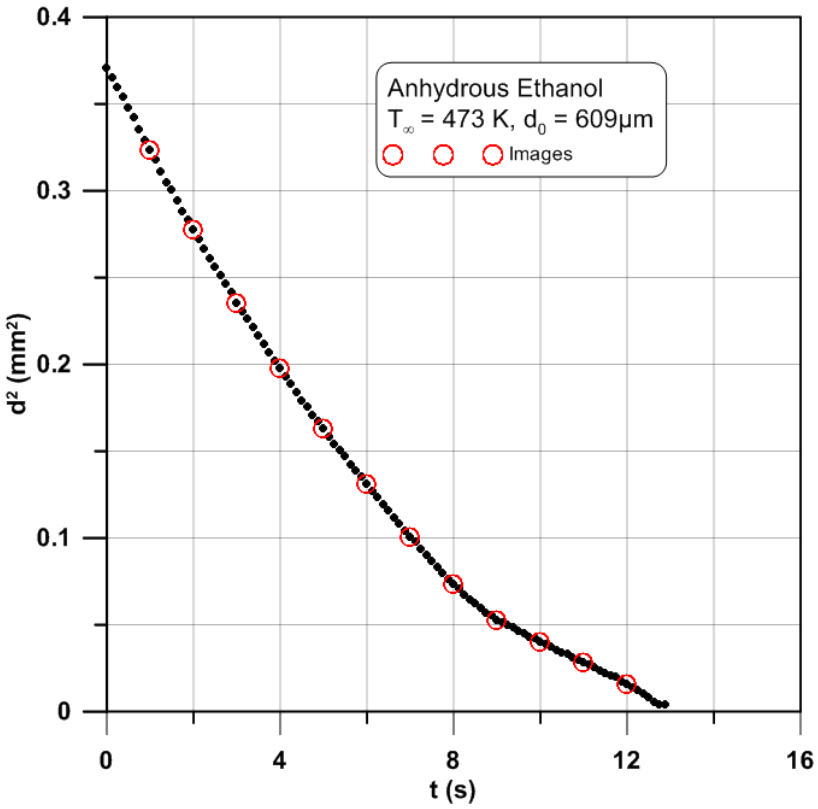

(b)

Figure 3.6: The evolution of the droplet life time for anhydrous ethanol at 473K (a) Images extracted from the video, and (b) their corresponding time reporting on the figure.

2. Estimation of the Droplet Size Measurement

It is possible to determine the droplet size directly from the image captured. As the coordinates of the image are in pixels, one can deduce the droplet size as the conversion of pixel to the width is known (1 pixel corresponds to 9.8 micrometer).

3. Measurement of Uncertainties and Experimental Reproducibility

The method for determining the droplet diameter mainly includes two sources of errors; the first is the conversion factor from pixels to actual measured size in mm. To determine this

factor we use a calibration target types USAF that has been positioned in place of the droplet. The manual operation causes a pointing accuracy of ± 1 pixel on each of the lines of sight to give a conversion factor of 9.5 µm/pixel of ±0.06. The rod (0.5 mm square) had eight squares in X and Y direction. A standard measurement (Photoshop) gave us H = 421 pixels and L = 420 pixels with a magnification factor of Gr = 9.5 µm /pixel. If now we consider a pointing error of 1 pixel outward in each direction we obtain 423 pixels in H and L where the magnification factor, Gr = 9.46 µm/pixel. If we now consider a pointing error of 1 pixel inward in each direction, we obtain 418 pixels in H and L where Gr = 9.57 µm/pixel. Therefore, the magnification factor is defined as, Gr = 9.5 ± 0.06% µm/pixel.

The second source of error is from the automatic treatment of images. To determine the surface droplet in squared-pixel, it is necessary for the binarization of the droplet and the bottom. However, this procedure uses a threshold value which is a constant for any given sequence of vaporization. A variation of the voluntary value of this threshold (± 20 grey level) around its nominal value (S = 70/256) causes a variation of ± 3.5% in the droplet diameter of a 450 µm initial diameter of a droplet. However it should be noted that this error is not constant throughout the life of the drop, and significantly increases at the end of droplet lifetime (> 10%). If a real calculation of uncertainty is taking into account the possible error in the beginning and at the end of life of the droplet, with addition on the magnification and the time, one will obtain,

Table 3-2: Uncertainties Calculation at ± 15 greylevel

Item	Unit	Value	Error	
d_0	In pixels	48.6	±1	X
d	In pixels	13.5	±1.2	Y
Gr	µm/pixel	9.5	±0.06	Z
t	s	3	±0.001	W
K	**0.065572943**	**±0.003132**	**4.78%**	

K consists of linear formula between d_0 and d and defined as follows;

$$K = (x^2 - y^2) \cdot \left(\frac{z^2 \cdot 10^{-6}}{w}\right) \tag{3-1}$$

The values of d and d_0 are taken in pixels, before the intervention of Gr. Their uncertainties are taken to a variation of ± 15 greylevel thresholds, which is already excessive as error. During the time, an error of 1 ms is made knowing that in general the snapshots frame rates are between 200 and 1000 frames/s. Again the value is overestimated relative to the variability of the camera. If we refer to a more realistic error, i.e. ± 10 greylevel, we obtain the following result:

Table 3-3: Uncertainties Calculation at ± 10 greylevel

Item	Unit	Value	Error	
d_0	In pixels	49.1	±0.6	X
d	In pixels	14.1	±0.8	Y
Gr	µm/pixel	9.5	±0.06	Z
t	s	3	±0.001	W
K	**0.066544333**	**±0.002041**	**3.07%**	

With the images treatment utilized in this study, the vaporization rates are obtained between 3 and 5% of error depending on the size of the initial diameter of the droplet. With one manual analysis of the images, we could not obtain a good precision result. However, with our treatment technique, we could achieve a considerable time of treatment with sufficient images to analyze. In our present experimental work, minimum of 700 images are captured and recorded for each experiment with at least 6 repetitive experiments performed for each test condition to permit sufficient temporal resolution.

Concerning the variability and reproducibility between the different tests, mean and standard deviation of the average vaporization rate for all test runs at each condition are calculated. Figure 3.7 shows the measurements of the droplet vaporization rate of 1-propanol at T_∞ = 673K were repeatable within ± 2%.

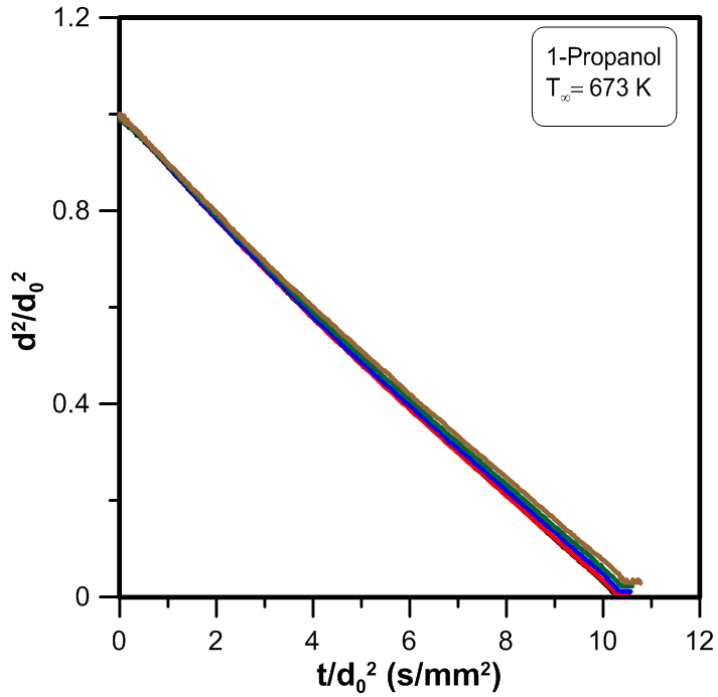

Figure 3.7: Representative set of runs showing the reproducibility of droplet vaporization experiments

3.2 Experimental studies of autoignition alcohols and alcohol-water mixture on Rapid Compression Machine (RCM)

In this section a detailed description of experimental studies on autoignition behaviour of ethanol, propanol and ethanol/water mixture will be given. The experimental works have been carried out using a rapid compression machine (RCM) courtesy of Chemistry of Combustion Centre, National University of Ireland, Galway (NUIG), Ireland (Director: Dr. Henry Curran).

3.2.1 Experimental Apparatus and Equipment

A rapid compression machine (RCM) is a device designed to perform the compression stroke of a reciprocating Diesel engine, such that the autoignition of fuels may be studied un-

der more defined conditions than those found in an engine by excluding the complicating influences of blow-by, spatial inhomogeneities etc. A RCM must be capable of the near-adiabatic compression of a low-pressure test gas into a confined volume of elevated pressure and temperature and of maintaining these conditions. Achievable post-compression conditions in RCM studies are ≈ 10–60 atm and ≈ 600–1100 K, and as such the RCM is a valuable tool for the study of the principles of homogenous charge compression ignition (HCCI). HCCI involves the compression of a homogenous (fuel) lean mixture of fuel/air. The use of a dilute and premixed fuel/air mixture allows ignition to occur at many points simultaneously when the piston is close to top-dead-centre, preventing thermal runaway of the combusting mixture and eliminating the high temperature combustion zones responsible for NO_x and particulate matter production.

Figure 3.8: The NUIG RCM

The RCM in NUIG has its origins in the Shell-Thornton (Affleck and Thomas, (1969)) research laboratory, where it operated since its creation in 1969 until the mid 1980's. The machine arrived in NUIG, Galway in 1995 where it was re-commissioned and modified to operate in its new environment. A description of these initial minor modifications and a detailed description of the workings of the machine are given by Brett (2001). A schematic of the NUIG RCM is given in Figure 3.9 (Affleck and Thomas, (1968)). Briefly, to compress the test gas the RCM uses two horizontally opposed pistons which are tightly sealed inside two compression sleeves which adjoin the reaction chamber. The RCM is symmetrical; two large drive chambers are positioned behind each piston and serve as a reservoir for high pressure

compressed air to drive the pistons forward at high speed. The two halves of the RCM are distinguished by the terms “fixed” and “free” referring to the non identical compression sleeves which allow the reaction chamber to be attached in the centre of the RCM. Following compression the pistons may be withdrawn to their pre-fired position by applying a vacuum to these same drive chambers. Adjacent to each drive chamber is an oil-containing hydraulic chamber through which the piston must pass as part of a complicated oil-hydraulic system which controls the starting, stopping and velocity of the pistons. By pressurising the hydraulic system the pistons are held in the pre-fired position whilst the drive pressure is applied. Once the desired pressure is contained in the drive chamber and the test gas has been admitted to the reaction chamber assembly, the pistons may be driven forward instantaneously by venting a portion of the pressure applied to the hydraulic system. This motion confines the test gas in the reaction chamber at an elevated temperature and pressure. All experiments were performed with creviced piston heads, an idea that was first engineered by Park and Keck (1990) and further developed by Lee and Hochgreb (1998). According to Silke *et al*. (2007), provided their optimal size and shape, piston head crevices effectively swallow the cooler boundary that is scraped from the chamber wall during the piston movement, thus preventing it from mixing with the hot compressed gas. The net effect is a more homogeneous distribution of temperature during the post-compression period. Since the rates of chemical reactions are extremely sensitive to temperature, non-homogeneous temperature fields render realistic kinetic modelling very difficult or even impossible. Würmel and Simmie (2005) highlighted the importance of an optimal piston head design. It was shown, by means of a computational fluid dynamic (CFD) study, that the crevice volume, its distance from the chamber and the ease with which the gas can flow into the crevice are crucial design considerations.

Figure 3.9: Schematic diagram of the NUIG RCM

3.2.2 RCM Experimental Procedure

The procedure for performing an experiment with the RCM is briefly described below, with details in *Appendix A-2*.

Mixture preparation

In this study test mixtures are prepared in one of the three stainless steel mixing tanks using standard manometric methods. Oxygen and diluents gases are obtained from BOC Ireland Ltd. and are presented in Table 3-4 and are used without further purification. All fuels are obtained from Aldrich Chemical Co. Ltd. and are presented in Table 3-5. Gaseous fuels of anhydrous ethanol and propanol also are used without further purification. The mixing tank is always flushed with the diluent as it is to contain for the next test mixture before being evacuated to 10^{-2} Torr (~10^{-5} bar). Liquid fuel is then allowed to vaporize into the evacuated mixing tank. Partial pressures of fuel and all gases are measured using a 2000 mbar digital manometer (Chell cd101) to an accuracy of ±0.2 mbar. Test gas mixtures are typically made up to a final pressure of 2000 mbar and are allowed standing for at least a couple of hours to ensure homogeneity.

The preheat temperature is set above the saturation temperature of each alcohol to ensure complete vaporization of the fuel. A magnetic stirrer mixes the reactants which are heated to avoid condensation of the mixtures. The temperature inside the mixing tank is allowed approximately 1.5 to 2 hours to reach a steady-state condition. Both reactive and non reactive (absent of O_2) mixtures are prepared for all experiments. The non reactive (NR) mixtures are prepared as a reference to be used for species reaction calculation and kinetics modelling.

Each compressed temperature condition is repeated at least three times to ensure reproducibility.

The reaction chamber is fitted with pressure and temperature sensing devices to measure the initial conditions in the reaction chamber. A pressure transducer (Kistler type 603B, SN 51740) is mounted flush with the reaction chamber wall and is used to monitor the change in pressure inside the reaction chamber during compression and any post-compression includeng ignition. The pressure experienced by the transducer is recorded as a charge signal. This signal is sent to a charge proportional amplifier (Kistler type 5001) where it is amplified to a known setting determined by the user, before being recorded as a voltage–time profile by an oscilloscope (Nicolet TDS). For all experiments with the rapid sampling chamber the charge amplifier is set to 20 Mechanical Units/Volt and the transducer sensitivity is set to 4.684 pC/V, as calibrated by the manufacturer for this specific pressure transducer (SN 51740). The temperature is measured by thermocouple type-J. There is first a characterisation of the inside gas temperature as a function of the wall temperature. This is then used in order to determine the initial gas temperature before the shot.

Table 3-4: Diluent gases used in RCM experiments.

Gas	Purity (%)	Major Contaminations (volume per million)
N_2 (CP Grade)	99.95	Ar <250 vpm O_2 <1 vpm Hydrocarbon < 0.0014% H_2O < 0.025% CO_2 < 0.0014% CO < 0.0014%
O_2	99.50	

Table 3-5: Fuels used in RCM experiments.

Fuel	Purity (%)
Anhydrous Ethanol	99.5
1-Propanol	99.9

Determination of gas compressed temperature, T_c

The adiabatic compression/expansion facility in the application *GasEq* (C. Morley, http://www.gaseq.co.uk/) is used to calculate the initial test gas pressure required to reach a specific compressed gas temperature, T_c. To do so *GasEq* requires the initial mixture composition, the values of initial pressure, P_i and initial temperature, T_i as well as an accurate value of P_c. The compressed temperature T_c can be defined from adiabatic process as;

$$\ln\frac{P_c}{P_i} = \int_{T_i}^{T_c} \frac{\gamma}{\gamma - 1}\frac{dT}{T} \tag{3-3}$$

where γ is the ratio of specific heat at constant pressure (C_p) to specific heat at constant volume (C_v),

$$\gamma = \frac{C_p}{C_v} \tag{3-4}$$

3.2.3 Experimental Operating Conditions

The details of operating conditions for autoignition experiments for alcohols and alcohol/water mixture have been performed using a NUIG rapid compression machine and are presented as below (Table 3-6):

Table 3-6: Autoignition operating conditions.

Fuel	P_i (bar)	T_i (K)	P_c (bar)	T_c (K)
C_2H_5OH	1	330 - 380	30	780 - 860
C_3H_7OH	1	340 - 380	30	750 - 850
C_2H_5OH (70% vol)/H_2O(30% vol)	1	350 - 370	30	790 - 835

Anhydrous ethanol (Sigma-Aldrich, 99.5%), 1-propanol (Sigma-Aldrich, 99.9%) and pure water (Mili-Q-Milipore, 0.22 µm) are used as the reactants. To determine the mixture composition, the mass of fuel, equivalence ratio and oxidizer ratio are specified. The diluents gas used is Nitrogen (N_2). Equivalence ratio is fixed to φ = 1.0 (stoichiometric condition) at all experiments. Proportions of O_2 and N_2 in the mixture are determined manometrically and added at room temperature (Table 3-7, 3-8 and 3-9).

For molar calculations,

$$C_xH_yO_z + m(O_2 + 3.76\,N_2) \rightarrow xCO_2 + \frac{y}{2}H_2O + 3.76mN_2 \qquad \text{(R1)}$$

Where m = $x + \frac{y}{4} - \frac{z}{2}$

For Ethanol,

m= 3,

$C_2H_6O + 3\,O_2 + 11.28\,N_2 \rightarrow 2CO_2 + 3H_2O + 11.28N_2$

For 1-propanol,

m= 4.5

$C_3H_8O + 4.5\ O_2 + 16.92\ N_2 \rightarrow 3CO_2 + 4H_2O + 16.92N_2$

Table 3-7: Mixture Preparation of Anhydrous Ethanol for both Reactive and Non Reactive.

Species	No. of Mole	Calculated Partial Pressure (mbar)	Accumulated Partial Pressure (mbar)	Reactive Measured Partial Pressure (mbar)	Non Reactive Measured Partial Pressure (mbar)
C_2H_5OH	1.0	131	131	125	125
O_2	3.0	393	524	500	0
N_2	11.28	1476	2000	1909	1910
Total	**15.28**				

Table 3-8: Mixture Preparation of 1-Propanol for both Reactive and Non Reactive.

Species	No. of Mole	Calculated Partial Pressure (mbar)	Accumulated Partial Pressure (mbar)	Reactive Measured Partial Pressure (mbar)	Non Reactive Measured Partial Pressure (mbar)
C_3H_8O	1.0	89	89	88	88
O_2	4.5	401	491	482	0
N_2	16.92	1509	2000	1965	1965
Total	**22.42**				

Table 3-9: Mixture Preparation of Anhydrous Ethanol/H_2O for both Reactive and Non Reactive.

Species	No. of Mole	Calculated Partial Pressure (mbar)	Accumulated Partial Pressure (mbar)	Reactive Measured Partial Pressure (mbar)	Non Reactive Measured Partial Pressure (mbar)
C_2H_5OH	1	138	138	133	133
H_2O	1.39	192	330	314.10	314
O_2	3	414	744	714	0
N_2	11.28	1557	2300	2208	2207
Total	**16.67**				

3.2.4 Experimental Reproducibility

The typical uncertainty in ignition delay time measured by NUIG RCM based on the observation and measurement of Wurmel *et al*. (2007) is around ±10%. This uncertainty is mostly due to the properties change with temperature and pressure. In present studies, each compressed pressure and temperature condition is repeated at least three times to ensure good reproducibility. The mean and standard deviation of the ignition delay for all test runs at each condition are calculated, as an indication of reproducibility (cf. Figure 3.10). The results show that the standard deviation calculation is less than 10% of the mean in every case. This estimation of uncertainties is in agreement with Weber *et al.* (2011) and Lee *et al*. (1993) in terms of RCM calculated error of ignition delay that represents the indication of reproducibility.

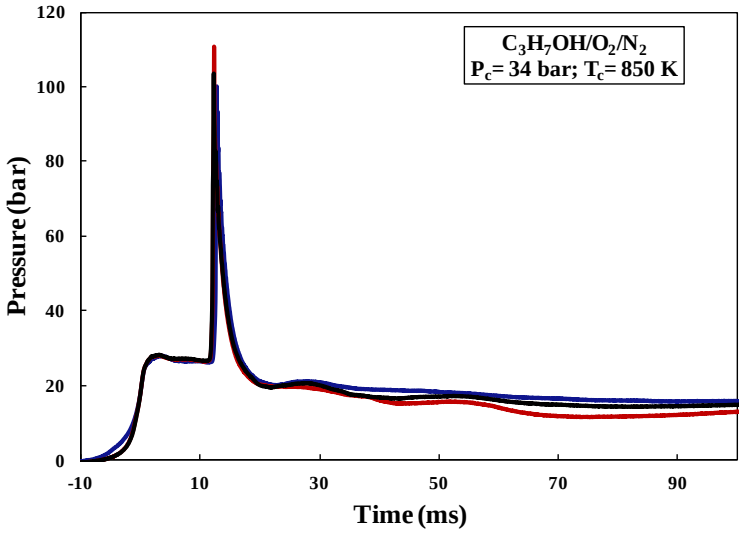

Figure 3.10: Representative set of runs showing the reproducibility of experiments.

3.3 Conclusions

A detailed description of the vaporization of an isolated droplet has been carried out in this experimental study intended at investigating ethanol and 1-propanol. The experimental set-up consists of a pressure chamber in which the furnace, the droplet formation, the droplet support and motion devices are located. An alcohol droplet is located at the intersection of the cross quartz fiber (diameter of 14 µm) with a controlled initial diameter (range of 300 – 600 µm) in Nitrogen medium to allow pure vaporization and to avoid any oxidation or ignition to occur at various ambient temperatures from 298 to 973 K; the ambient pressure is maintained at atmospheric pressure; at various ambient relative humidity. When the droplet is exposed to the hot environment in the furnace, the temporal regression is recorded using a high-speed video camera with various frame rates. For each experiment set, a minimum of 700 images are recorded to allow sufficient temporal resolution and at least six experiments are performed for each test condition. The images captured by the high speed video camera are transferred to a computer and are analyzed by post-processing to deduce the droplet instanta-

neous surface area and hence its diameter temporal variation. Note that the error analysis in determining the droplet diameter is calculated to be around 3%.

The study of autoignition of ethanol, 1-propanol and blends of ethanol and water have been performed in a rapid compression machine (RCM) at a compressed pressure of 30 bar over a temperature range of 750-860 K for stoichiometric mixture of fuel and air. The thermodynamic conditions are pertinent to those encountered in internal combustion engines. The experiments have been carried out in the twin piston at NUIG RCM. The compressed gas temperature was changed by adjusted the initial temperature. Fuel-oxidiser mixtures were prepared manometrically in stainless steel tanks. In present studies, each compressed pressure and temperature condition is repeated at least three times to ensure good reproducibility. The mean and standard deviation of the ignition delay for all test runs at each condition are calculated at less than 10%, as an indication of reproducibility.

4 THEORETICAL MODEL CALCULATIONS

A requirement of comparison between experimental and theoretical vaporization rate, K and K_{th} respectively is realized in this chapter. Theoretical vaporization rate, K_{th} is calculated by two methods; the first method based on the calculation of the binary diffusion coefficient, D, and the second method based on the estimation of the thermodynamic properties.

For these two methods we determine the vaporization rate based on the equations (2-15) and (2-16) that have been discussed and derived from the Chapter 2 based on assumption of unity value of Lewis number, where the vaporization rate, K is defined as;

$$K_{th1} = 8 \cdot \frac{\rho_{Fg}}{\rho_{Fl}} \cdot D \cdot \ln(1 + B) \tag{2-15}$$

$$K_{th2} = 8 \cdot \frac{\lambda_g}{C_{pg} \cdot \rho_{Fl}} \cdot \ln(1 + B) \tag{2-16}$$

4.1 First method: calculation and estimation of binary diffusion coefficient

In this calculation of the first method, the vaporization rate is calculated from equation (2-15). We should determine all the unknown and known variables such as;

ρ_F the density of the fuel where the subscript of l and g corresponds to the state of fuel liquid and gaseous respectively

D the binary diffusion coefficient

B the Spalding transfer number

This type of calculations was inspired mostly by Chesneau (1994) and Morin (1999).

In the case of droplet vaporization, the derivation of conservation equations shows the existence of thermal transfer number B_T and mass transfer number B_M. These numbers are equal

under the assumption of quasi-steady condition. The transfer number represents the ratio of the driving force for vaporization to the resistance to vaporization.

$$B_M = \frac{Y_{Fs} - Y_{Famb}}{Y_{Fl} - Y_{Fs}} \tag{4-1}$$

and when $Y_{Famb} = 0$ and $Y_{Fl} \approx 1$, equation 4.1 becomes,

$$B_M = \frac{Y_{Fs}}{1 - Y_{Fs}} \tag{4-2}$$

$$B_T = \frac{C_{pg}}{L_v} \cdot (T_{amb} - T_s) \tag{4-3}$$

$$B_T = B_M = B \tag{4-4}$$

with Y_{Fs} the mass fraction of gaseous combustible fuel at droplet surface, C_{pg} the molar calorific capacity of gaseous mixture, L_v the molar latent heat of vaporization, T_{amb} the ambient gas temperature and T_s the droplet surface temperature.

The equality of these two numbers permits us to determine the droplet surface temperature, T_s by iterations. For all calculation, we have utilized the software of mathematical calculation, MATHCAD™.

Figure 4.1 shows the calculated droplet surface temperature T_s of ethanol and 1-propanol droplets at any given ambient temperature, T_∞. The plot shows that at any given ambient temperature, T_s of 1-propanol droplet is always higher than those of ethanol.

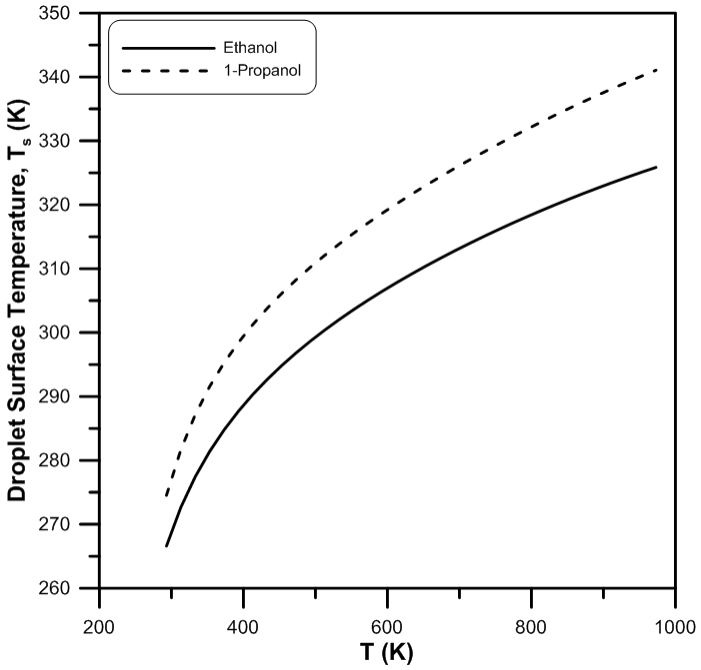

Figure 4.1: Calculated droplet surface temperature, T_s for 1-propanol and anhydrous ethanol droplets at various temperatures and P_∞ = 0.1 MPa.

4.1.1 Expression of mass transfer number, B_M

The mass transfer number is given by;

$$B_M = \frac{Y_{Fs}}{1 - Y_{Fs}} \tag{4-5}$$

or

$$B_M = \frac{P_{sat}}{P - P_{sat}} \cdot \frac{M_F}{M_O} \tag{4-6}$$

The saturated vapor pressure, P_{sat} is calculated from equation of Wagner for alcohols studies (Reid *et al*. 1987);

$$\ln\left(\frac{P_{sat}}{P_c}\right) = \frac{A \cdot x + B \cdot x^{1.5} + C \cdot x^3 + D \cdot x^6}{1 - x} \tag{4-7}$$

with $x = 1 - \frac{T_s}{T_c}$, A, B, C and D are constants for alcohols properties.

4.1.2 Expression of thermal transfer number

The thermal transfer number, B_T is given as;

$$B_T = \frac{C_{pg}}{L_v} \cdot (T_{amb} - T_s) \tag{4-8}$$

The calorific capacity is calculated according to the reference temperature, T_r as defined by Sparrow and Gregg (1958) where

$$T_r = T_s + \frac{T_{amb} - T_s}{3} \tag{4-9}$$

and it is estimated by the method of Joback (Reid *et al*. 1987) where

$$C_p = A + B \cdot T_r + C \cdot {T_r}^2 + D \cdot {T_r}^3 \tag{4-10}$$

with A, B, C and D are constants.

To calculate the latent heat of vaporization at droplet surface temperature, the Watson relationship is used (Reid *et al.* 1987);

$$L_v = L_{vTb} \cdot \left(\frac{T_c - T_s}{T_c - T_b}\right)^n \tag{4-11}$$

where *n* is defined as per relation of Viswanath and Kuloor (Rei *et al.* 1987);

$$n = \left[0.00264 \left(L_{vTb} \cdot \frac{1}{R \cdot T_b}\right) + 0.8794\right]^{10} \tag{4-12}$$

and the latent heat of vaporization at normal boiling temperature, L_{vTb} is calculated based on the method suggested by Vetere (Reid et al. 1987) and defined as;

$$L_{vTb} = R \cdot T_b \cdot \frac{0.4343 \ \ln P_c - 0.69431 + 0.89584 \cdot \frac{T_b}{T_c}}{0.37691 \ + 0.89584 \cdot \frac{T_b}{T_c} + \frac{0.15075}{P_c \cdot \left(\frac{T_b}{T_c}\right)^2}} \tag{4-13}$$

where R is the perfect gas constant, T_b is the normal boiling temperature; T_c and P_c are the critical temperature and the pressure respectively. For alcohols, the average absolute percentage of error between calculated (Vetere method) and experimental values of latent heat of vaporization at normal boiling point is estimated around 3.8% (Reid *et al.* 1987). Figure 4.2 shows the comparison of L_v between ethanol and 1-propanol in terms of various surface temperature of the droplet T_s.

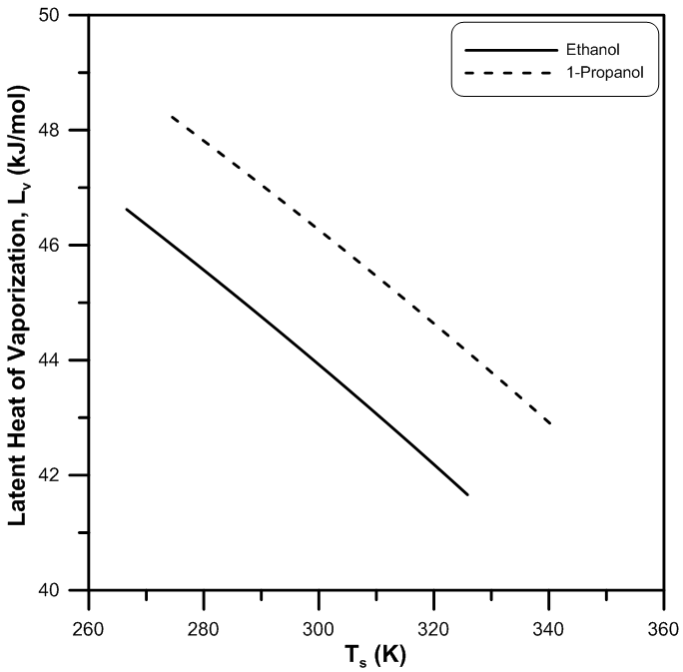

Figure 4.2: Calculated latent heat of vaporization, L_v for 1-propanol and anhydrous ethanol droplets at various droplet surface temperatures and P_∞ = 0.1 MPa.

4.1.3 Calculation of binary diffusion coefficient, D

In the case where experimental values are not available, such as ethanol-water gas diffusivity, ethanol-nitrogen gas diffusivity, and water-nitrogen gas diffusivity, the Chapman- Enskog correlation (Reid *et al*. (1987) was used to approximate the binary diffusivity coefficient of combustible fuel *F* in ambient *O*.

$$D = \frac{0.00266 \cdot {T_r}^{3/2}}{P \cdot {M_{FO}}^{1/2} \cdot {\sigma_{FO}}^2 \cdot \Omega_D} \tag{4-14}$$

where T_r is the reference temperature, P is the pressure, M is the molecular weight, σ is the characteristic length and Ω_D, the diffusion collision integral.

This equation is derived directly from the resolution of the equation of Boltzmann, indicated for diffusion in a binary system.

M_{FO} is given by the molar masses of components F and O;

$$M_{FO} = \frac{2}{\frac{1}{M_F} + \frac{1}{M_O}} \tag{4-15}$$

The diffusion collision integral, Ω_D, depends strongly on temperature and the intermolecular forces between the collided molecules. The function of Lennard-Jones potential gives a good description of the transport properties where it relies on the intermolecular energy between these two molecules, ψ and their separation distance, r;

$$\psi = 4 \cdot \varepsilon \left[\left(\frac{\sigma}{r} \right)^{12} - \left(\frac{\sigma}{r} \right)^{6} \right] \tag{4-16}$$

with ε and σ are the characteristic energy and length of Lennard-Jones respectively.

The integral collision depends on term defined as kT/ε_{AB}, with k is Boltzmann constant and is given by the relationship of Neufield (Reid *et al.* 1987);

$$\Omega_{\mathrm{D}} = \frac{\mathrm{A}}{(\mathrm{T}^*)^{\mathrm{B}}} + \frac{\mathrm{C}}{\exp(\mathrm{D}\cdot\mathrm{T}^*)} + \frac{\mathrm{E}}{\exp(\mathrm{F}\cdot\mathrm{T}^*)} + \frac{\mathrm{G}}{\exp(\mathrm{H}\cdot\mathrm{T}^*)} \tag{4-17}$$

with A, B, C, D, E, F, G, H are constants, and

$$T^* = \frac{k \cdot T_r}{\varepsilon_{FO}} \tag{4-18}$$

where *k* is Boltzmann constant.

The characteristic energy and length are defined by:

$$\varepsilon_{FO} = (\varepsilon_F \cdot \varepsilon_O)^{\frac{1}{2}} \tag{4-19}$$

and

$$\sigma_{FO} = \frac{(\sigma_F + \sigma_O)}{2} \tag{4-20}$$

The relations between ε_F, ε_O, σ_F, σ_O, and the critical parameters are used to determine the values (Hirschfelder *et al*. 1954):

$$\frac{\varepsilon}{k} = 0.77 l T_c \tag{4-21}$$

and

$$\sigma = \left(\frac{3}{2} \cdot \frac{b_0}{\pi \cdot N}\right) \tag{4-22}$$

where

$$b_0 = 18.4 \cdot \frac{T_c}{P_c} \tag{4-23}$$

and *N* is Avogadro number.

Figure 4.3 shows the calculated value of binary diffusion coefficient, *D* of ethanol and 1-propanol. The value of *D* is positive temperature dependent with ethanol is always higher than 1-propanol at all temperatures.

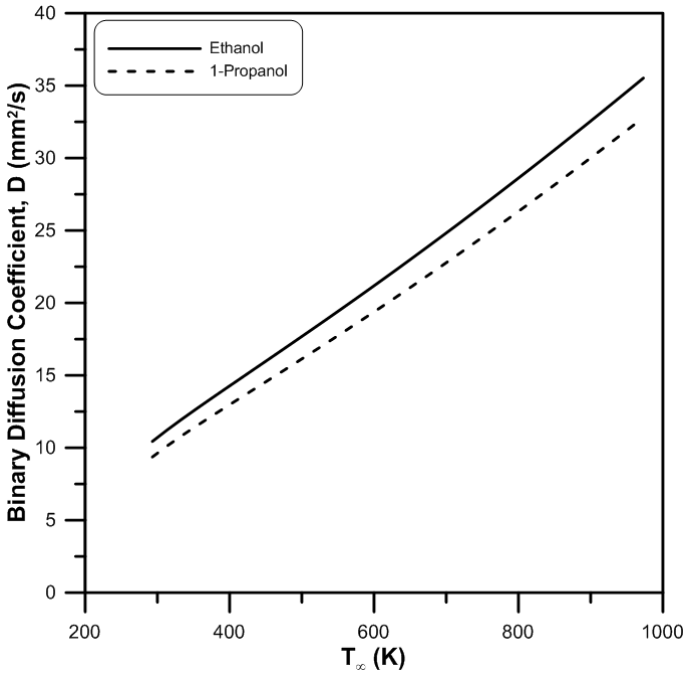

Figure 4.3: Calculated binary diffusion coefficient, *D* for 1-propanol and anhydrous ethanol droplets at various ambient temperatures and P_∞ = 0.1 MPa.

4.2 Second method: estimation of the thermodynamic properties

For the second method calculation, we determine the vaporization rate from equation (2-16),

$$K_{th2} = 8 \cdot \frac{\lambda_g}{C_{pg} \cdot \rho_{Fl}} \cdot \ln(1 + B)$$

Therefore it is imperative to calculate these followings terms;

λ_g the thermal conductivity of the gaseous mixture

C_{pg} the specific heat per unit mass of the gaseous mixture

ρ_{Fl} the volumetric mass of liquid combustible

B the Spalding transfer number

The calculation of this method is using the similar methodology than the previous first method. By the assumption of equality of mass transfer number B_M and thermal transfer number B_T, the droplet surface temperature, T_s is determined iteratively and used for the calculation of thermodynamics and transport properties of the combustible droplet. The main difference between the previous method and this method is the utilisation of the thermodynamics and transport properties of the mixtures.

4.2.1 The expression of transfer numbers, B_M and B_T

$$B_M = \frac{Y_{Fs}}{1 - Y_{Fs}} \qquad B_M = \frac{P_{sat}}{P - P_{sat}} \cdot \frac{M_F}{M_O} \tag{4-24}$$

where Y_{Fs} is defined in terms of molecular weight and pressure as;

$$Y_{Fs} = \left[1 + \left(\frac{P}{P_{sat}} - 1\right) \cdot \frac{M_O}{M_F}\right]^{-1} \tag{4-25}$$

where M_O and M_F are the molecular weight of the gaseous oxidant and liquid combustible fuel respectively. P_{sat} is defined as the saturated vapor pressure calculated at the droplet surface temperature (equation 4-8).

$$B_T = \frac{C_{pg}}{L_v} \cdot (T_{amb} - T_s)$$

with

$$L_v = L_{vTb} \cdot \left(\frac{T_c - T_s}{T_c - T_b}\right)^n$$

4.2.2 Estimation and calculation of thermodynamic and transport properties

The physical parameters in the droplet film region such as thermodynamics (C_{pg}) and transport properties (k_g) are evaluated at temperature defined as reference temperature, T_r (Hubbard *et al.* 1975; Lefebvre, 1989);

$$T_r = T_s + A_r(T_{amb} + T_s) \tag{4-26}$$

where A_r is the averaging parameter. For the one-third rule, A_r = 1/3.

To calculate the specific heat of gaseous mixture C_{pg}, one needs to calculate first the individual molar specific heat of the oxidant and the combustible fuel, represented by C_{pO} and C_{pF} respectively at reference temperature, T_r and by utilizing the method of Joback.

However, in our study we define the molar fraction of combustible fuel as;

$$x_F = \frac{P_{sat}}{P_{amb}} \tag{4-27}$$

where P_{amb} is the ambient gas pressure.

Therefore by considering the concentration of combustible fuel droplet at infinity is zero, the molar concentration of oxidant will be;

$$x_O = 1 - x_F \tag{4-28}$$

The specific heat of the gaseous mixture of combustible fuel and oxidant C_{pg}, therefore could be written off as;

$$C_{pg} = x_F \cdot C_{pF} + (1 - x_F) \cdot C_{pO} \tag{4-29}$$

And the thermal conductivity of gaseous mixture is estimated by utilizing the relation proposed by Euckan (Reid et al. 1987) for polyatomic gases;

$$\lambda_g = x_F \cdot \lambda_F + (1 - x_F) \cdot \lambda_O \tag{4-30}$$

Where

$$\lambda_F = \frac{\left(C_{pF} - R\right)}{M_F} \cdot \mu_F \left[1 + \frac{\frac{9}{4}}{\left(\frac{C_{pF}}{R}\right) - 1}\right] \tag{4-31}$$

and

$$\lambda_O = \frac{\left(C_{pO} - R\right)}{M_O} \cdot \mu_O \left[1 + \frac{\frac{9}{4}}{\left(\frac{C_{pO}}{R}\right) - 1}\right] \tag{4-32}$$

where μ_F and μ_O are the viscosities of combustible fuel and oxidant respectively and they are defined by equation proposed by Chapman-Enskog (Reid et al. 1987) as;

$$\mu_F = \frac{26.69d(M_F \cdot T_r)^{\frac{1}{2}}}{\sigma^2 \cdot \Omega_{\mathrm{D}}} \tag{4-33}$$

$$\mu_O = \frac{26.69)(M_O \cdot T_r)^{\frac{1}{2}}}{\sigma^2 \cdot \Omega_{\mathrm{D}}} \tag{4-34}$$

4.3 Comparison between the two methods

K_{th1} and K_{th2} are the theoretical vaporization rates that are calculated using two different calculations. The difference between these two methods comes from the calculation of thermodynamic and transport properties. In the second method, K_{th2} is determined by evaluating the thermodynamics properties at a reference temperature) as the first method, but also by evaluating a reference composition. Therefore, it is closer to the real case of droplet vaporization. In the first method of calculation, we use semi-empirical relationships to determine the

binary diffusion coefficient of the liquid into the mixture using the characteristic length and the diffusion collision integral of the molecules.

Droplet surface temperature, T_s and binary diffusion coefficient, D are the main factors in influencing the increase of vaporization rate of both alcohols droplets. These two factors are calculated theoretically for both 1-propanol and anhydrous ethanol and plotted against various ambient temperatures in Figure 4.1 and Figure 4.3.

As mentioned before, the increase of average vaporization rate, K is influenced by the droplet surface temperature and binary diffusion. From the theoretical calculation, it demonstrates that as the temperature increases, both droplet surface temperature T_s and the binary diffusion D, for both 1-propanol and anhydrous ethanol droplets also increase accordingly (Figure 4.1 and Figure 4.3). The value of the binary diffusion D is higher for anhydrous ethanol at all temperatures. On contrary, 1-propanol droplet surface temperature T_s is higher than anhydrous ethanol at all temperatures.

Figure 4.4 and Figure 4.5 show the measured experimental and calculated theoretical average vaporization rate of anhydrous ethanol and 1-propanol droplets respectively. At a temperature T_∞ lower to 473 K, the value of the average vaporization K of anhydrous ethanol droplet is higher than that of 1-propanol. Nevertheless, as the temperature increases beyond this limit, the average vaporization rate of 1-propanol droplet is superior to anhydrous ethanol. By the presentation of both K_{th} and K values for both alcohols, one can conclude that for temperature T_∞ lower than 473 K, the average vaporization rate of both alcohols is mainly influenced by the diffusion factor and at T_∞ higher to 473 K, the droplet surface temperature, T_s is more dominant in increasing the average vaporization rate, K compared to the binary diffusion coefficient.

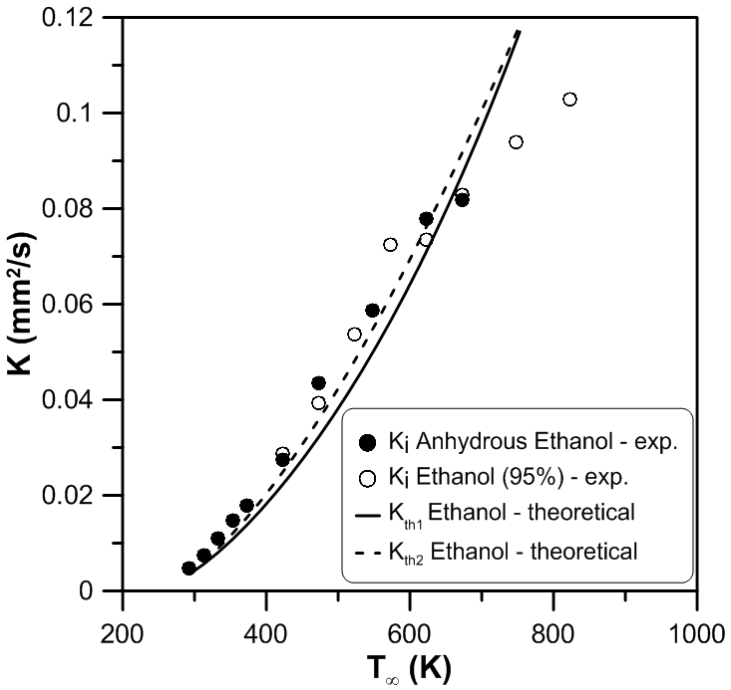

Figure 4.4: Theoretical and experimental average vaporization rates, K_{th} and K for ethanol droplet at various temperatures and P_{∞} = 0.1 MPa.

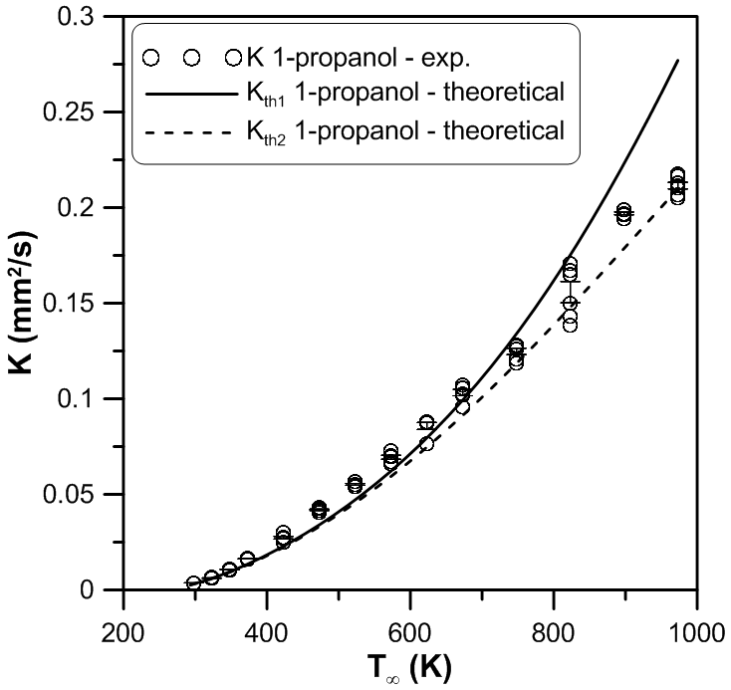

Figure 4.5: Theoretical and experimental average vaporization rates, K_{th} and K for 1-propanol droplet at various temperatures and P_{∞} = 0.1 MPa.

4.4 Estimation and calculation of Grashof , Prandlt, Schmidt and Lewis Numbers

From the theoretical calculation, a number of dimensionless properties could also be calculated. The Grashof number is defined in terms of surface droplet temperature and other thermodynamics properties by (Ebrahimian and Habchi (2011) :

$$Gr = g \cdot {d_0}^3 \cdot \frac{(T_{amb} - T_s) \cdot \left(\rho_g\right)^2}{(\mu_O)^2 \cdot T_{amb}} \tag{4-35}$$

with g the gravitational acceleration, ρ_g is the volumetric mass of ambient gas, T_{amb} the gas ambient temperature, T_s the droplet surface temperature, μ_O the dynamic viscosity of ambient gas, d_o is the droplet initial diameter, The volumetric mass and the dynamic viscosity are determined by the reference temperature.

Grashof number is calculated and estimated to determine the effect of buoyancy on the droplet vaporization. Figure 4.6 shows the variation of Grashof number with ambient temperature, T_∞. At lower temperature range (T_∞ < 373 K), the Gr number is increased with T_∞, however it is then negatively dependent at higher T_∞ range.

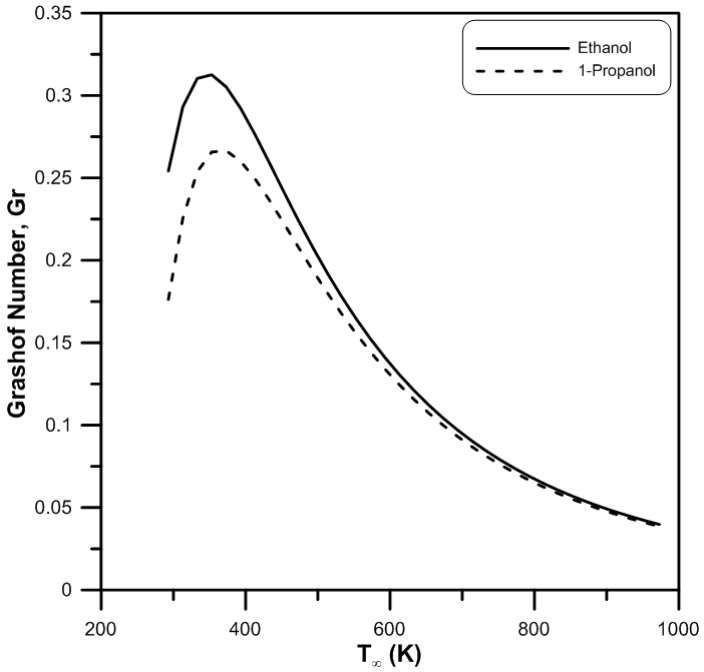

Figure 4.6: Evolution of Grashof number in function of temperature for ethanol and 1-propanol droplets vaporized in N_2 ambient at various temperatures and P_∞ = 0.1 MPa.

Meanwhile, the Prandtl number could be defined as:

$$Pr = \frac{\mu_g \cdot C_{pg}}{\lambda_g} \tag{4-36}$$

where the specific heat and thermal conductivity of gaseous mixture are estimated by the reference composition and the temperature according to equation (4-25).

In order to calculate the Lewis number, a dimensionless Schmidt number could be defined as:

$$Sc = \frac{\mu_g}{\rho_g \cdot D} \tag{4-37}$$

where μ_g the viscosity and ρ_g the density of gaseous mixture and D the binary diffusion coefficient of fuel-oxidant.

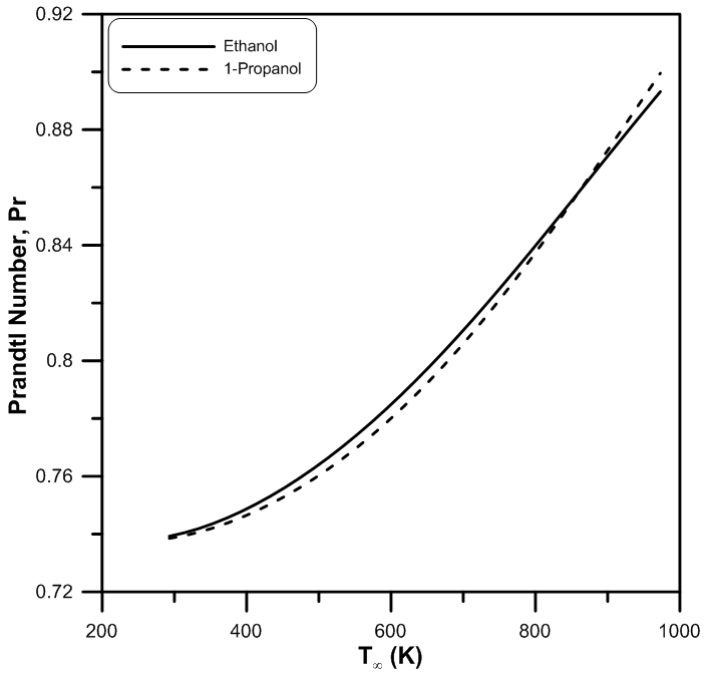

Figure 4.7: Evolution of Prandtl number in function of temperature for ethanol and 1-propanol droplets vaporized in N_2 ambient at various temperatures and P_∞ = 0.1 MPa.

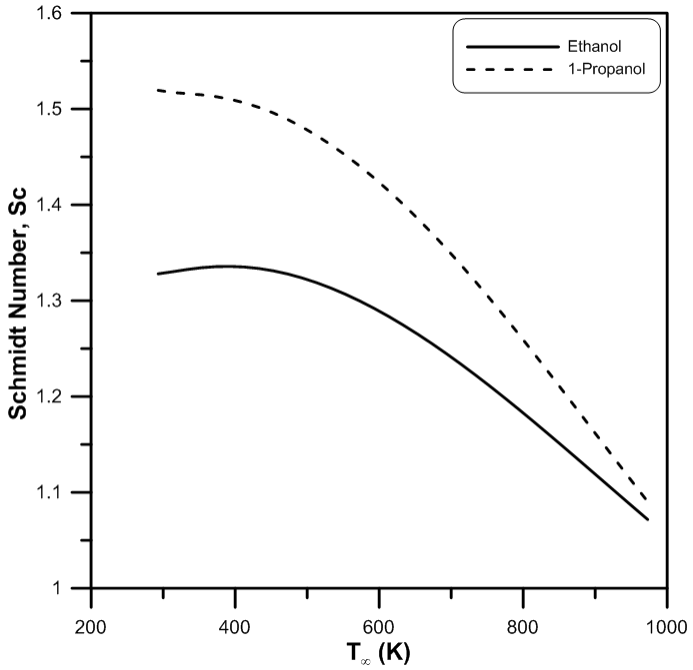

Figure 4.8: Evolution of Schmidt number in function of temperature for ethanol and 1-propanol droplets vaporized in N_2 ambient at various temperatures and P_∞ = 0.1 MPa.

One of the major assumptions applied in 'Quasi-Steady' model utilised in this study is that the properties of transport in gas phase are always constant. Such properties are thermal conductivity and molar specific heat. Therefore, the Lewis number must be equal to unity. In other words, the thermal diffusivity will always equal the mass diffusivity. The Lewis number is defined as:

$$Le = \frac{\lambda_g}{\rho_g \cdot C_{pg} \cdot D} \tag{4-38}$$

where the thermal conductivity λ_g, the density ρ_g and the specific heat C_{pg} of the gaseous mixture are estimated and calculated based on the reference temperature and composition and D the binary diffusion coefficient.

Lewis number could also be calculated directly from the correlation of Schmidt and Prandlt numbers:

$$Le = \frac{Sc}{Pr} \tag{4-39}$$

In our case of ethanol and 1-propanol fuels vaporization, the calculations of the Lewis number (Figure 4.9) show that the values are not unity (the Lewis number varies between 1 and 2). At lower temperature 1-propanol fuel seems to have higher value of Lewis number compared to ethanol fuel. Nevertheless, the Lewis number seems to converge to unity for both alcohols as the ambient temperature increases, therefore they are in almost agreement with the principal assumption of quasi-steady theory.

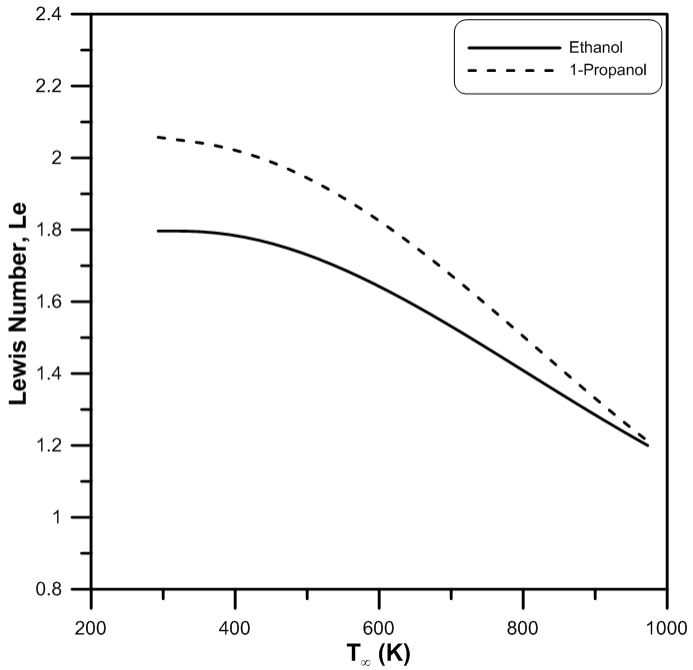

Figure 4.9: Evolution of Lewis number in function of ambient temperature for ethanol and 1-propanol droplets vaporized in N_2 ambient at various temperatures and P_∞ = 0.1 MPa.

4.5 Conclusions

Theoretical calculation of average vaporization rate for both anhydrous ethanol and 1-propanol droplets have been realized in this chapter. The theoretical calculations are based on the concept of 'quasi-steady' where the assumptions as explained in chapter 2 are applied. Two different methods; one is based on the functionality and influence of binary diffusion coefficient D and the other is determined by evaluating the thermodynamics properties at a reference temperature and also at reference composition. The comparison of experimental average vaporization rate, K for both alcohols with these theoretical calculated vaporization rates, K_{th1} and K_{th2} is in a very good agreement. Various dimensionless numbers are calculated to determine the influence of buoyancy (Gr Number) and the assumption of 'quasi-steadiness' (Le number).

5 RESULTS AND DISCUSSIONS

5.1 Ethanol and Anhydrous Ethanol

5.1.1 Average Vaporization Rate

Average vaporization rate from the experiments is calculated by a linear least-square fit in the quasi steady zone of the d^2 curves. However in the case of both ethanol (95%) and anhydrous ethanol, the apparent 'quasi-steady' period occurs two times throughout the droplet lifetime (Figure 5.1). The normalized temporal evolutions of squared-diameter, d^2 against time of anhydrous ethanol and ethanol 95% droplets, at various ambient temperatures are shown in Figure 5.2 and 5.3 respectively. In these experiments, the so-called 'quasi-steady' period for both ethanol (95%) and anhydrous ethanol occurs two times throughout the droplet lifetime. Average vaporization rates are deduced from the d²-curves presenting two parts: the first linear part allows in determining a first average vaporization rate called hereafter "initial vaporization rate K_i", and the second linear part a second average vaporization rate called "final vaporization rate K_f". Both Figures 5.2 and 5.3 show few common features, the d^2/d_0^2 versus t/d_0^2 curves for all temperatures are deviated from the d^2-law. The initial average vaporization rate, K_i ceases to be constant at a certain point through the droplet life. For ethanol (95%) the deviation from the linear part occurs at mid stage of the vaporization of the droplet (and $d^2/d_0^2 < 0.4$) whereas for anhydrous ethanol, the deviation only starts towards the end of the droplet life (and $d^2/d_0^2 < 0.2$). When the droplets are formed in a closed chamber filled with nitrogen gas, one prevents the combustion of the droplets and excludes the effect of ambient moisture on the evaporation process. Even so, there is still some humidity in the chamber (leak, wall adsorption…). This could explain why even anhydrous ethanol produces a non-linear d^2-law.

Note that these figures do not exhibit the droplet heat-up periods for the reason that during this period of the droplet lifetime, the droplet is moved from the so-called 'cold chamber' to the furnace. This movement is accompanied by vibrations and subsequently induces oscillations. It was decided then to show the evolution of surface area of the vaporized droplet only when the droplet was stabilized.

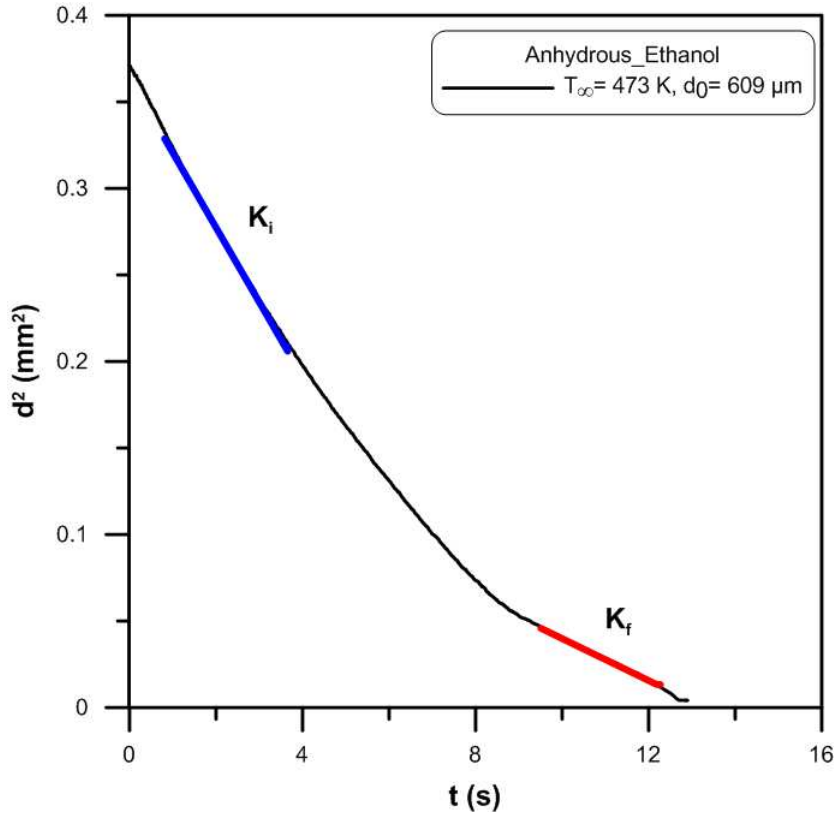

Figure 5.1: Definition and calculation of initial average initial, K_i and final vaporization rates, K_f from the d^2 *(t)* curve for anhydrous ethanol droplet; T_∞= 473 K and P_∞=0.1 MPa. K_i and K_f are calculated from the blue and red part respectively.

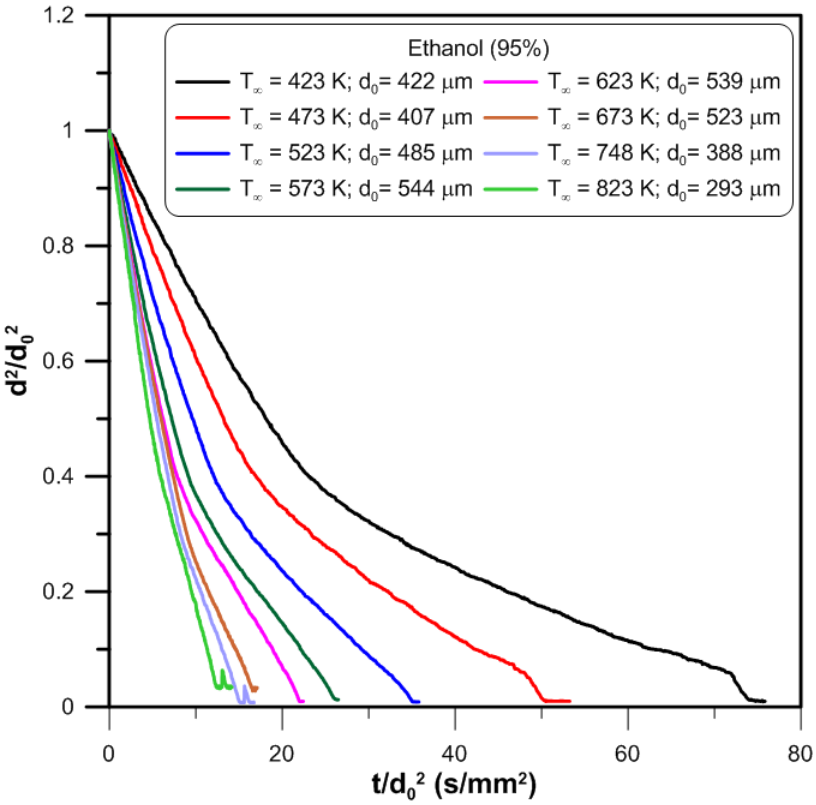

Figure 5.2: Normalized squared-diameter curves for ethanol (95%) at different temperatures; P_{∞}=0.1 MPa.

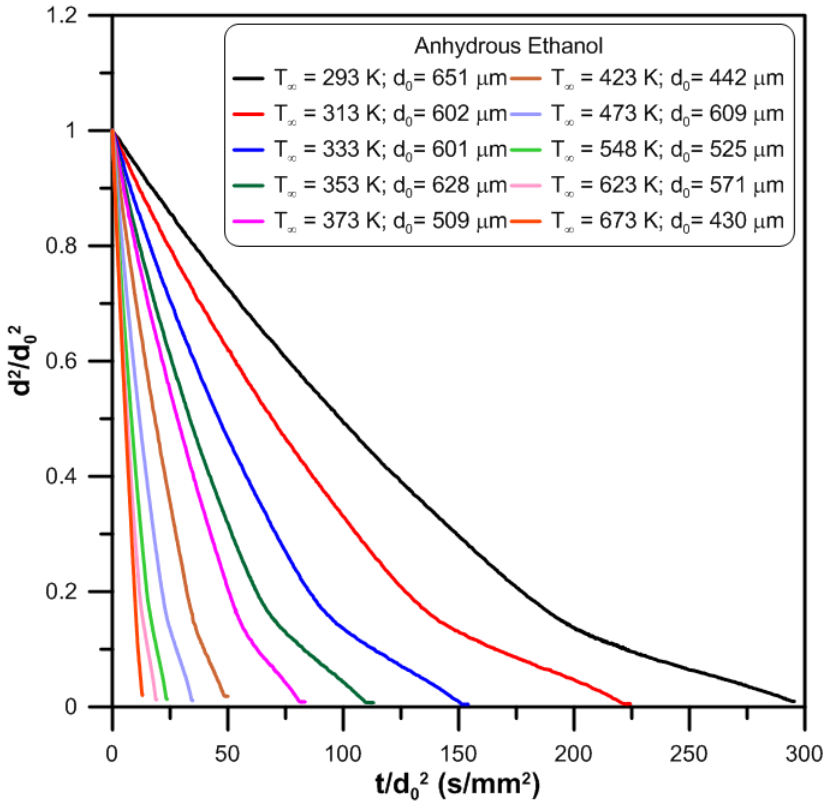

Figure 5.3: Normalized squared-diameter curves for anhydrous ethanol at different temperatures; P_{∞}=0.1 MPa.

The different values in initial water concentration in both ethanol forms are also affecting the droplet lifetime. With greater initial water concentration, the droplet lifetime is significantly prolonged (+30%) as shown in Figures 5.4 and 5.5.

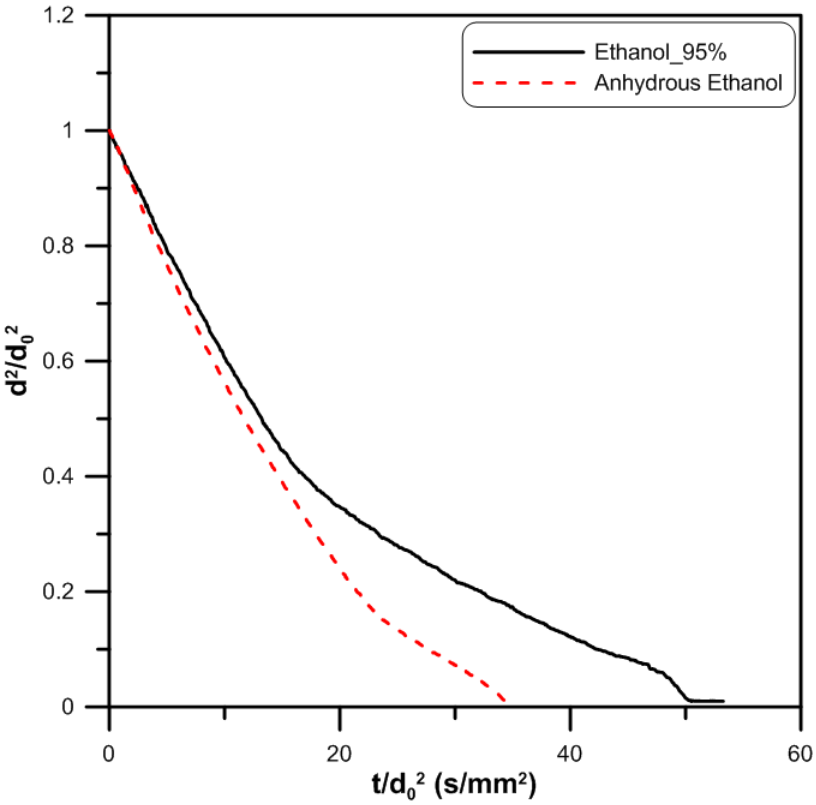

Figure 5.4: Normalized squared-diameter curves for ethanol (95%) and anhydrous ethanol at temperature, T_{∞}= 473 K and; P_{∞}=0.1 MPa.

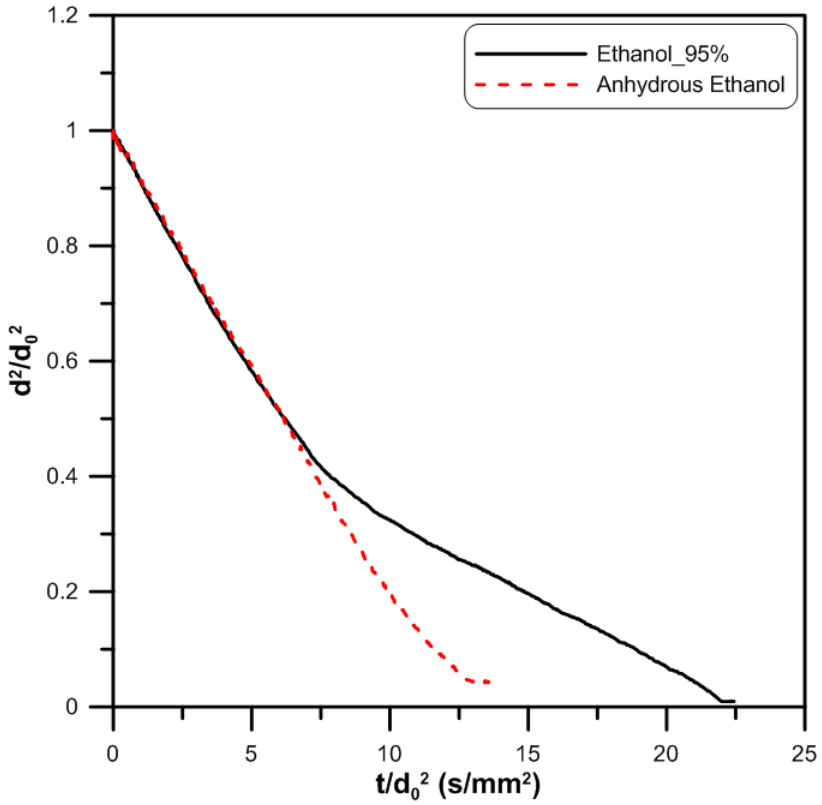

Figure 5.5: Normalized squared-diameter curves for ethanol (95%) and anhydrous ethanol at temperature, T_∞= 673 K and; P_∞=0.1 MPa.

As shown in Figure 5.6, the average vaporization rates, K_i calculated from the first linear part of the d^2 curves are similar for both ethanol forms. Therefore it shall be noted that the first linear part of d^2 curves for both ethanol (95%) and anhydrous ethanol may entirely and totally consist only of ethanol vaporization. Ethanol is the major component evaporating at this first stage as it has lower boiling temperature than water.

Meanwhile, a second 'linear' part of the d^2-curves could be observed towards the end of the curve for all temperatures of anhydrous ethanol vaporization. We define previously that the gradient at this period as a final vaporization rate, K_f. For the calculation of the final average vaporization rate, K_f, a comparison is made with the theoretical calculation of water vaporization rate. The theoretical water vaporization rate, $K_{th1}H_20$ and $K_{th2}H_20$ are calculated based on

the ‘quasi-steady’ model of equations 4-1 and 4-2. As observed in Figure 5.6, the evolution of K_f for anhydrous ethanol is in a very good agreement with the theoretical water vaporization rate, $K_{th1}H_20$. This comparison is important as to correlate the ‘deviation’ of the anhydrous droplet from the quasi-steady of the d^2-law to the fact that it is entirely due to the disturbance and interference of water vapour from ambient in the vaporization behaviour of anhydrous ethanol.

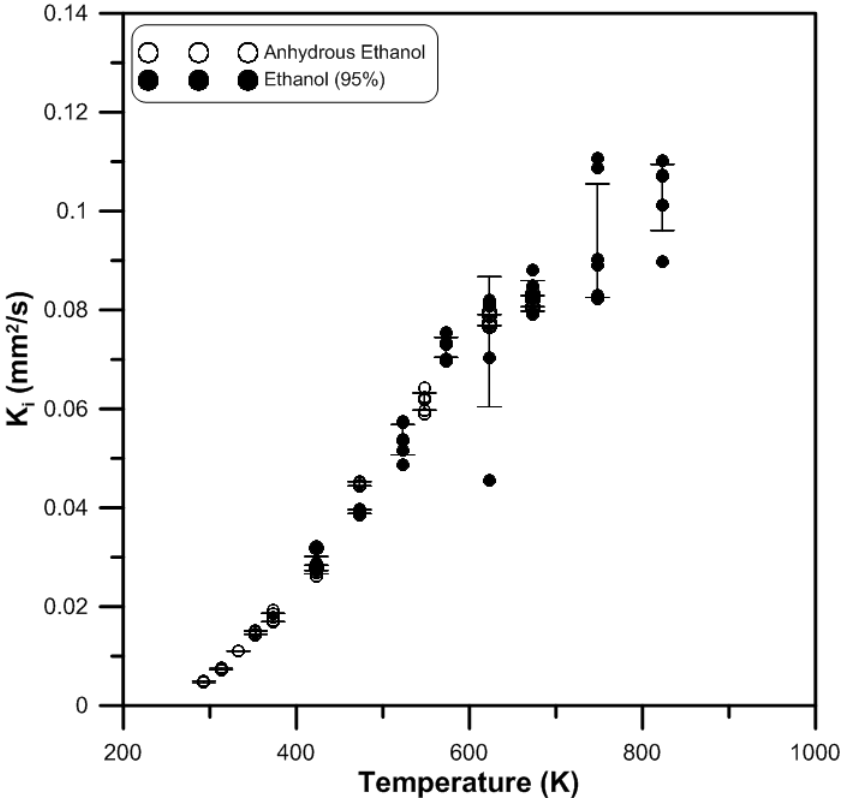

(a)

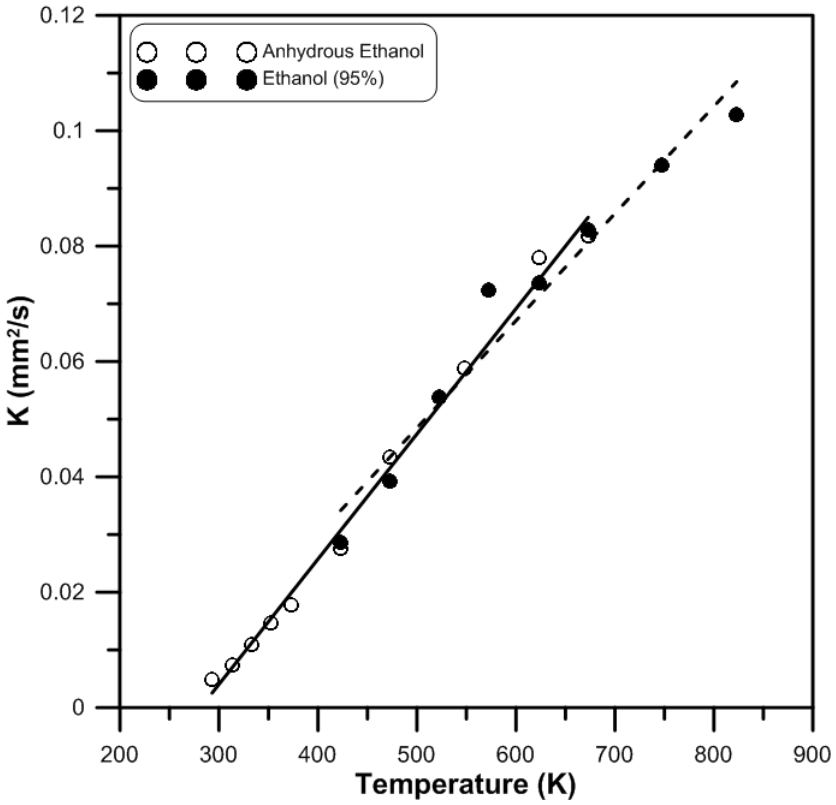

(b)

Figure 5.6: Average vaporization rates K_i for anhydrous ethanol and ethanol (95%) at different temperatures. K_i is calculated from the first linear part of the d^2-curves; (a) all tests and (b) average value.

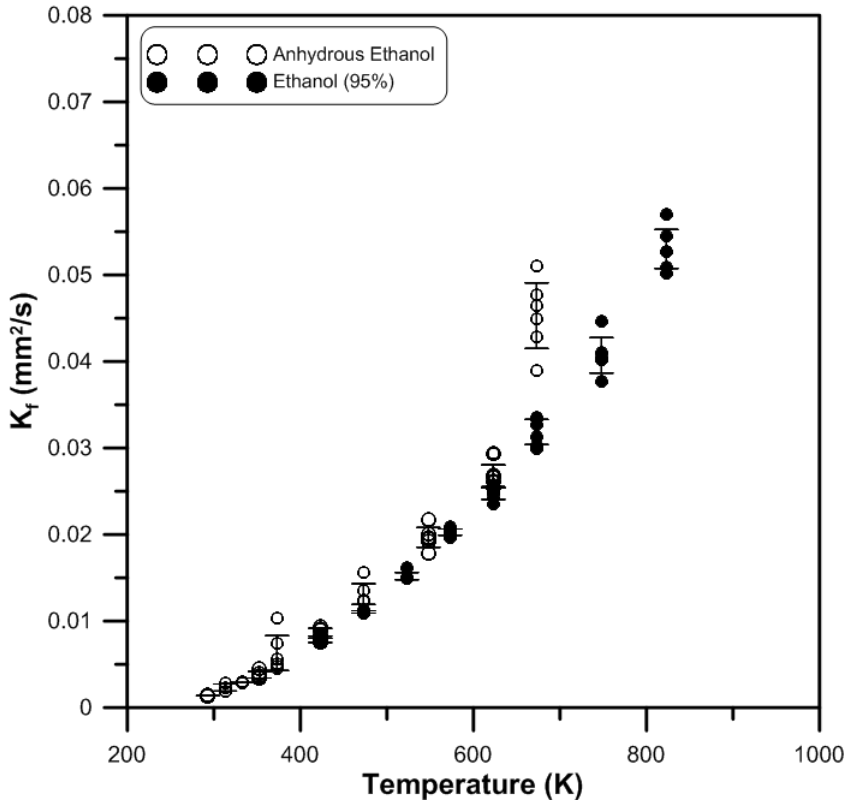

Figure 5.7: Average vaporization rates calculated during second linear part of the d^2 curves for ethanol (95%), anhydrous ethanol, K_f.

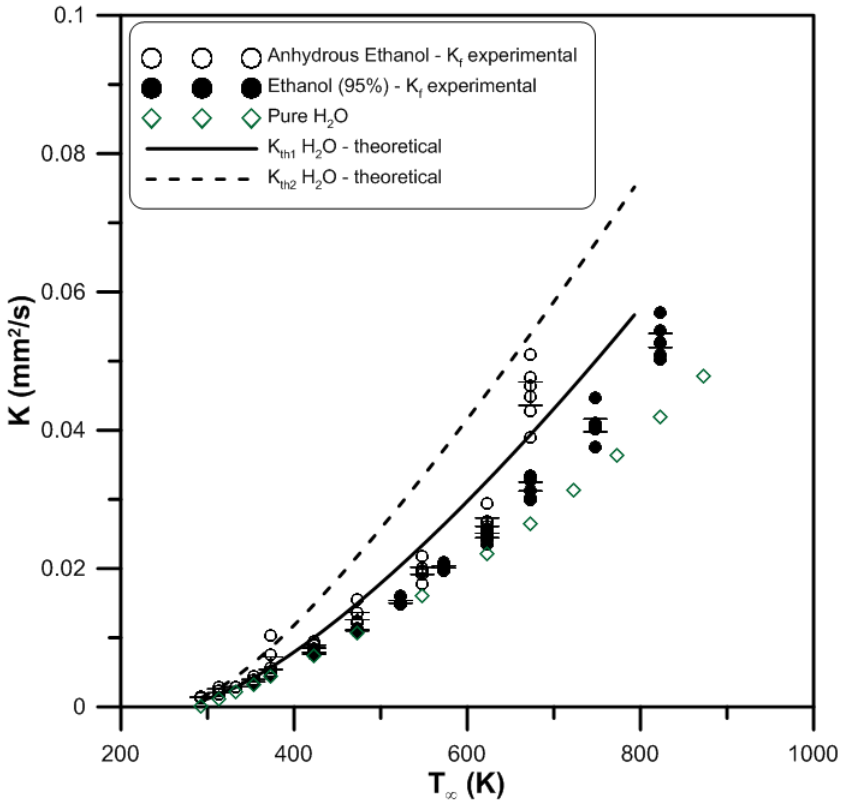
Anhydrous Ethanol - K_f experimental
Ethanol (95%) - K_f experimental
Pure H2O
K_th1 H2O - theoretical
K_th2 H2O - theoretical
K (mm²/s)
T∞ (K)
0.1
0.08
0.06
0.04
0.02
0
200
400
600
800
1000

(a)

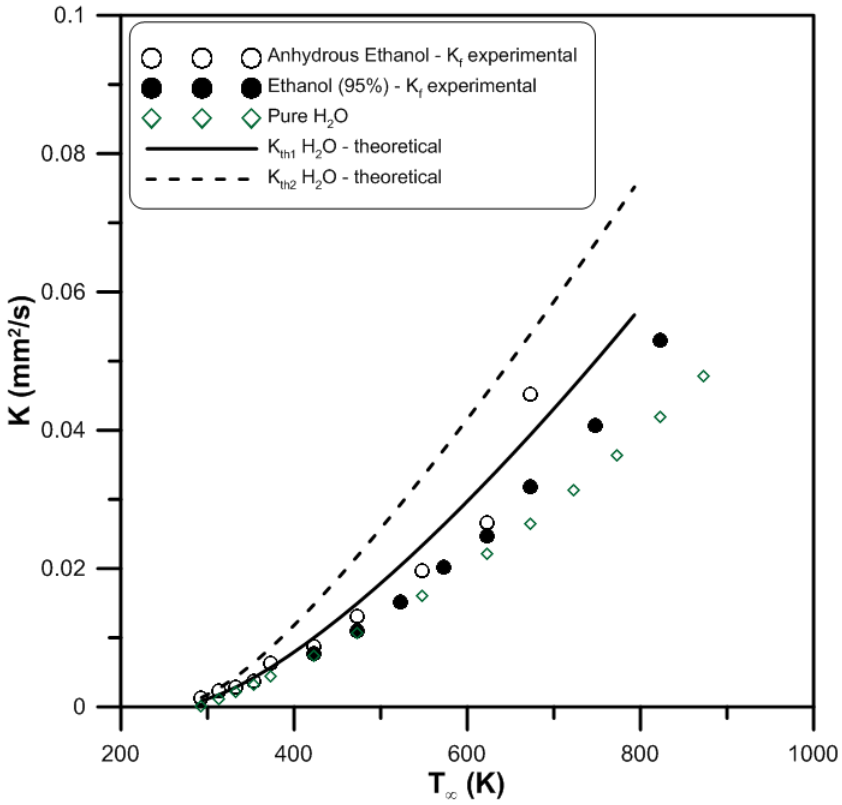

(b)

Figure 5.8: Theoretical and experimental average vaporization rates of the second part of the d²-curves for ethanol (95%) and anhydrous ethanol (noted K_f) and the theoretical average vaporization rates calculated for water droplets (noted K_{thH20}) at various temperatures and P_∞ = 0.1 MPa; (a) all tests and (b) average value.

5.1.2 Instantaneous Vaporization Rate

The instantaneous vaporization rate, K_{inst}, is calculated from the d^2-curves by determining the derivative of these curves. According to Law et al. (1987), the derivative of the d^2 *(t)* will give the instantaneous vaporization rate,

$$K_{inst} = -\frac{d}{dt}\left[d^2(t)\right] \tag{5-1}$$

In order to avoid errors in the calculation of the derivative, a smoothing is carried out on the d^2 (t) curves by using a FFT (Fast Fourier Transfer) low-pass filter. This method removes only the high frequency components with a parabolic window (Origin® function). Then the derivative is calculated on this smoothed curve.

Figure 5.9 and Figure 5.10 show the original d^2 (t) curve and their corresponding instantaneous vaporization rate, K_{inst} versus time for both ethanol (95%) and anhydrous ethanol. It is clearly observed, that in both cases the instantaneous vaporization rate, K_{inst} is significantly unsteady for the initial part corresponding to the ethanol vaporisation period, K_i. The second period, K_f, attributed to the water vaporization is almost quasi steady. In order to illustrate that, the equivalent average value of K_{inst} is plotted in Figures 5.9 and 5.10, corresponding to the vaporizing rate K_i and K_f respectively. That shows that although it is easy to determine a linear trend on the d^2 (t) curve, the unsteadiness of the phenomenon is clearly revealed by the evolution of K_{inst} according to time. This evolution is certainly due to the interference of water concentration on the ethanol droplet vaporization and also to the water condensation from the ambient moisture, due to the temperature decrease at droplet surface.

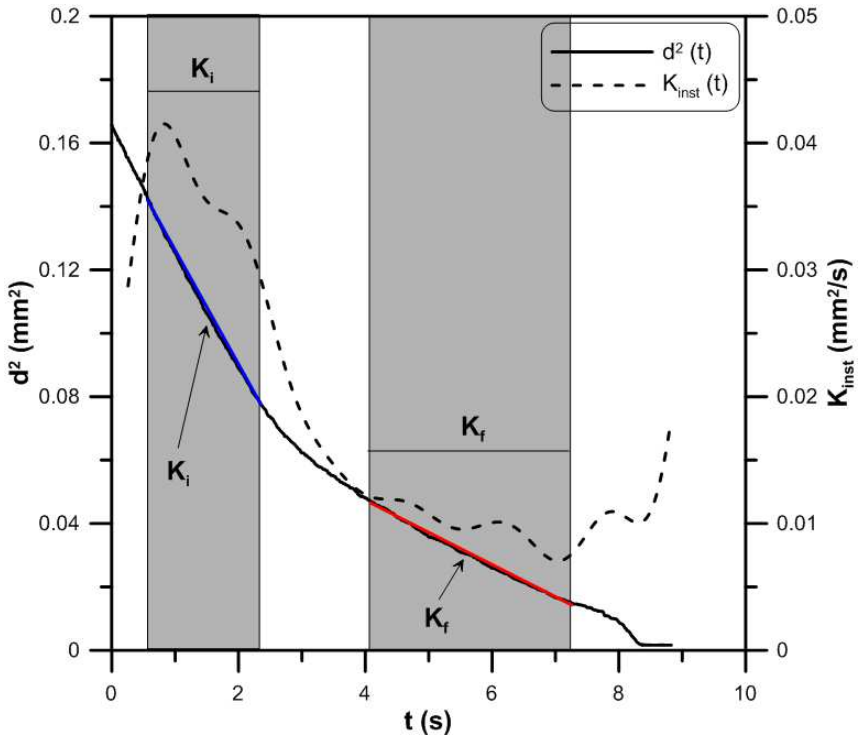
0.2
0.16
0.12
0.08
0.04
0
0.05
0.04
0.03
0.02
0.01
0
0
2
4
6
8
10
t (s)
d² (mm²)
K_inst (mm²/s)
d² (t)
K_inst (t)
K_i
K_f
K_i
K_f

(a)

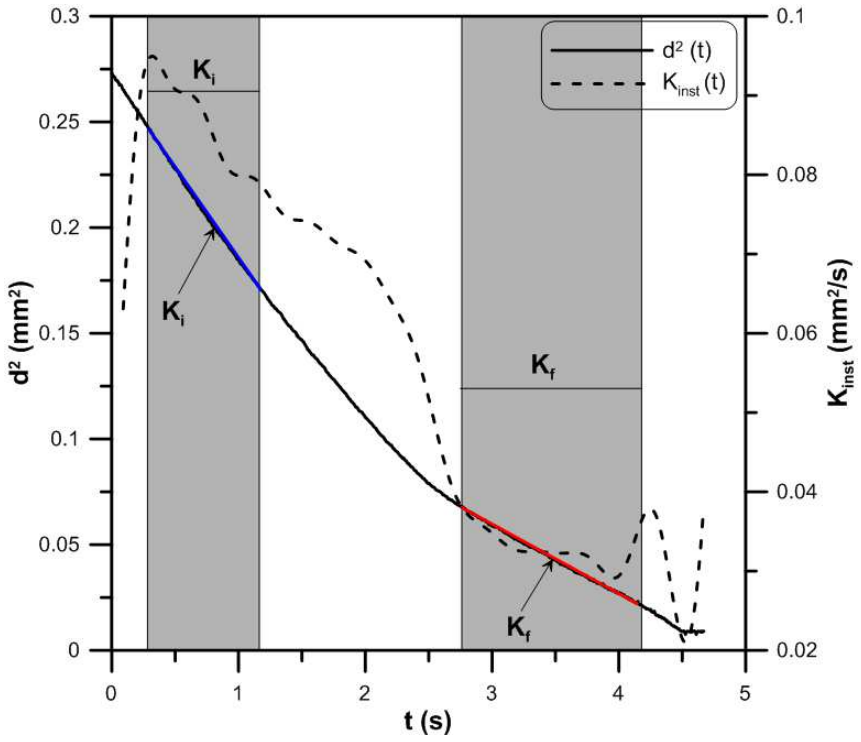

(b)

Figure 5.9: Evolution of the instantaneous vaporization rate, K_{inst} *(t)* and the squared droplet diameter for ethanol (95%) droplet at (a) T∞= 473 K (d0 = 407 μm) and (b) T∞= 673 K (d0 = 523 μm); P∞= 0.1 MPa.

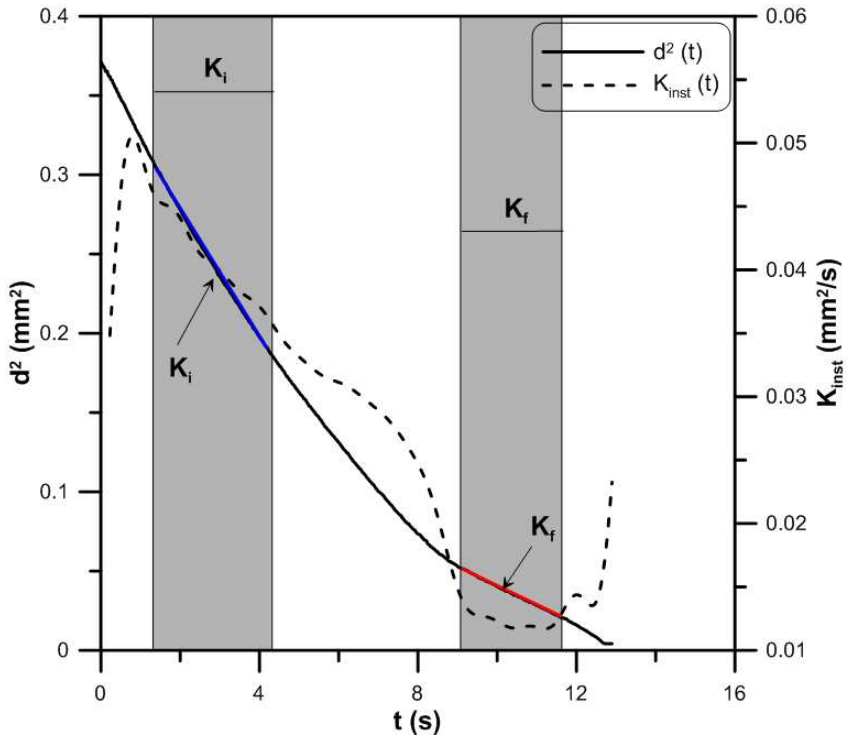
0.4
0.3
0.2
0.1
0
0.06
0.05
0.04
0.03
0.02
0.01
0
4
8
12
16
t (s)
d² (mm²)
K_inst (mm²/s)
d² (t)
K_inst (t)
K_i
K_i
K_f
K_f

(a)

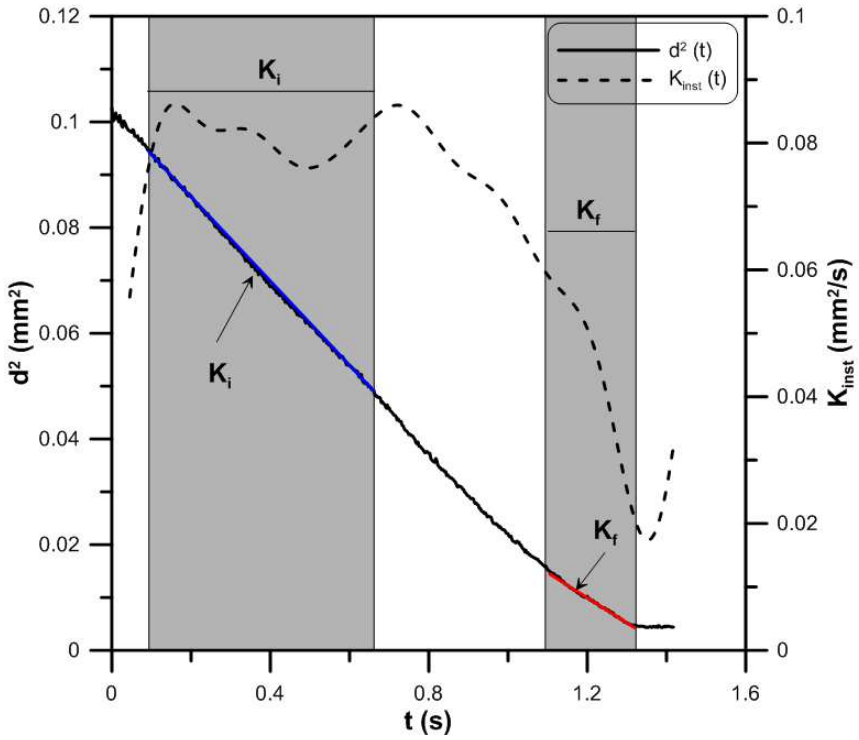

(b)

Figure 5.10: Evolution of the instantaneous vaporization rate, K_{inst} *(t)* and the squared droplet diameter for anhydrous ethanol droplet at (a) T_∞= 473 K (d_0 = 609 μm) and (b) T_∞= 673 K (d_0 = 320 μm); P_∞= 0.1 MPa.

In order to compare these evolutions for different temperatures, a normalization of these curves has been conducted. The time has been normalized by the droplet total vaporization time t_{vap}. Figures 5.11 and 5.12 show the variation of normalized instantaneous vaporization rate, K_{inst} for both ethanol (95%) and anhydrous ethanol against the time normalized by t_{vap}. It is observed that by considering normalized time by t_{vap}, the instantaneous vaporization rate, K_{inst} presents the two domains, previously described, ethanol vaporization first and then the water vaporization. In this figure one can observe that the first part of the vaporization process occurs mainly at 1/3 of the total vaporization time for the ethanol (95%), even though this occurs around at 70% of the total vaporization time for the anhydrous ethanol.

Nevertheless, one can observe in Figure 5.13, that the instantaneous vaporization rate for the anhydrous ethanol is always higher than the ethanol (95%) for the initial part of the total vaporization time, corresponding to the K_i. This can be explained by the fact that for the calculation of a mean vaporization rate the variation of instant vaporization rates is divided by a time period. For the anhydrous form the time period considered is longer thus compensating the systematic higher values observed for instant vaporization rates and therefore making mean values equivalent to (95%) form.

Another interesting observation that could be made from Figure 5.13 is the behaviour of anhydrous ethanol at temperature 673 K where the K_{inst} is always almost a constant, 'quasi-steady' and equal to K_i throughout droplet lifetime. The disappearance of ethanol component only occurs at the end of the lifetime, as underlined also by Marchese and Dryer (1996). It seems that at this higher temperature anhydrous ethanol behaves as a single component without or with slight water concentration interference.

Morin (2000) had studied the vaporization of n-alkanes droplet. The results showed that the instantaneous vaporization rate increases with time. However, for alcohol fuels such as ethanol and 1-propanol as in our current studies show the opposite results. The K_{inst} decreases with time. The nature of alcohols which is miscible with water has changed the overall process of vaporization.

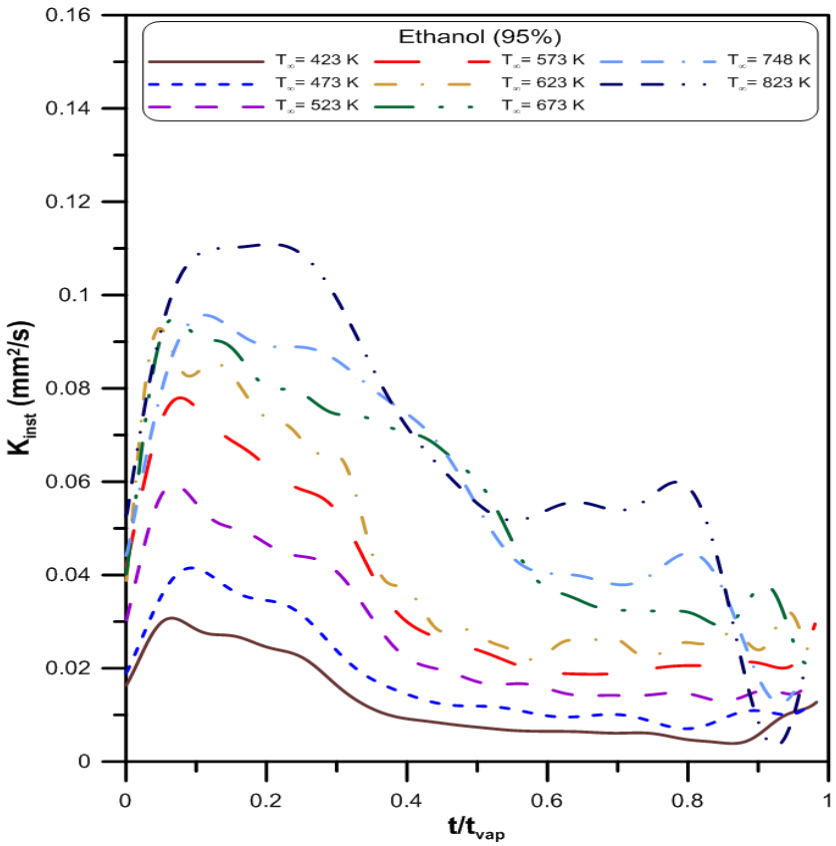

Figure 5.11: Comparison of the instantaneous vaporization rate, K_{inst} *(t)* of ethanol (95%) droplet at various temperatures; P_{∞}=0.1MPa

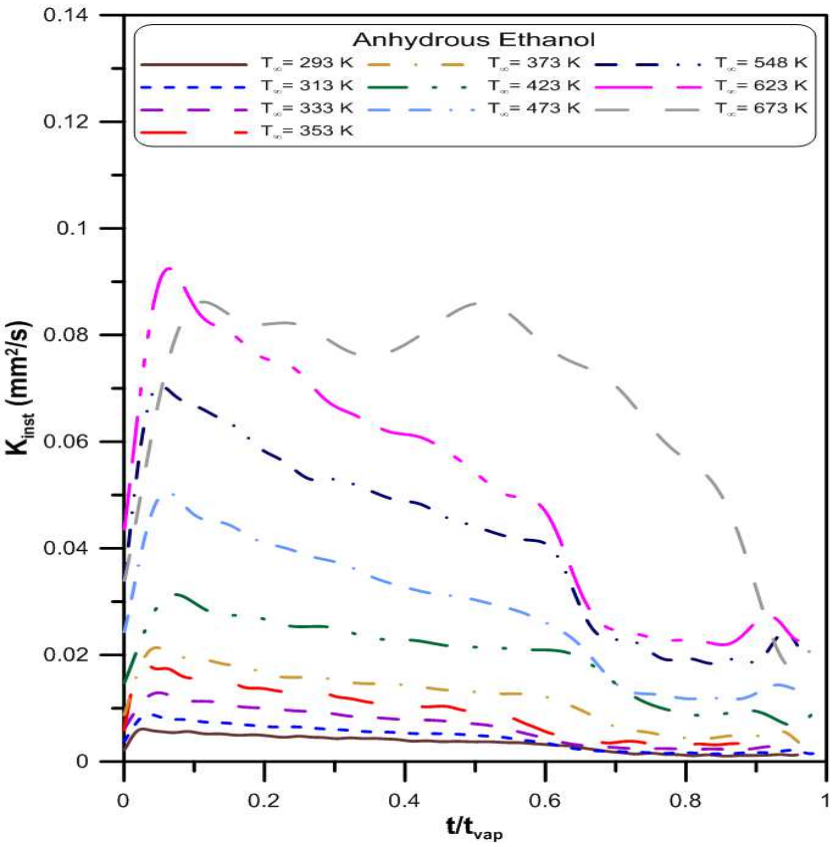

Figure 5.12: Comparison of the instantaneous vaporization rate, K_{inst} *(t)* of anhydrous ethanol droplet at various temperatures; P_{∞}=0.1MPa

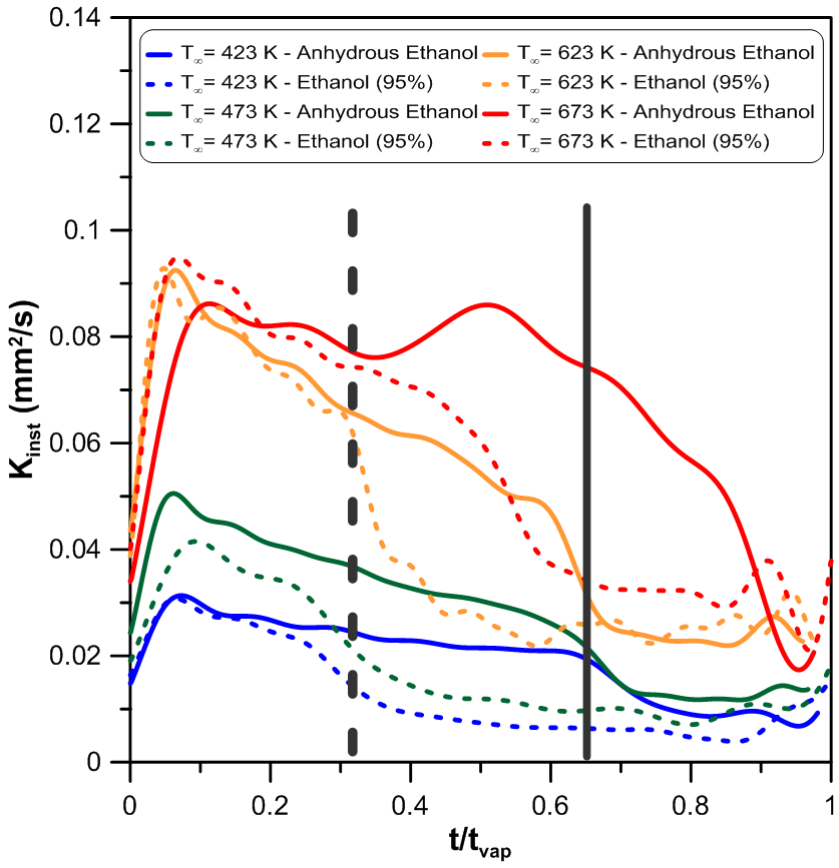

Figure 5.13: Comparison of the instantaneous vaporization rate, K_{inst} *(t)* of anhydrous ethanol and ethanol (95%) droplets at various temperatures; P_{∞}=0.1MPa

5.1.3 Influence of Water Vapour on Ethanol Vaporization

To further substantiate the effect of environment water content on ethanol droplet vaporization under different temperatures, calculations of estimated water inside the droplet has been carried out (Saharin *et al*., 2012). One of the possible approaches is to estimate the initial diameter of the droplet from the second linear part of the vaporization called afterwards "the condensed water" droplet, from the existing d^2/d_0^2 against t/d_0^2 curve. By identifying the inception point where the start of constant K_f is attained, a horizontal extrapolation will give the equivalent value of d^2/d_0^2 (Figure 5.14). Therefore, as the value of d_0 is known, the squared diameter of the water droplet d^2 is determined. Figure 5.15 shows the volume per-

centage of condensed water for anhydrous ethanol. The volume percentage of measured condensed water is almost constant at all temperature for anhydrous ethanol (approximately 3-6 %), and as the initial water content in anhydrous ethanol is low at value less than 0.4%, therefore it verifies that the water vaporization observed for anhydrous ethanol is caused by ambient constant relative humidity.

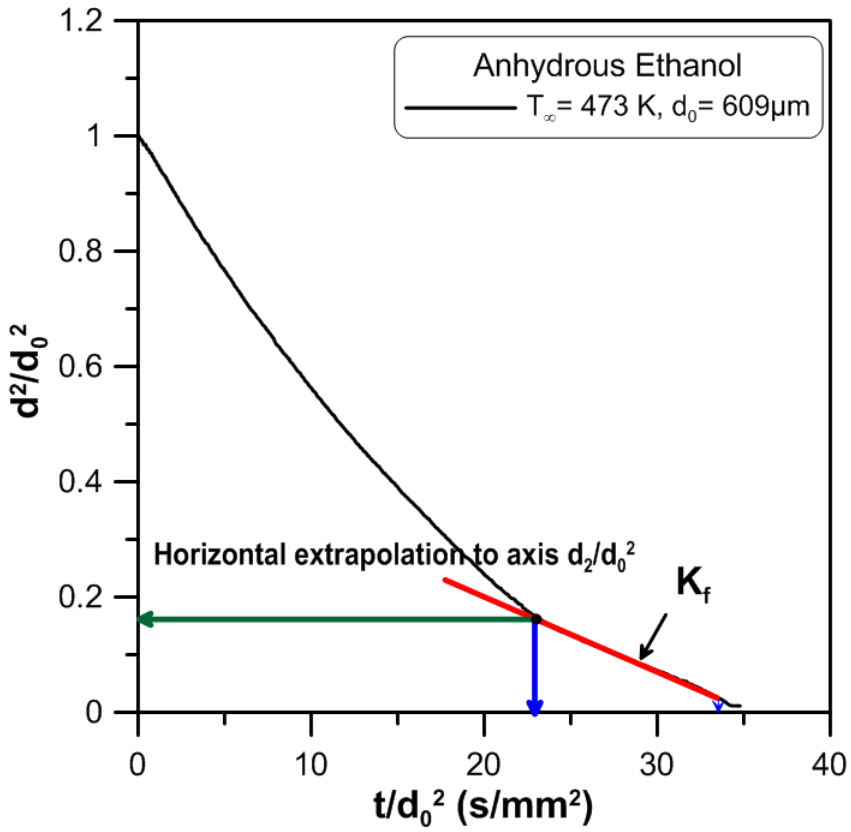

Figure 5.14: Example of determination of water diameter in the droplet from d^2 *(t)* curves for anhydrous ethanol at 473K.

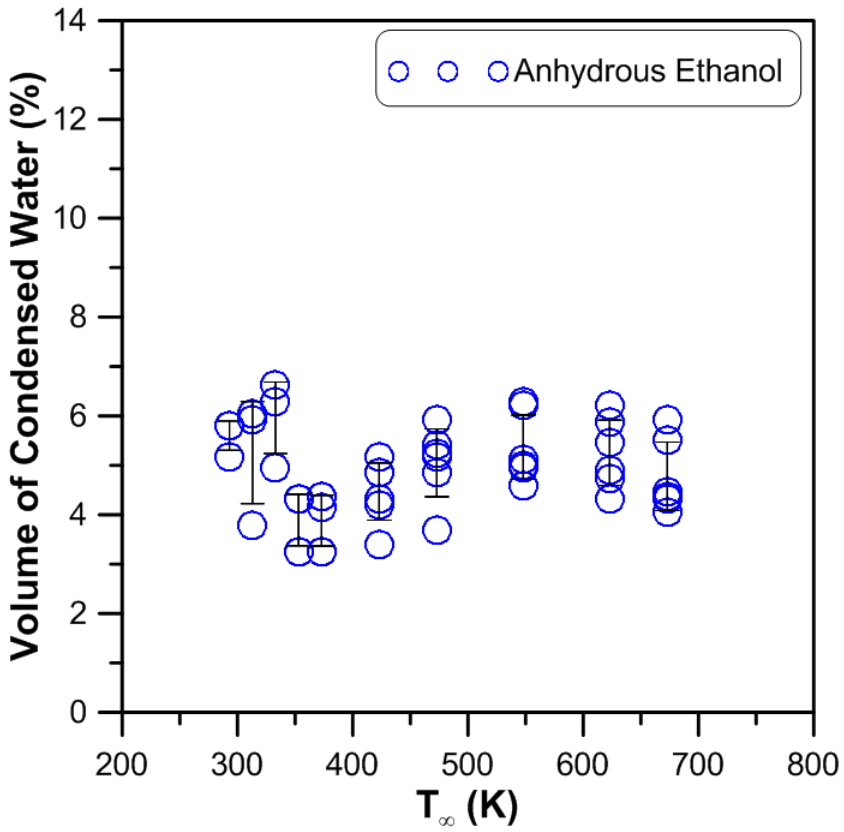

Figure 5.15: Volume percentage of condensed water at different temperatures for anhydrous ethanol droplets.

Zang and Williams (1996) studied the combustion of spherical alcohol droplets under microgravity conditions by theoretical analyses. They explained the water dissolution phenomena. The same observation arises from Marchese and Dryer (1996) on methanol droplet combustion where the d^2 curve deviated significantly from the d^2-law predictions. This behaviour is a result of the absorption of combustion intermediates and products. Water is one of the main combustion products and it produces non-linear d^2-law behaviour. During the alcohol droplet combustion, water first diffuses back to the droplet, and it is then absorbed during the first half of the burning history. Then, the water gradually builds up inside the liquid and during the second half of the combustion history, vaporizes along with alcohol. Lee and Law (1992) reported the vaporization and combustion of freely-falling methanol and ethanol drop-

lets in dry and humid environments. They demonstrated that water vapour, either from the ambience or generated at the flame, can freely condense at the droplet surface and subsequently dissolve into the droplet interior. Cho *et al.* (1991) did the same observations earlier. As mentioned and fully described by Law *et al*. (1987) one can assume that the same phenomena can occur for the vaporization phenomenon alone. During the initial fuel vaporization, the surrounding water vapour condenses at the droplet surface. Then the condensed water further diffuses into the droplet interior because of its miscibility with ethanol. Since the present vaporization rate is based on the rate of change of the droplet diameter, the condensed water tends to artificially increase the droplet size, slowing down the instantaneous vaporization rate as can be observed in Figure 5.9 and Figure 5.10 during the K_i period. However, this continuous water condensation will decrease because of the reduction in the water vapor pressure difference between the ambience and the droplet surface. Law *et al*. (1987) have reported the evolution of the droplet temperature for methanol droplets vaporizing in humid air, and demonstrated that T_s decreases to a minimum and then increases again. These authors have explained this increase by the condensation heat release as well as the favourable wet-bulb temperature of water. In our work, this temperature increase at the end of the ethanol vaporizing period could explain the increase of vaporization rate of water, K_f, observed in Figure 5.8, comparatively to the theoretical water curve. The longer condensation period for the anhydrous ethanol, could explain the higher level of vaporization rate, K_f, especially at high temperatures.

5.2 1-Propanol

5.2.1 Average Vaporization

In these experiments, the temporal evolution of squared-diameter, d^2 against time of 1-propanol droplet is significantly linear with constant vaporization rate throughout the droplet lifetime. So-called 'quasi-steady' behaviour is preserved and it is seen that the vaporization of 1-propanol is clearly described by the classical d^2-law as illustrated in Figure 5.16.

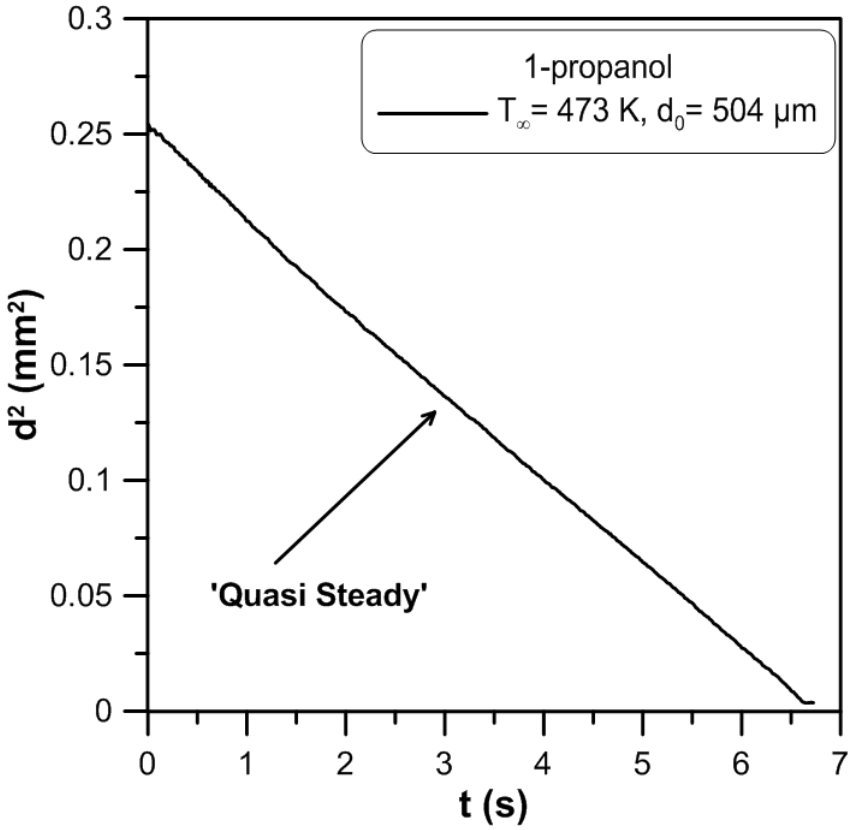

Figure 5.16: Evolution of squared diameter, d^2 against time, t for 1-propanol droplet at T_∞ = 473 K; P_∞ = 0.1 MPa

Meanwhile, Figure 5.17 portrays the time histories of normalized squared-diameter of 1-propanol droplet at different ambient gas temperatures. The average vaporization rate, *K* also increases significantly with temperatures. The common main phenomena in the vaporization

process are the increase of the droplet surface temperature and the increase of the binary diffusion coefficient with increasing temperature. Both phenomena contribute to the increase of the vaporization rate.

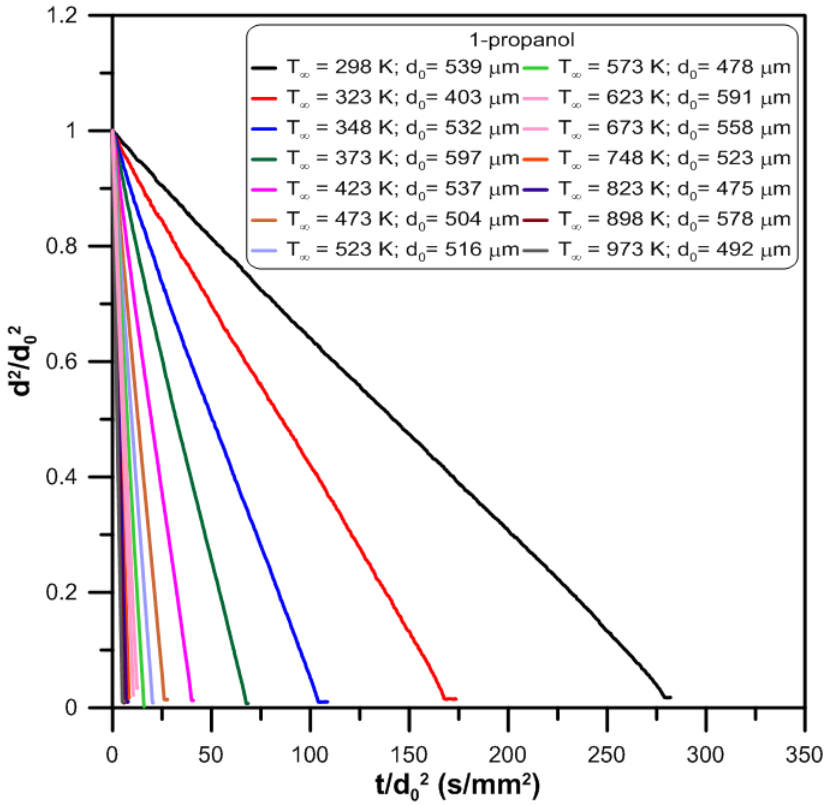

Figure 5.17: d^2 (t) curves for 1-propanol at various temperatures; P∞ = 0.1 MPa

A plot of average vaporization rates against ambient gas temperature is shown in Figure 5.18 where a polynomial fit of degree two is plotted (with the value of R^2 = 0.999873). It is clearly shown that at all ambient temperatures, the average vaporization *K* follow the fit predominantly, with slightly lower values observed at higher temperatures.

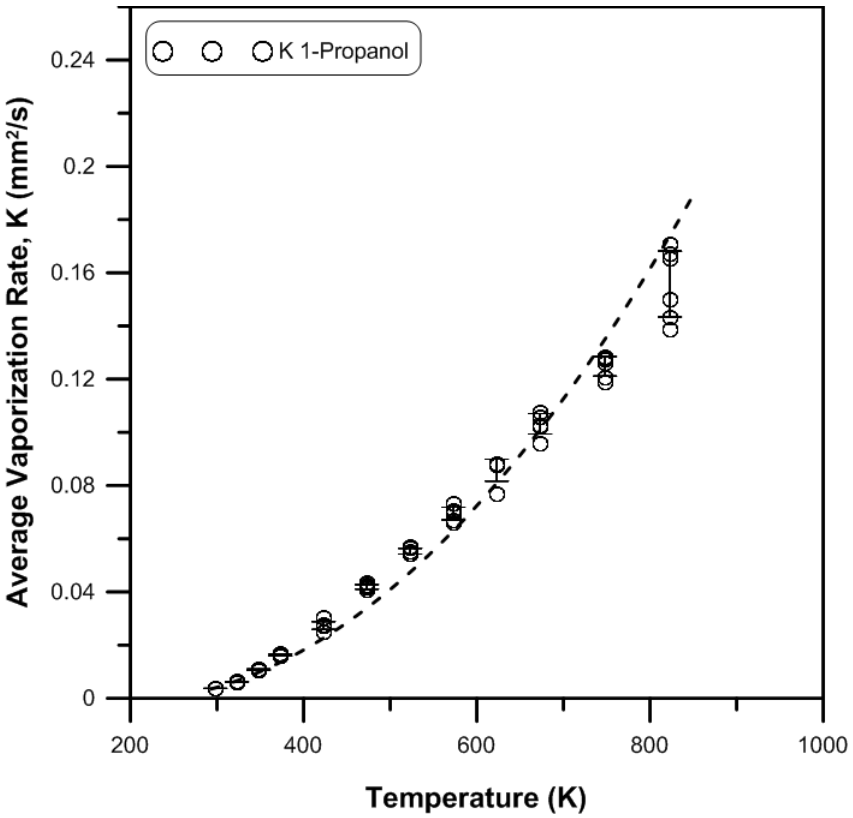

Figure 5.18: Average vaporization rates, K for 1-propanol droplet at various temperatures; P∞ = 0.1 MPa. The dotted line is the polynomial fit of the data.

5.2.2 Instantaneous Vaporization Rate

The calculation of instantaneous vaporization rate of 1-propanol is similar to that of ethanol droplet. In order to avoid errors in the calculation of the derivative, a smoothing is carried out on the d^2 *(t)* curves by using a FFT filter. This method removes only the high frequency components with 40 to 50 points of window (Origin® function). Then the derivative is simply calculated on this smoothed curve. Figure 5.19a shows the original d^2 *(t)* curve and their corresponding instantaneous vaporization rate, K_{inst} against time for 1-propanol droplet at ambient gas temperature of 473 K. It is clearly illustrated that a 'quasi-steady' vaporization period occurs throughout the droplet lifetime. The same behaviour but with a slight 'unsteadiness' is observed at ambient gas temperature of 673 K (Figure 5.19b).

In order to compare lucidly these evolutions for different temperatures, a normalization of these curves has been carried out. The time has been normalized by the droplet total vaporization time, t_{vap}. We can observe from Figure 5.20 that the quasi-steady behaviour of 1-propanol droplet is achievable for all lower temperatures up to T_∞= 673 K. However, an interesting observation could be seen beyond this temperature, where the instantaneous vaporization rate, K_{inst} reveals a bit of unsteady behaviour with the values of K_{inst} gradually decreasing over time.

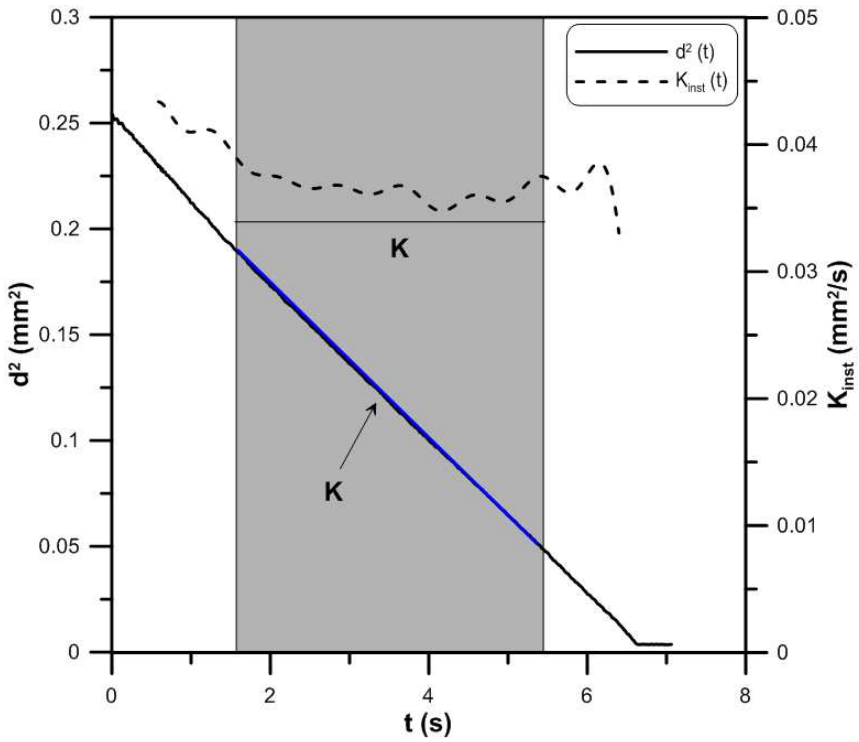

(a)

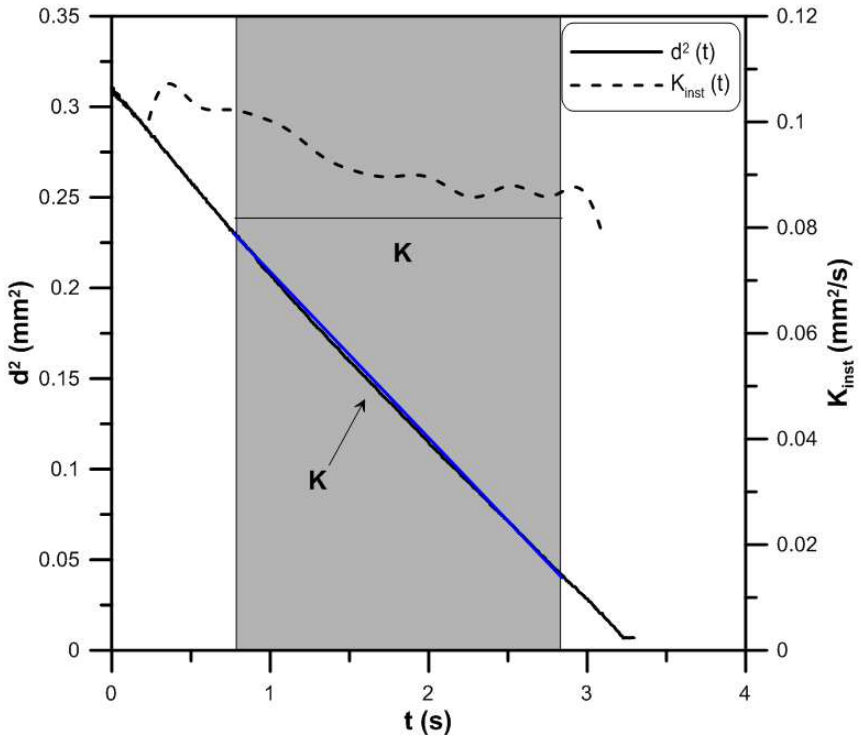

(b)

Figure 5.19: Evolution of the instantaneous vaporization rate, K_{inst} *(t)* and the squared droplet diameter curves for 1-propanol droplet at T_{∞} = (a) 473 K and (b) 673 K.

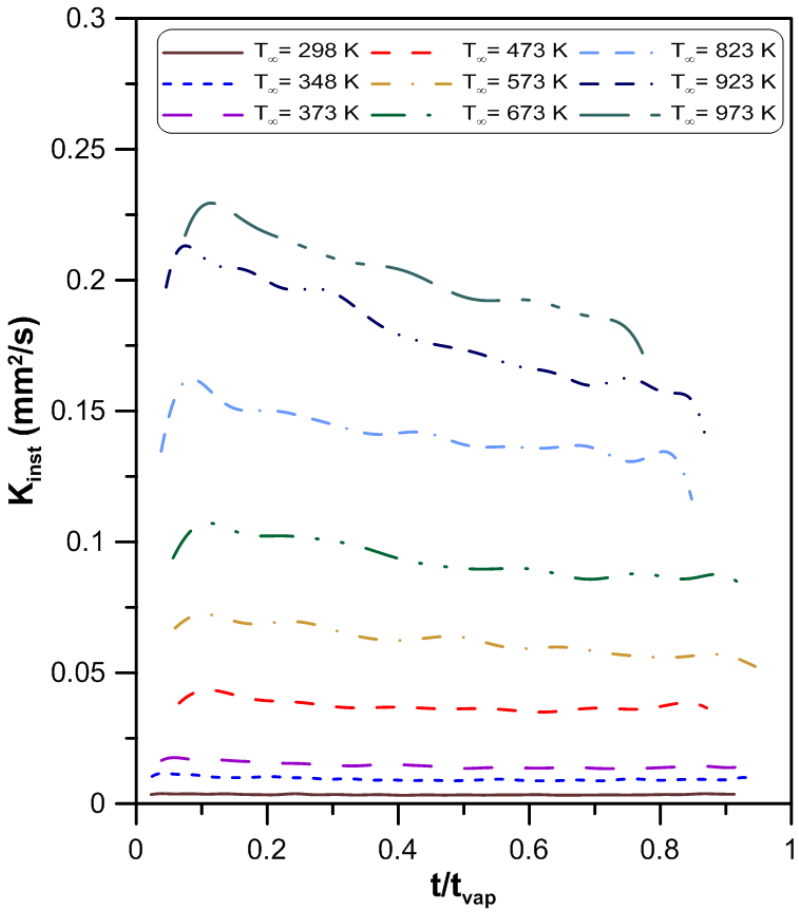

Figure 5.20: Comparison of the instantaneous vaporization rate, K_{inst} *(t)* of 1-propanol droplet at various temperatures; P_{∞}=0.1MPa.

5.3 Comparison between Ethanol and 1-Propanol Vaporization Characteristics

In this section a comparison of the vaporization behaviour has been carried out between anhydrous ethanol and 1-propanol droplets in terms of average vaporization and instantaneous vaporization rates.

The normalized temporal evolutions of squared-diameter, d^2 against time of 1-propanol and ethanol, at various ambient temperatures are shown in Figures 5.21a and 5.21b. The vaporization of 1-propanol is clearly described by the classical d^2-law. The change of squared-diameter, d^2 of 1-propanol droplet is almost linear with constant vaporization rate throughout

the droplet lifetime. On the other hand, the curve representing the vaporization behaviour of anhydrous ethanol shows a significant deviation from the linear d^2-law. The so-called 'quasi-steady' behaviour is apparently not preserved in anhydrous ethanol vaporization. However, as the ambient temperature is increased (Figure 5.21b), the significant deviation from linearity gradually diminishes. In other words, the slope is approaching almost a constant value for ethanol droplets at extremely higher temperatures.

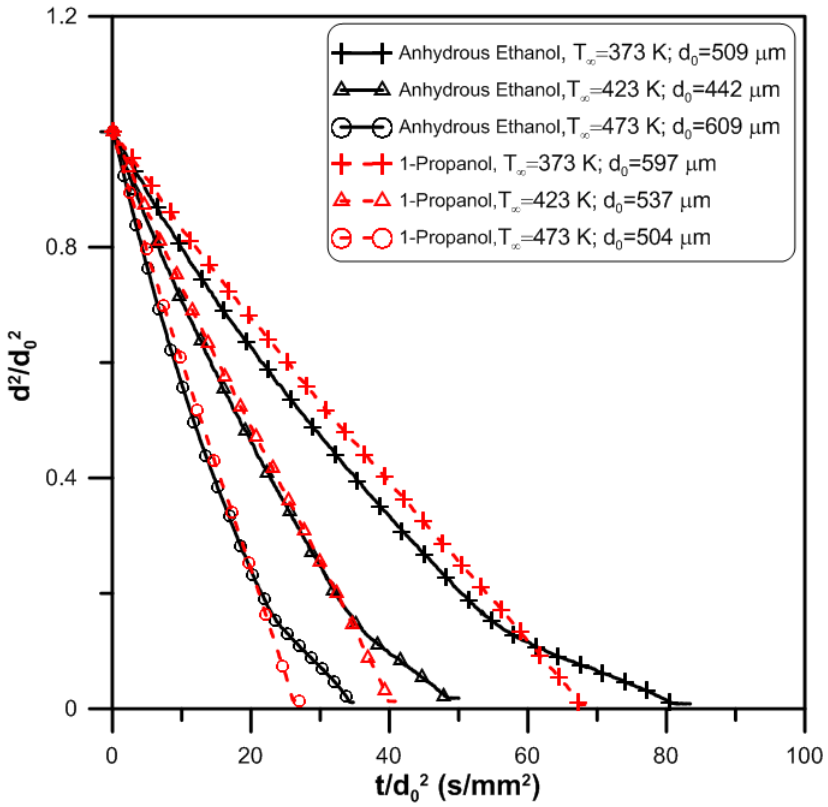

(a)

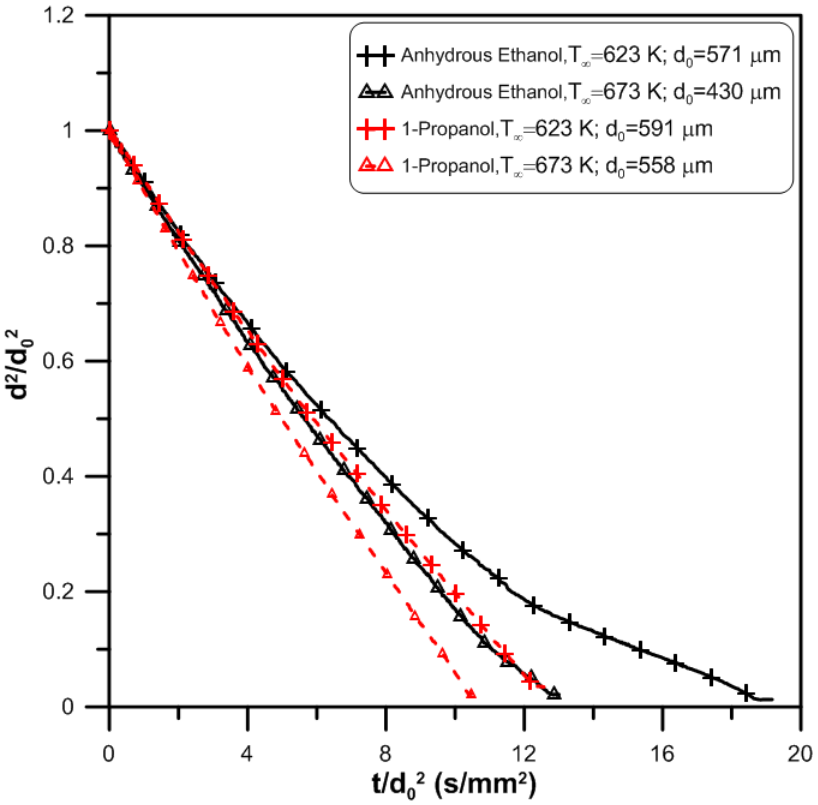

(b)

Figure 5.21: Normalized squared-diameter curves for anhydrous ethanol and 1-propanol droplets at (a) low temperature T_∞ (b) high temperature T_∞ and pressure P_∞ = 0.1 MPa.

As observed in Figures 5.22a and 5.22b, at two different ambient temperature T_∞ = 473 and 673 K respectively, the instantaneous vaporization rate, K_{inst} for 1-propanol droplet is almost always a constant, unlike the anhydrous ethanol droplet which shows the unsteadiness over time. There is also an obvious sudden change in K_{inst} value of anhydrous droplet at the deviation point which we define as the start point of water vapour vaporization. The histories of the instantaneous vaporization rate, K_{inst} also confirm that the steady-state behaviour of vaporization is achievable in 1-propanol droplet.

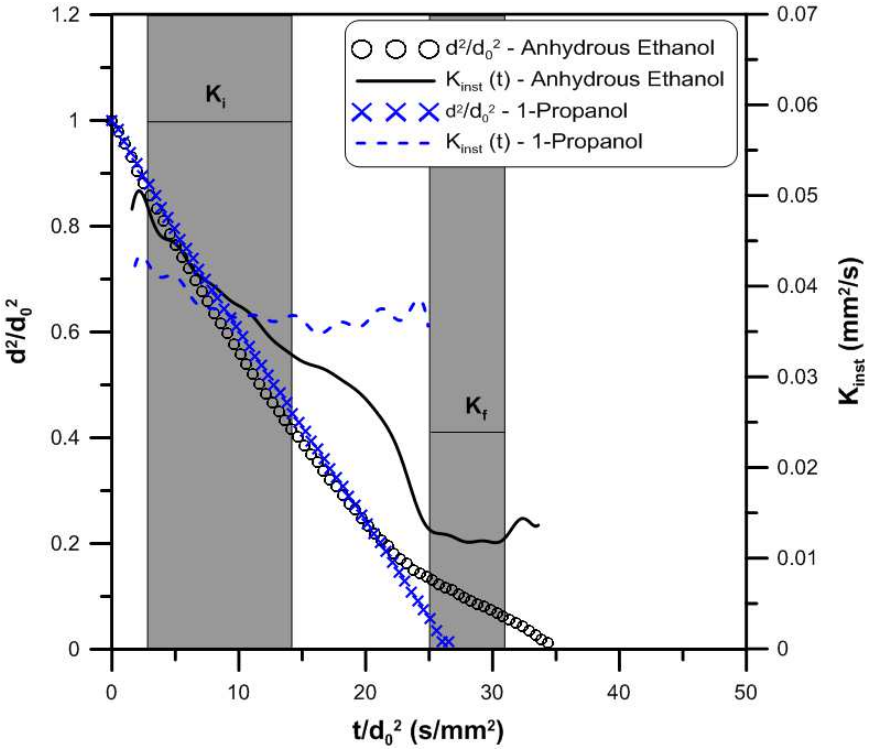
d²/d₀² - Anhydrous Ethanol
K_inst (t) - Anhydrous Ethanol
d²/d₀² - 1-Propanol
K_inst (t) - 1-Propanol
K_i
K_f
d²/d₀²
K_inst (mm²/s)
t/d₀² (s/mm²)
0
0.2
0.4
0.6
0.8
1
1.2
0.01
0.02
0.03
0.04
0.05
0.06
0.07
10
20
30
40
50

(a)

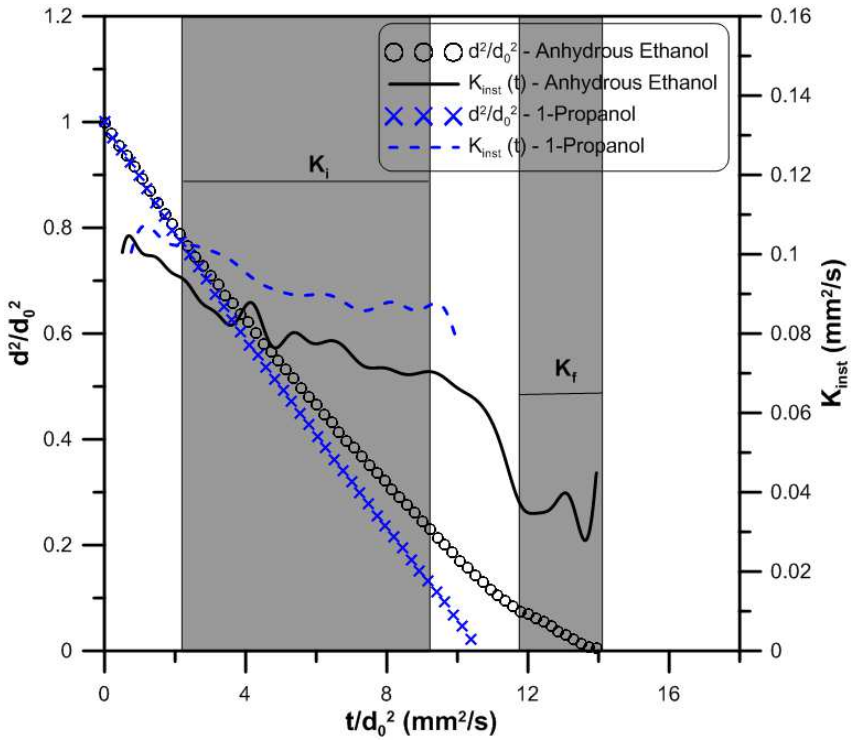

(b)

Figure 5.22: Evolution of the instantaneous vaporization rate, K_{inst} *(t)* and the normalized squared diameter for anhydrous ethanol and 1-propanol droplets at T_∞ = 473 K (a) and (b) T_∞=673 K.

5. 4 Effect of Ambient Relative Humidity

Figures 5.23 (a-d) show the variation of so-called initial and final vaporization rate, K_i and K_f of ethanol droplet at various temperatures respectively. In this section we attempt to correlate the effect of ambient relative humidity on the behaviour of K_i and K_f. It is clearly demonstrated from these figures that the initial vaporization rate K_i is always constant despite the change of ambient relative humidity. However, the value of final vaporization rate K_f is clearly affected as the ambient humidity is altered. The value of K_f is observed to decrease as the ambient relative humidity increases. This observation shows that the values of the first linear part of d^2 curves (K_i) for both ethanol (95%) and anhydrous ethanol consist entirely and

totally only of ethanol vaporization. Ethanol is the major component evaporating at this first stage as it has lower boiling temperature than water. In the meantime, K_f undoubtedly correlates to the water vaporization phenomenon as these values are negative dependent on the ambient humidity due to the droplet prolonged lifetime at the end of the droplet vaporization (see also *Appendix C*).

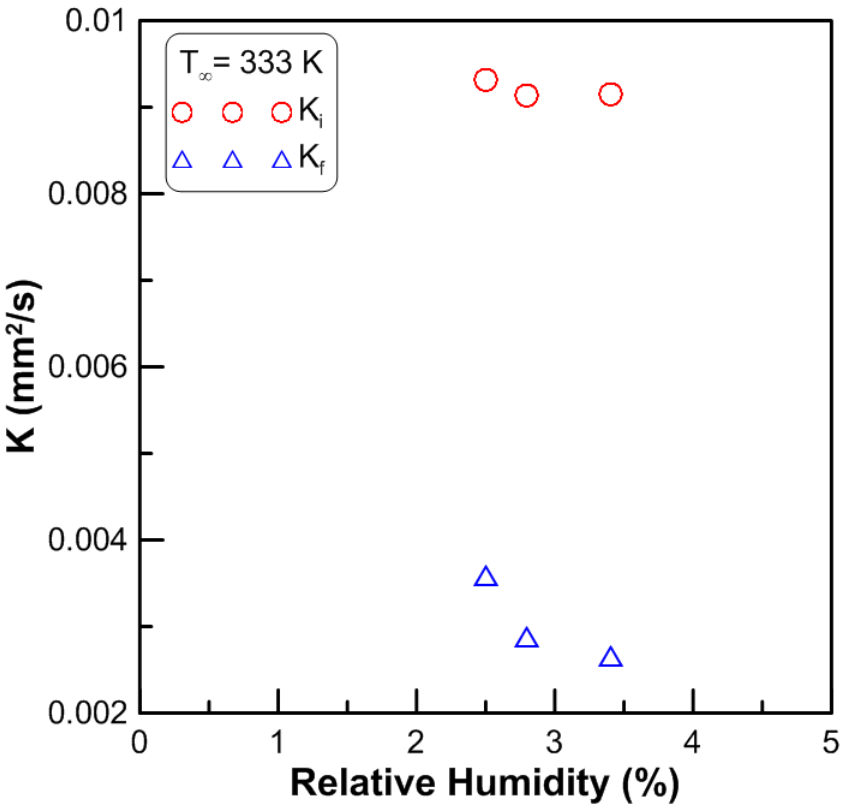

(a)

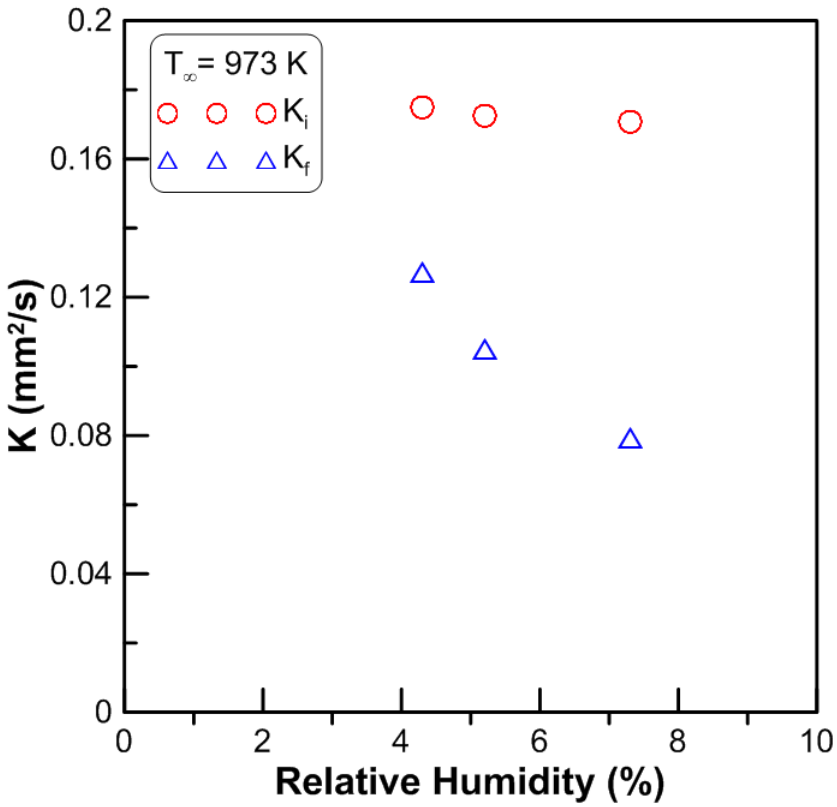

(b)

Figure 5.23: The disparity of initial vaporization rate K_i and final vaporization rate K_f of ethanol droplets at different values of ambient relative humidity; T_∞ = (a) 333 K and (b) 973 K.

5. 5 Effect of Droplet Initial Diameter

During the experiments of vaporization of ethanol and 1-propanol droplets, the effect of the droplet initial diameter has been observed closely. The droplet initial diameter d_0 has been varied from as small as 250 µm up to almost 600 µm. An obvious observation of d_0 impact can be made on 1-propanol vaporization. Results show that the average vaporization rate K, increases as the droplet initial diameter d_0 increased (Figure 5.24). However, as the environment humidity was also varied, and most of the experiments experienced an almost similar range of droplet initial diameter, the exact and direct influence of d_0 on the vaporization rate of ethanol remains ambiguous due to the fact that ethanol are extremely affected by the ambi-

ent humidity. Moreover the findings from literature concerning the impact of d_0 especially on vaporization and burning rate are still tenuous and indecisive. According to Jackson and Avedisian (1994), on *n*-heptane combustion experiment in microgravity condition, the burning rate decreased as the droplet initial diameter, d_0 increased, with the argument that the residence times inside the flame structure for fuel vapour to undergo pyrolisis reactions leading to soot formation was prolonged. However, Hara and Kumagai (1994) carried out a similar experiment and concluded that there was a negligible variation of burning rate with d_0. Yozgatligil *et al.* (2003) have conducted experimental study on ethanol combustion at elevated pressure and enhanced oxygen concentrations. Concerning the effect of droplet initial diameter d_0 on ethanol burning rate, the results showed that the burning rate was positive dependent on the d_0. Nomura *et al.* (2003) have experimentally investigated the effects of suspender diameter and natural convection on measured evaporation constant of an *n*-heptane droplet. The evaporation constant was obtained for various initial droplet diameters and suspender diameters. They concluded that the dependence of the evaporation constant on initial droplet diameter changes when the suspender diameter is varied. That is when the suspender diameter is large as compared with the initial droplet diameter, the evaporation constant decreases as the increase of initial droplet diameter. Conversely, when the suspender diameter is small as compared with the initial droplet diameter, the evaporation constant increases as the increase of initial droplet diameter. An experimental study to investigate the effect of initial droplet diameter on droplet heat-up period and steady-state vaporization regime of kerosene droplet has been conducted by Khan *et al.* (2007). The results revealed that both heat-up period and evaporation rate have increased with an increase of droplet initial diameter at all ambient temperatures and pressures.

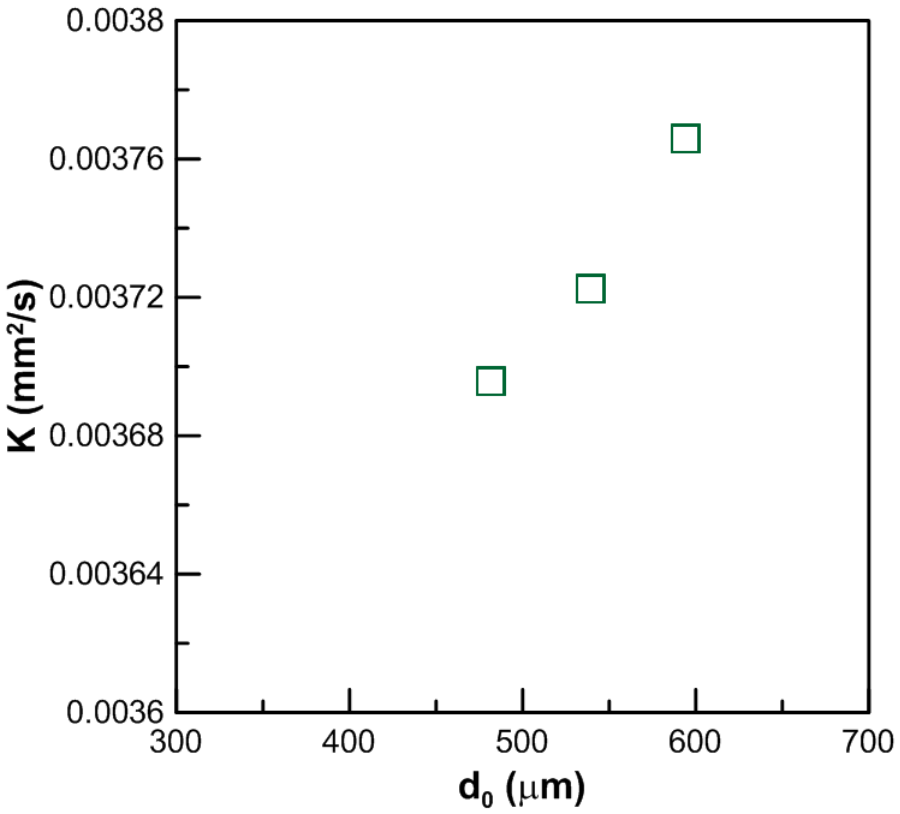
0.0038
0.00376
0.00372
0.00368
0.00364
0.0036
K (mm²/s)
300
400
500
600
700
d0 (μm)

(a)

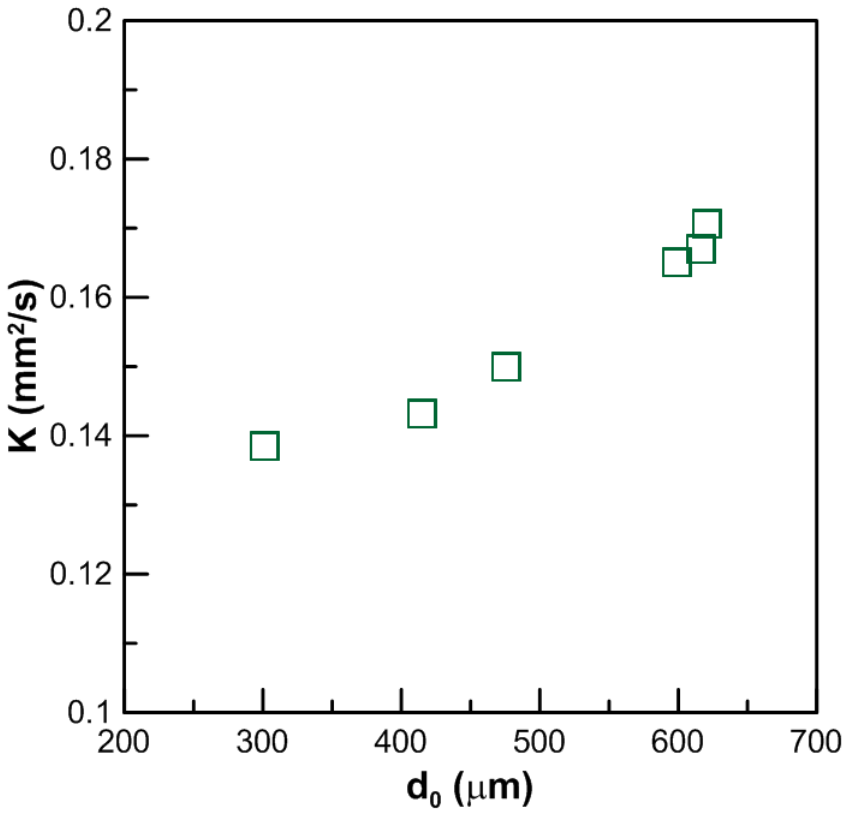

(b)

Figure 5.24: The disparity of average vaporization rate of 1-propanol droplets at various initial droplet diameters; T_{∞} = (a) 298 K and (b) 823 K.

5.6 Effect of Initial Water Content on Ethanol Vaporization

Figures 5.25 to 5.29 show the plots of normalized squared diameter of the ethanol droplet against normalized time at a variety of initial water content at ambient temperature of 473 K. The mixtures of ethanol and water have been prepared by manually mixing the absolute ethanol with pure water. The percentage of initial water in ethanol solution is calculated by volume. The tests were run at different values of ambient relative humidity. As expected, a so-called 'quasi-steady' period for ethanol in all cases occurs two times throughout the droplet lifetime. The obvious effect of ambient relative humidity on the ethanol vaporization is in the droplet lifetime. The droplet lifetime is prolonged with increase of ambient relative humidity.

However the values of initial and final average vaporization rate K_i and K_f are not directly affected by the increase of ambient relative humidity.

The figures also show that the deviation of the curve from the linearity of the d^2-law becomes more prominent with the increase of initial water content and instead the values of the first linear part of all d^2-curves remain unchanged.

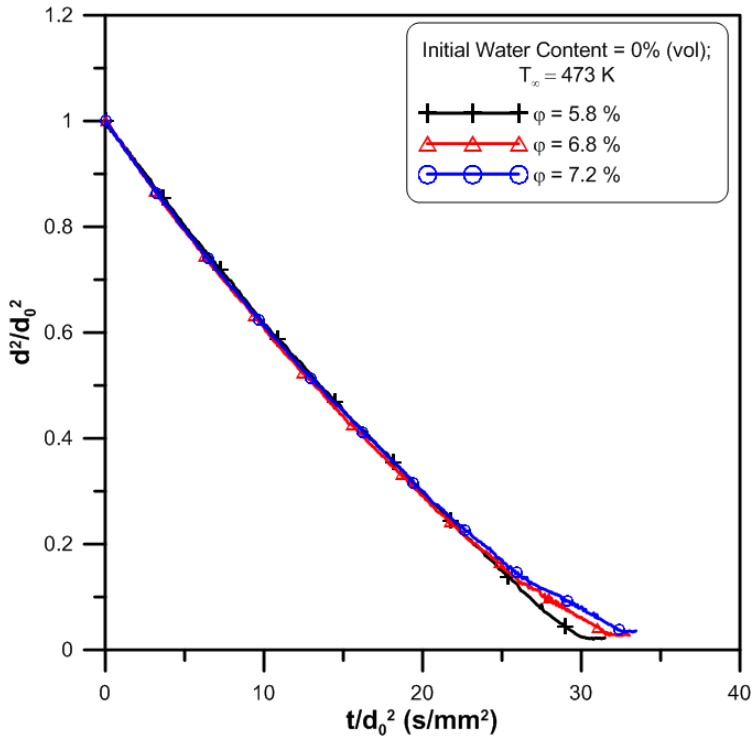

Figure 5.25: Normalized d^2- curves for ethanol droplets (absolute, no additional water content) at various ambient relative humidity (%); T_∞ = 473 K and pressure P_∞ = 0.1 MPa.

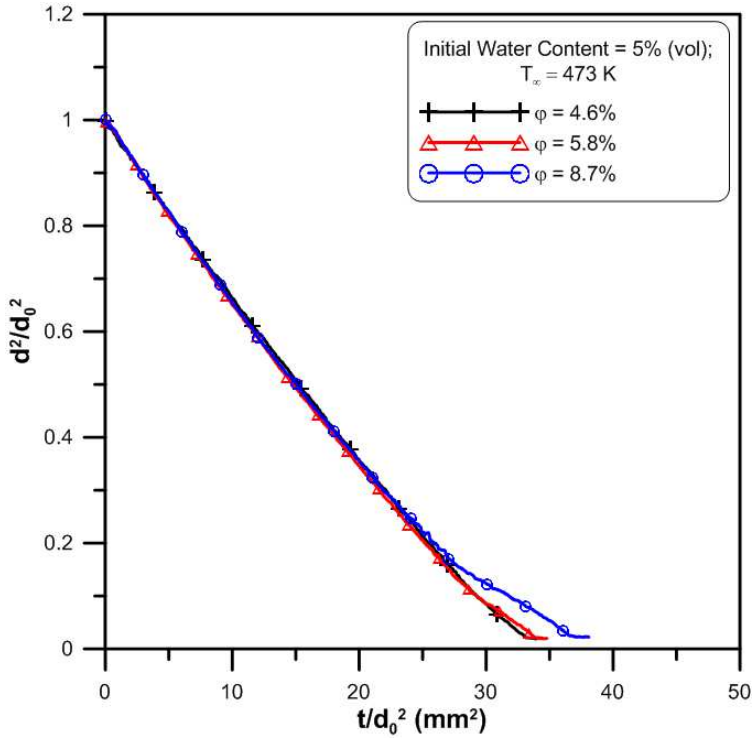

Figure 5.26: Normalized d^2- curves for ethanol droplets (initial water content = 5% volume) at various ambient relative humidity (%); T_∞ = 473 K and pressure P_∞ = 0.1 MPa.

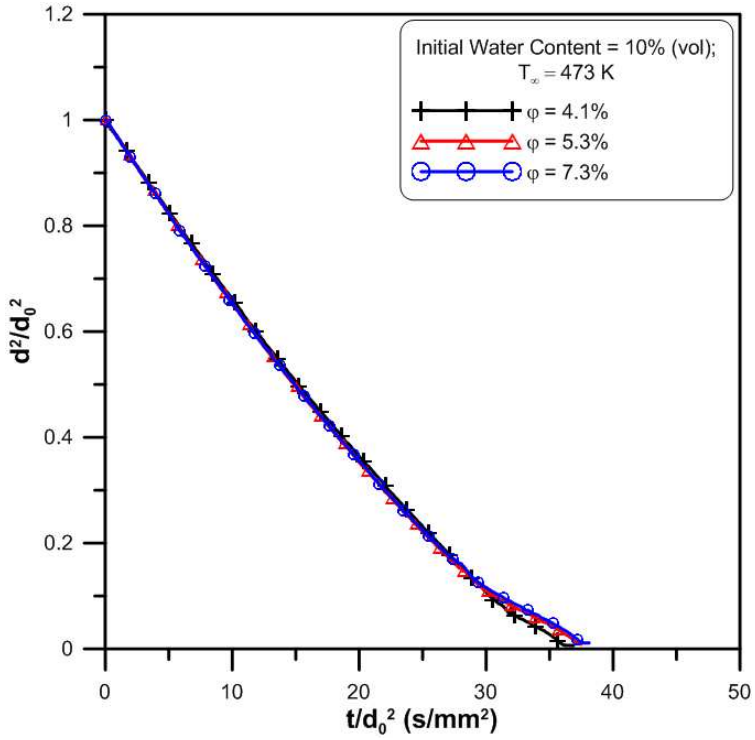

Figure 5.27: Normalized d^2- diameter curves for ethanol droplets (initial water content = 10% volume) at various ambient relative humidity (%); T_∞ = 473 K and pressure P_∞ = 0.1 MPa.

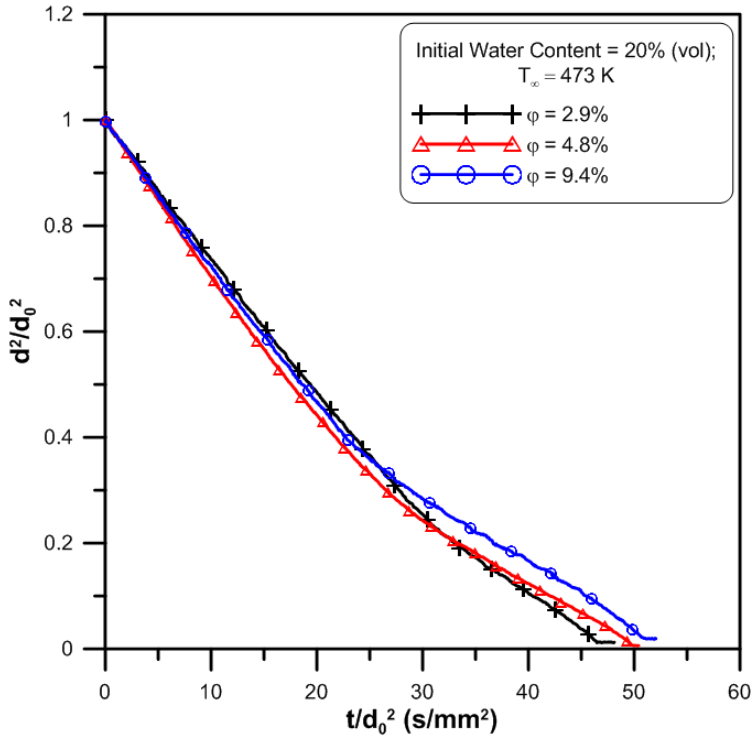

Figure 5.28: Normalized d^2- diameter curves for ethanol droplets (initial water content = 20% volume) at various ambient relative humidity (%); T_∞ = 473 K and pressure P_∞ = 0.1 MPa.

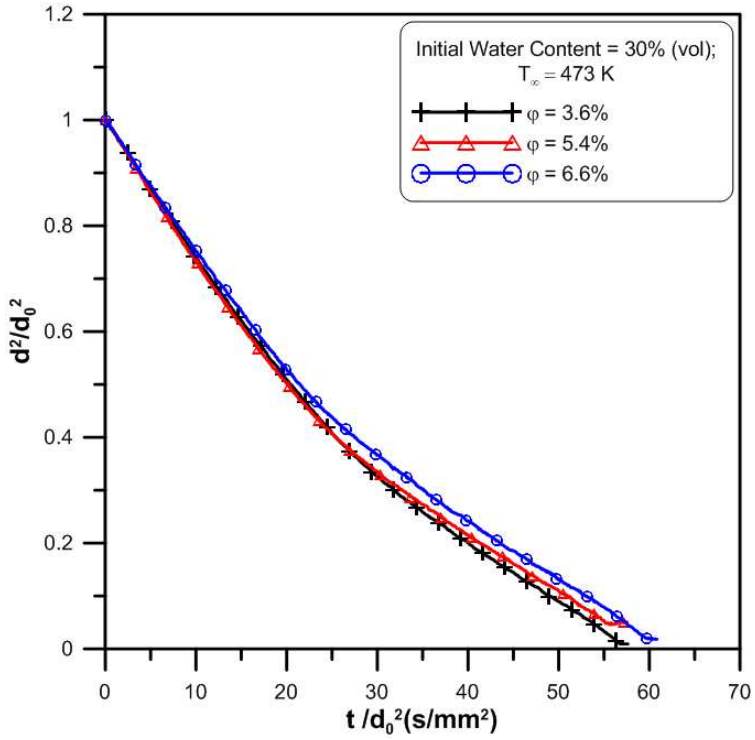

Figure 5.29: Normalized d^2- diameter curves for ethanol droplets (initial water content = 30% volume) at various ambient relative humidity (%); T_∞ = 473 K and pressure P_∞ = 0.1 MPa.

5.7 Conclusions

From the d^2 curves, average and instantaneous vaporization rates for the two ethanol forms are presented and discussed. The d^2-curves results show that the so-called 'quasi-steady period for both ethanol forms occurs two times throughout droplet lifetime. These two linear part have been defined as initial vaporization rate K_i and final vaporization rate K_f. The results also show that the different in initial water content of ethanol affect the droplet lifetime but not to the vaporization rate values. The measured K_i for both ethanol forms shows an obvious similarity. Therefore it might be conclusive to note that the first linear part of the d^2-curve is entirely due to ethanol vaporization. The final vaporization rate K_f, measured from the second linear part of the d^2-curve shows the similar values for both ethanol forms. Theoretical water vaporization rate based on 'quasi-steady' model as per discussion in Chapter 4

has been calculated and comparison is made with experimental K_f. The results show that they are in a good agreement. The deviation from the d^2-law of ethanol droplet vaporization might due entirely to the interference of water absorption and dissolution on ethanol droplet surface. The experimental instantaneous vaporization rates are calculated and show that in both cases, they are significantly unsteady especially at the initial part corresponding to ethanol vaporization. This unsteadiness is certainly due to the interference of water concentration on the ethanol droplet vaporization and also to the water condensation from the ambient moisture, due to the temperature decrease at droplet surface. The miscibility nature of ethanol to water has changed the overall process of vaporization.

The effect of various ambient temperatures on the vaporization of 1-propanol droplet shows that at various temperatures, the d^2-law holds quite steadily and the 'quasi-steady' behaviour is preserved. The time histories of instantaneous vaporization rate, K_{inst} confirm this stationary aspect of 1-propanol droplet at various ambient temperatures. The results also conclusively demonstrate that the 1-propanol vaporization is not affected by the water vapour from the environment even though it posses the miscibility property with water.

An attempt to correlate the effect of ambient relative humidity on the behaviour of K_i and K_f has been carried out. It is clearly demonstrated that the initial vaporization rate K_i is always constant despite the change of ambient relative humidity. On the other hand, the value of final vaporization rate K_f is apparently affected when the ambient relative humidity is changed. The value of K_f is observed to decrease as the ambient relative humidity increases. This observation might conclude that the values of the first linear part of d^2 curves (K_i) for ethanol consist entirely and totally only of ethanol vaporization. Ethanol is the major component evaporating at this first stage since it has lower boiling temperature than water. In the meantime, K_f undoubtedly correlates to the water vaporization phenomenon as these values are negative dependent on the ambient.

Eventhough the droplet initial diameter d_0 has been varied during the experiments, the actual effect on the ethanol remains ambiguous due to the fact that ethanol are extremely affected by the ambient humidity. However, an obvious observation of d_0 impact can be made on 1-propanol vaporization. Results showed that the average vaporization rate K, increases as the droplet initial diameter d_0 increased.

In experiments of different initial water content in ethanol, as expected, a so-called 'quasi-steady' period for ethanol in all cases occurs two times throughout the droplet lifetime. The results also show that the deviation of the curve from the linearity of the d^2-law becomes more prominent with the increase of initial water content and instead the values of the first linear part of all d^2-curves remain unchanged. The droplet lifetime is prolonged with increase of ambient relative humidity.

6 AUTOIGNITION CHARACTERISTIC AND KINETICS MECHANISM OF ETHANOL AND 1-PROPANOL

The chemical structure of biofuels such as alcohols significantly differs from fossil fuels due to the incorporation of oxygen atoms into the alkyl chain, as such the chemical details of their combustion is currently poorly understood relative to more conventional fuels. The chemical processes of a combustion reaction are extremely complicated. This has become obvious with the continued development of kinetic models and their capacity to predict with accuracy the observations of sophisticated and well defined experiments. It has been shown that large numbers of chemical species and an even larger number of chemical reactions are required to predict experimental observations such as the evolution and consumption of intermediate species. In addition, kinetic modelling has guide to an understanding of how the chemistry of these species affects the reactivity of the global system. Since so many intermediates species can be produced during the combustion process, the number of reactions required to describe this process can be up to hundreds or even thousands of chemical reactions depending on the size of the fuel molecule undergoing oxidation.

Both experimental and kinetic modelling techniques have shed light upon the chemical mechanism of combustion as being a radical chain reaction. Although the well known chain initiating, branching, propagation and termination reactions are dependent on the chemical composition and structure of the fuel, it is also reliant in a complicated non-linear way on the temperature and pressure at which the combustion is occurring.

6.1 The Arrhenius Power Law Expression

The measured and computed ignition delay times for most experimental conditions are correlated to an Arrhenius, power law expression. According to Johnson *et al.* (2009) this corre-

lation form has been applied successfully in many previous studies for straight, branched and cyclic alkanes. The rate expressions which are the building blocks of the kinetic model consist of three main parameters, in terms of the modified Arrhenius-type plot of logarithm of the delay time versus reciprocal temperature equation;

$$\tau = AT^{n} \cdot e^{\frac{-E_A}{RT}} \tag{6-1}$$

Where τ is the rate constant, A the frequency factor which has units of $cm^3\ mol^{-1}\ s^{-1}$, T is the temperature in Kelvin, n the temperature exponent which is a constant, R the universal gas constant (cal K^{-1} mol^{-1}) and E_A the activation energy (cal mol^{-1}).

Nonetheless, there were also several findings from literature showed the occurrences of "two-stage" autoignition that led to the existence of "negative temperature coefficient" (NTC) region on alkanes. NTC behaviour has regularly been observed for hydrocarbons with alkyl chains of sufficient length ≥ C_3, (Silke *et al.* (2005)) to allow the gateway reaction class to NTC behaviour to occur: the isomerisation of alkylperoxyl to peroxyalkyl radicals.

Minetti *et al*. (1994) have studied experimentally the oxidation and autoignition of butane/air mixture in rapid compression machine (RCM). They found that the ignition delay of butane consisted of a "two-stage" phenomenon. Healy *et al*. (2010) have also observed the same existence of NTC region on isobutane mixtures autoignition experiments.

6.2 Computational Simulations

For the calculation of the modelling computations, ignition delay time is determined by a volume profile method, where it is resoluted from experiment with a non-reactive mixture using adiabatic compression/expansion assumption. The calculations have been performed by means of CHEMKIN 3.7 software.

The summary of simulation performed to determine the properties such as end of compression pressure P_c and temperature T_c and ignition delay time τ is shown in the block diagram as follows:

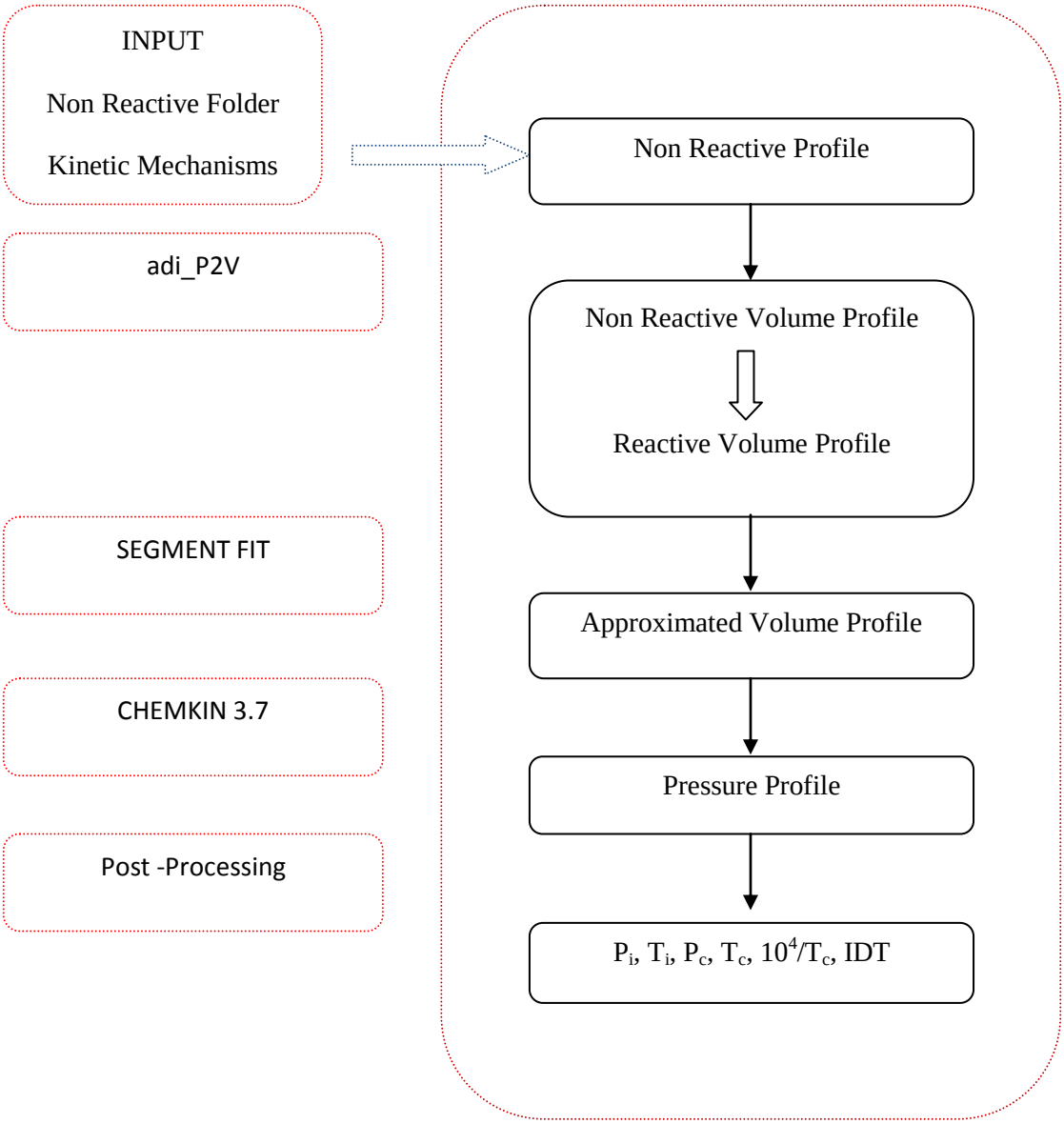

Figure 6.1: Presentation of ignition delay time calculation steps by modelling simulation.

where P_i and T_i are the initial pressure and temperature respectively.

In summary, the modelling simulation is based on a few main assumptions:

1. Adiabatic expansion of the core due to the cooling of the boundary layer (test gas).
2. Non Reactive mixtures, i.e. O_2 are replaced by N_2 (due to its similar thermodynamics properties).

6. 3 Detailed Kinetics Mechanism of Ethanol and 1-propanol

Alcohol have been defined as organic compounds characterized by a hydroxyl functional group OH, attached to a main carbon root, *R*. Figure 6.2 shows the oxidation pathways of alcohols, depends on which bond hydrogen abstraction occurs (Norton *et al.* (1991)). The reactions governing ignition delay time or chemical induction period combustion can be broken down into four categories:

1. Chain-initiating reactions: fuel is decomposed, usually by uni-molecular decomposition (pyrolysis at high temperatures and by $RH+O_2 \rightarrow \dot{R}+HO_2$ reaction at lower temperatures).
2. Chain-propagation reactions: keep the radicals concentration constant.
3. Chain-branching reactions: increase the radical pool where intermediate species are formed and radicals (reactive species with an unpaired electron) are released.
4. Chain-terminating reactions: decrease the radical pool where the final stable products such as H_2O and CO_2 are formed.

The pyrolysis and oxidation mechanism of ethanol and 1-propanol are very similar to those for hydrocarbon fuels. The development of a complete set of primary propagation reactions of fuel ethanol has been under studied and defined by Frassoldati *et al.* (2010) with a few new kinetics parameters for reactions involving bonds and *H*-atoms near to the OH group. This kinetic model consists of 1416 reactions involving 80 species. Another kinetics mechanism developed by C3 NUIG researchers called Aramco mechanism (courtesy of C3, NUIG and

still underdevelopment and yet to be published) is also applied for comparison purposes and it consists of 1542 reactions with 253 species. A kinetic mechanism of methanol and ethanol by Frassoldati *et al*. (2010) is reasonably well-known and has been revised recently by numerous authors. According to them, the mechanism is evolving from the initiation reactions where the activation energy equal to the bond energy by assumption of a reference frequency factor, to the metathesis reactions to define the reactivity of the H atoms in hydroxyl position and the H atoms in α position. Decomposition reactions of the corresponding alkoxy and parent radicals from alcohols fuels and finally the class of the four-centre molecular dehydration reactions are required to complete the kinetics mechanism of fuel ethanol and 1-propanol.

For 1-propanol fuel, a mechanisms developed by Johnson *et al*. (2009) has been utilised in this study. The model consists of 1415 reactions involving 237 species. The 1-propanol mechanism was developed based on the hierarchical structure of chemical kinetic mechanisms and uses the updated C_3-chemistry (Bourque *et al.* (2008) and Johnson *et al.* (2009)) for the baseline chemistry, with the propanol isomer sub mechanisms added. These sub mechanisms were systematically generated considering (i) unimolecular fuel decomposition reactions, (ii) hydrogen atom abstraction reactions, and (iii) β-scission reactions associated with the alkyl/alkoxy radicals generated from the parent fuel.

Figure 6.2: Alcohol oxidation pathway (Adopted from Norton *et al.*, (1991)).

6.4 Sensitivity Analysis

A sensitivity analysis was performed on the kinetic model to explicate the important channels of reaction for alcohols under these rapid compression machine conditions. The sensitivity analysis was employed by multiplying the forward and reverse rate constants of a reaction or reaction class by a factor of two thereby leaving the thermo chemistry or thermodynamic

equilibrium constant within the chemical reaction unaffected and noting the effect on the computed ignition delay time (Marinov (1997)). The sensitivity coefficient, σ, is defined as:

$$\sigma = \frac{log\left(\frac{\tau_1}{\tau_2}\right)}{log\left(\frac{2}{0.5}\right)} \tag{6-2}$$

where τ_1 is equal to the multiplication of A by a factor of 2 and τ_2 is equal to the division of A by a factor of 2. Thus, a positive sensitivity coefficient represents a longer ignition time, indicating that this reaction impedes reactivity and a negative coefficient indicates a shorter ignition time, indicating that this reaction promotes reactivity.

Two mechanisms have been applied for the sensitivity analysis for ethanol. The evaluation of the most sensitive reactions has been realized by Aramco mechanism and by Frassoldati *et al.* Meanwhile, the 1-propanol mechanism is realized by Johnson *et al.* mechanism.

6.5 Pressure Profile Measurements

Figure 6.3 shows the major feature of the RCM, namely the ability to vary compressed temperature at constant compressed pressure. As seen in Figures 6.3, 6.4 and 6.5 the ignition delay times of fuel ethanol, 1-propanol and ethanol/water decreases monotonically as compressed temperature increases, indicating that these experiments are not in the negative temperature coefficient (NTC) region (all experiments were carried out at stoichiometric condition). It is also obvious from these figures that two-stage ignition did not occur. These pressure profiles represent the most significant pressure profile over various experiments performed at one condition. The reproducibility is within ± 10% in terms of ignition delay time measurement.

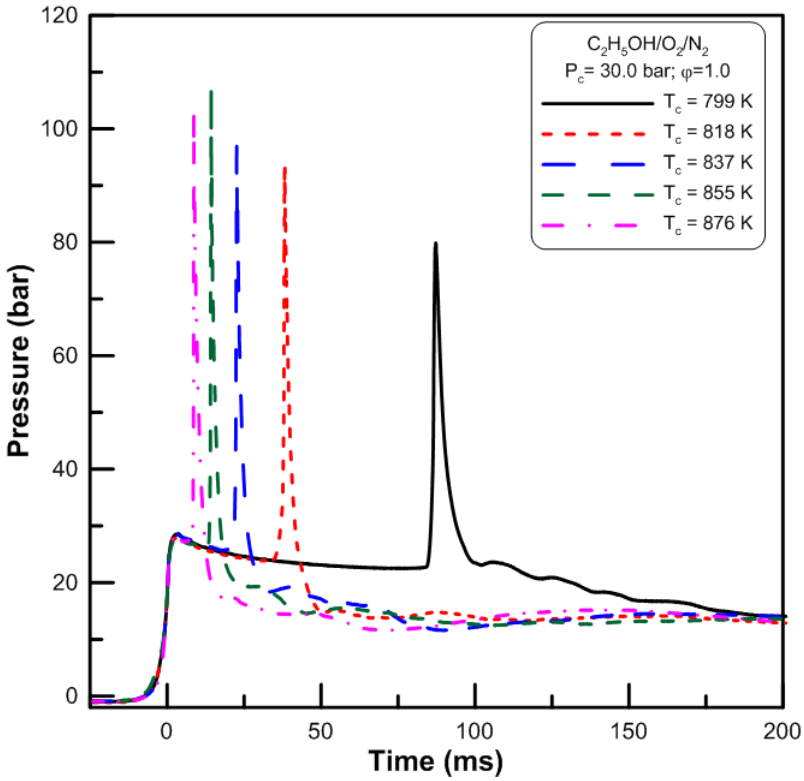

Figure 6.3: Experimental pressure profile measured in the RCM of Ethanol at all temperatures; P_c=30.0 bar, φ=1.0.

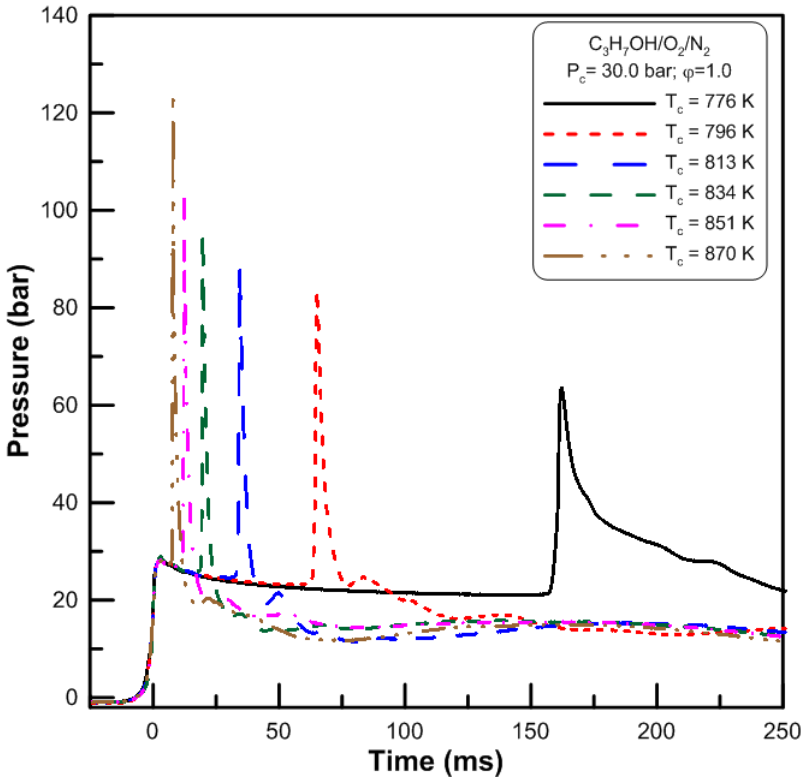

Figure 6.4: Experimental pressure profile measured in the RCM of 1-propanol at all temperatures; P_c=30.0 bar, φ=1.0.

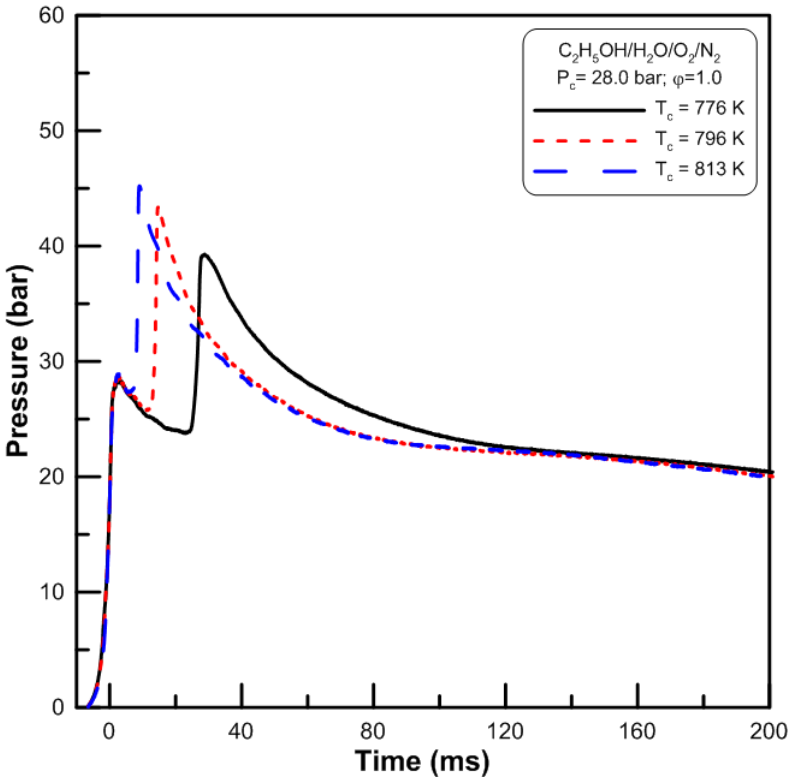

Figure 6.5: Experimental pressure profile measured in the RCM of Ethanol (70% vol)/water (30% vol) mixture at all temperatures; P_c=28.0 bar, φ=1.0.

Figure 6.6 illustrates the comparison of measured pressure profile between ethanol, 1-propanol and ethanol/water fuels at initial temperature T_i = 368 K. The results reveal that the addition of water to ethanol promotes the increase in reactivity; i.e. shorter ignition delay times. The trend could also be seen at other different temperatures. The heat release during the combustion process is significantly reduced to less than half with water addition to ethanol and it is apparently caused by the decreased ethanol concentration and energy absorption by water.

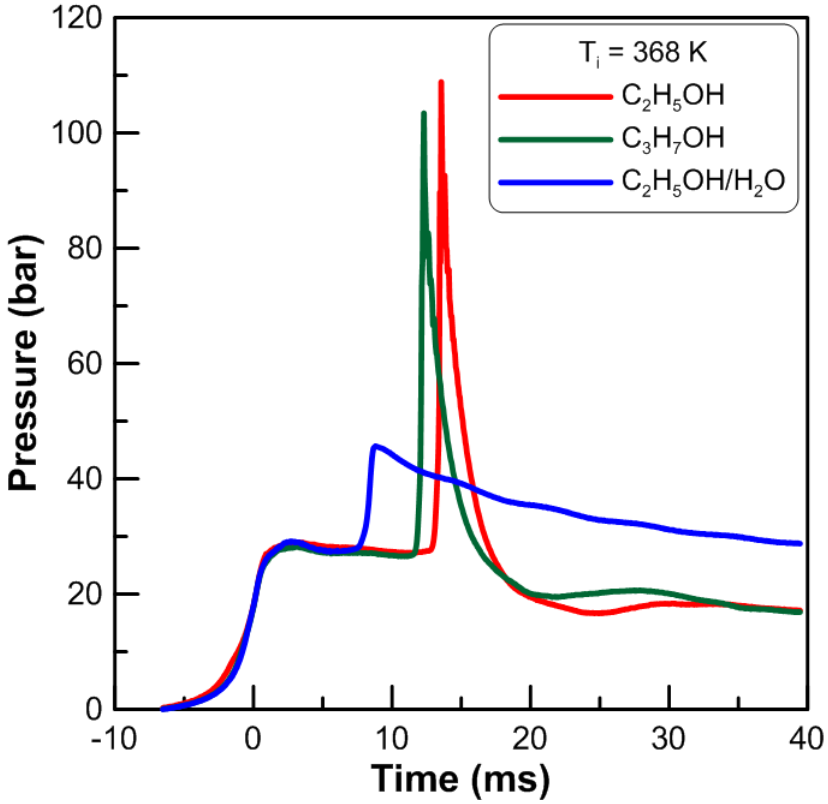

Figure 6.6: Comparison of experimental pressure profile measured in RCM of Ethanol and 1-propanol and Ethanol (70% vol)/water (30% vol) mixture at temperatures T_i= 368 K; P_i=1.0 bar, φ=1.0.

Figure 6.7 shows in more detailed the comparison between calculated pressure profiles of ethanol and 1-propanol by using the two different mechanisms. It is clearly shown that heavier alcohol, 1-propanol is more reactive (shorter ignition delay time) than ethanol. This finding is in agreement with the experimental results. Meanwhile the comparison between calculated pressure profiles for ethanol and ethanol/water mixture has been observed in Figure 6.8(see also *Appendix D*). Both mechanisms predict longer ignition delay time (less reactive) of ethanol ignition with addition of water.

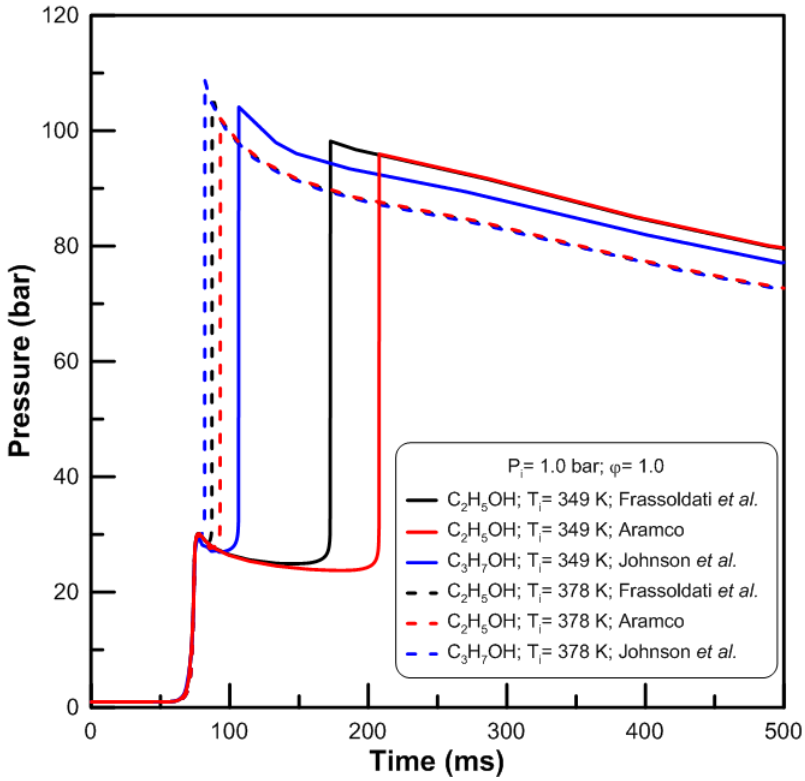

Figure 6.7: Comparison of calculated pressure profile of Ethanol and 1-propanol mixture using model predictions of Frassoldati *et al.*, Aramco and Johnson *et al.* at temperatures T_i= 349 and 378 K; P_i=1.0 bar, φ=1.0.

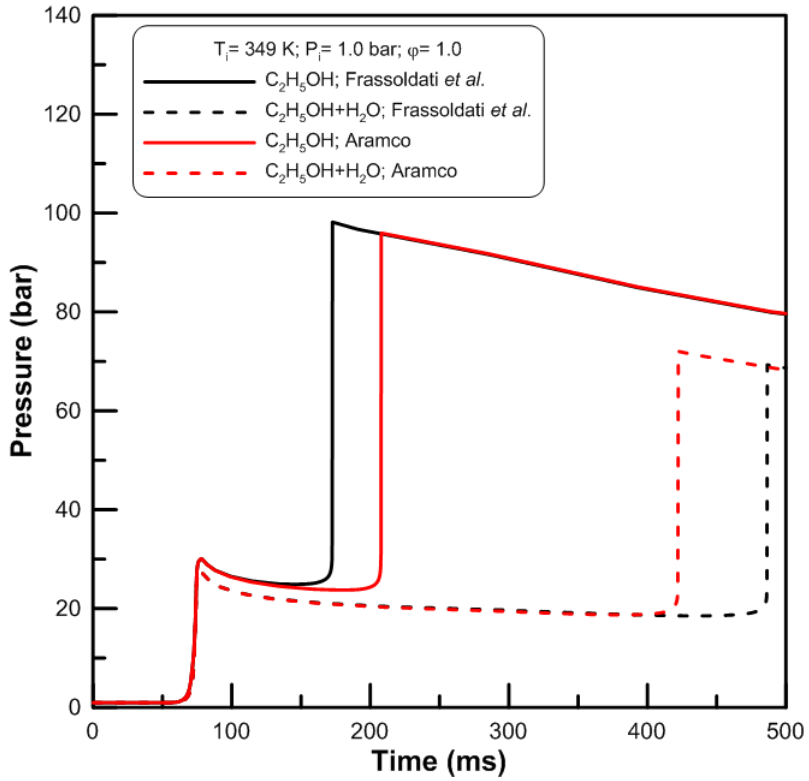
T_i= 349 K; P_i= 1.0 bar; φ= 1.0
C_2H_5OH; Frassoldati *et al.*
$C_2H_5OH+H_2O$; Frassoldati *et al.*
C_2H_5OH; Aramco
$C_2H_5OH+H_2O$; Aramco
Pressure (bar)
Time (ms)
0
20
40
60
80
100
120
140
0
100
200
300
400
500

(a)

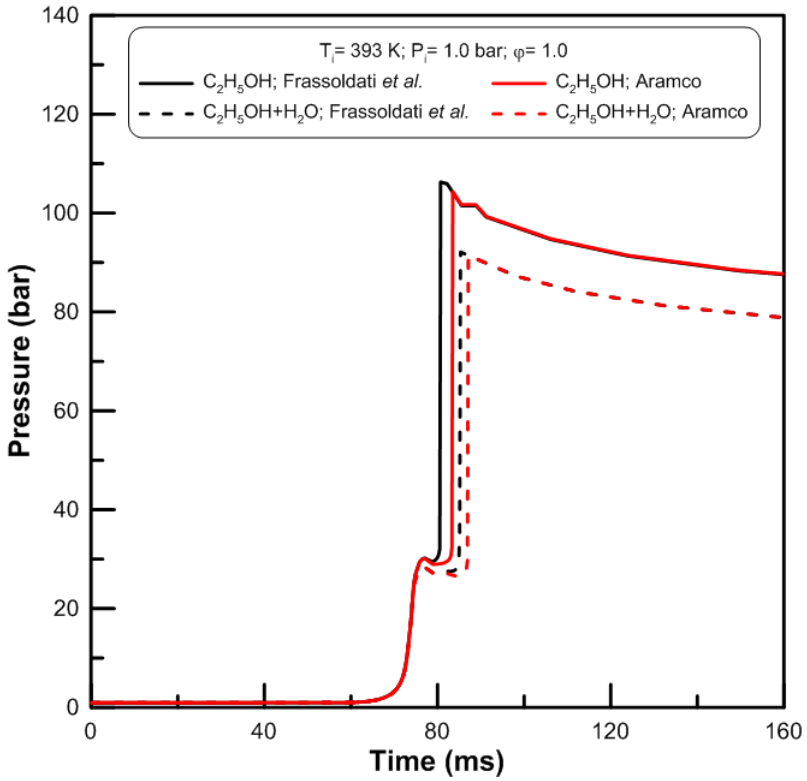

(b)

Figure 6.8: Comparison of calculated pressure profile of Ethanol and Ethanol (70% vol)/water (30% vol) mixture using model of Frassoldati *et al.* and Aramco at temperatures T_i= (a) 349 K and (b) 393 K; Pi= 1.0 bar; φ= 1.0.

6.6 Ignition Delay Time, τ Measurements

To further explain the definition and correlation of ignition delay time, an Arrhenius plot has been plot for all alcohols autoignition. Figure 6.9 shows the comparison of experimental autoignition delay times between ethanol, 1-propanol and mixture ethanol/water. Note that the ignition delay time for all fuels varies linearly with reciprocal temperature and hence exhibits Arrhenius behaviour. The ignition delay time of ethanol is observed to be longer in magnitude than 1-propanol. Therefore it shows that the higher molecular weight alcohol, 1-propanol is more reactive. As mentioned by Cooke et al. (1971) who investigated the ignition delay measurements of shock-heated ethanol-oxygen in argon mixes, on comparison of reac-

tivity between different molecular weight alcohols, have shown that ethanol is more reactive than methanol. In the meantime, the addition of water in ethanol appears to decrease the overall ignition delay time. The existence of water in ethanol/water mixture also shows an extended reactivity.

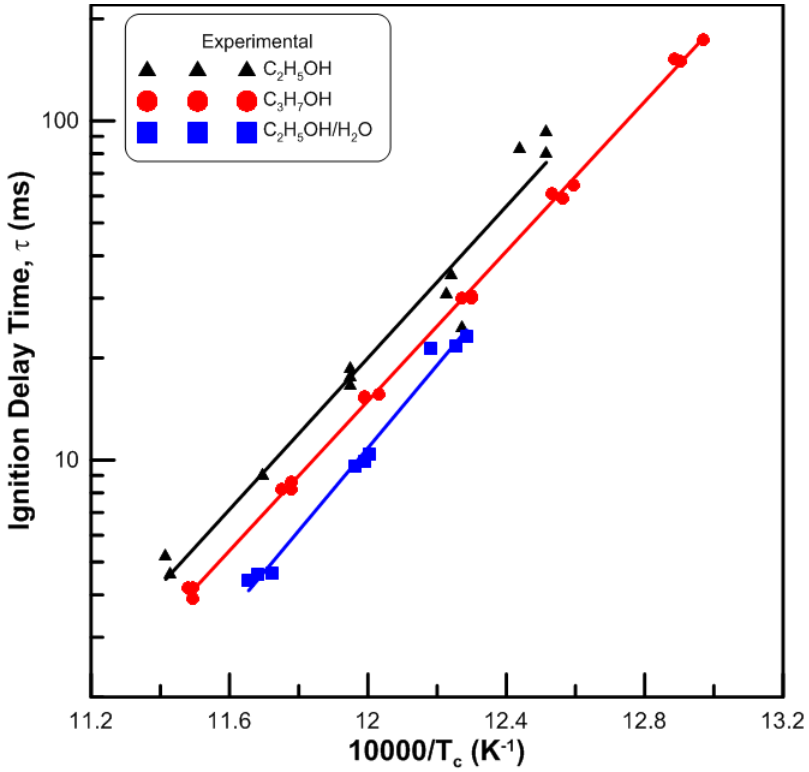

Figure 6.9: Experimental ignition delay time τ of Ethanol, 1-propanol and Ethanol (70% vol)/water (30% vol) fuels at all temperatures; P_c=34-35 bar, φ=1.0. Lines are linear square fits to the data.

Figure 6.10 shows the comparison of experimental and model predicted ignition delay time of ethanol and 1-propanol fuels. For ethanol, the model by Frassoldati *et al*. is observed to be in a good agreement with the experimental data. However there is a disturbing lack of agreement with the model under-predicting the reactivity of 1-propanol fuel.

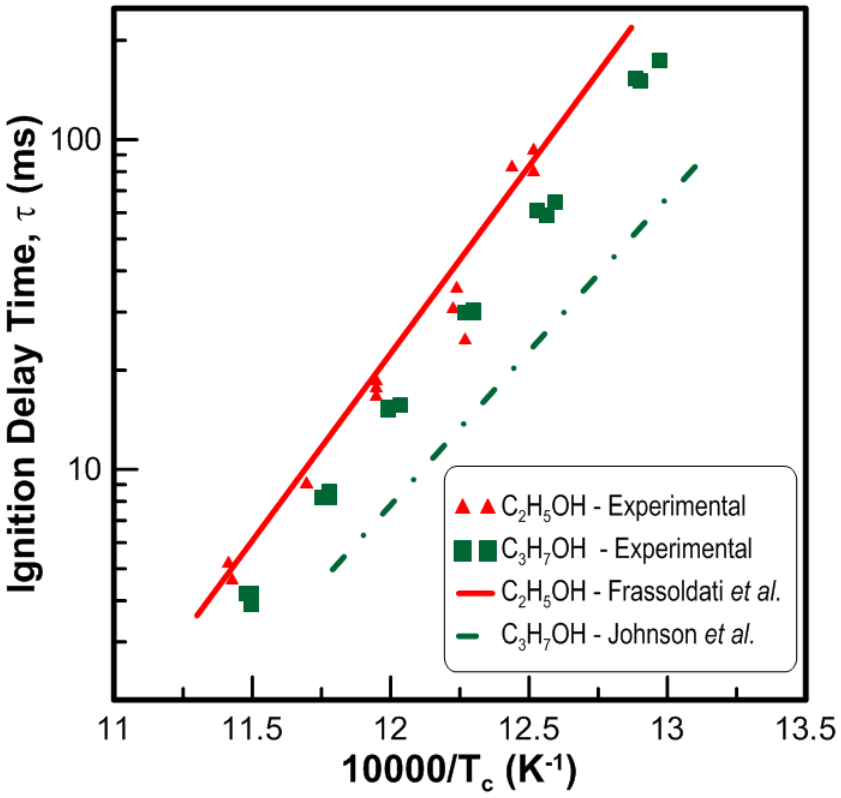

Figure 6.10: Experimental (symbols) and model predictions (lines) ignition delay time τ of Ethanol and 1-propanol fuels at all temperatures; P_c=34-35 bar, φ=1.0.

Meanwhile, Figure 6.11 illustrates the comparison between the experimental results and model prediction of both Frassoldati *et al.* and Aramco mechanisms of ethanol/water fuel mixture. Both models emerge to be in a good agreement with ethanol experimental results. However for the ethanol/water mixture, the Frassoldati *et al*. model shows increase of ignition delay time as water is added in ethanol or in the other word, reduction in reactivity, whereas the experimental data shows otherwise. On the other hand, model prediction by Aramco mechanism shows the increase of reactivity as water is added in ethanol, with an over prediction of the model to the experimental data. The Aramco modelling simulations predict that at higher compressed temperature *Tc* > 830 K approximately, the water addition to ethanol oxidation produces an increased in reactivity, which is in an agreement with the experimental results. However, at lower compressed temperature *Tc* < 830 K the opposite

occurs, i.e. reduced reactivity is observed and ignition delay prolongs. Unfortunately, in order to avoid condensation of water before the test run, the initial temperature is higher than 373 K, therefore our experiments on ethanol/water mixture could not be carried out at these lower compressed temperatures and therefore no definite conclusions could be made at these lower temperatures.

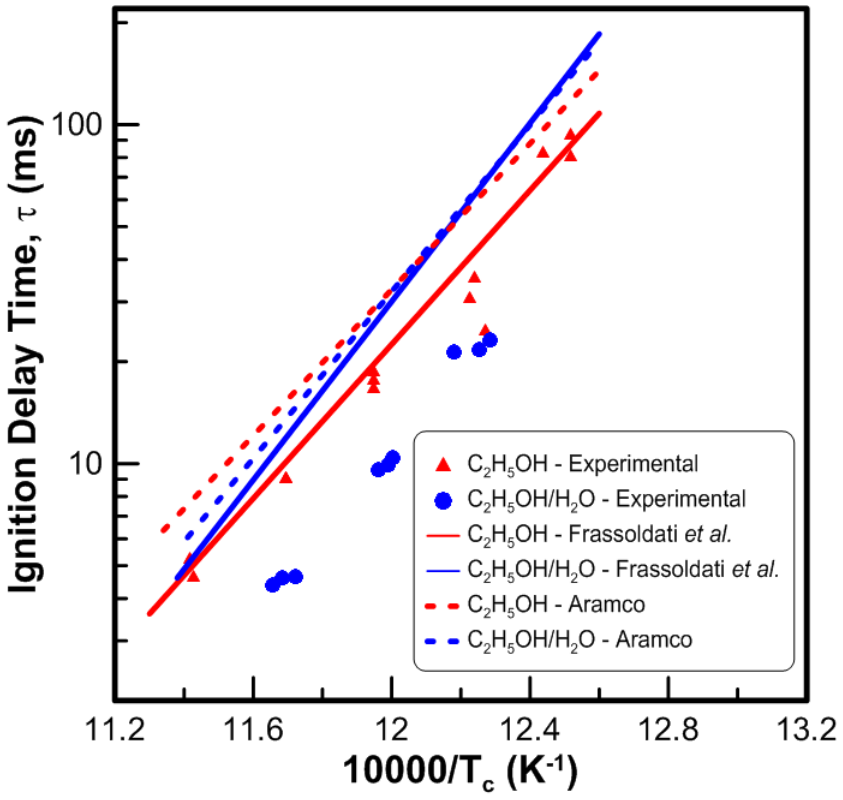

Figure 6.11: Experimental (symbols) and model predictions (lines) ignition delay time τ of Ethanol and Ethanol (70% vol)/water (30% vol) fuels at all temperatures; P_c=34-35 bar, φ=1.0.

6.7 Sensitivity Analysis Results

A sensitivity analysis study was conducted for the purposes of determining the most important reactions which strongly influence the overall rate of ethanol oxidation. Hydrogen peroxide radical and fuel dehydrogenation reactions control ignition delay time of ethanol and ethanol/water mixtures. Figures 6.12a and 6.12b show the most sensitive reactions for ethanol and ethanol/water mixtures sensitivity analysis by Frassoldati *et al*. mechanism at temperatures of 790 and 860 K. At all temperatures, the systems are sensitive to these reactions:

$$HO_2 + C_2H_5OH \rightarrow H_2O_2 + 0.33C_2H_4OH + 0.67CH_3CHOH \quad \text{(R2)}$$

$$O_2 + C_3CHO \leftrightarrow HO_2 + CH_3CO \quad \text{(R3)}$$

$$HO_2 + HO_2 \leftrightarrow H_2O_2 + O_2 \quad \text{(R4)}$$

$$OH + OH(+M) \leftrightarrow H_2O_2 \quad \text{(R5)}$$

Meanwhile, Figures 6.13a and 6.13b show the most sensitive reactions from the sensitivity analysis of ethanol and ethanol/water mixtures by Aramco mechanism at temperatures of 790 and 860 K. At all temperatures (also shown in *Appendix F*), the systems are sensitive to these reactions:

$$C_2H_5OH + HO_2 \leftrightarrow SC_2H_4OH + H_2O_2 \quad \text{(R6)}$$

$$H_2O_2(+M) \leftrightarrow OH + OH(+M) \quad \text{(R7)}$$

$$HO_2 + HO_2 \leftrightarrow H_2O_2 + O_2 \quad \text{(R8)}$$

$$C_2H_5OH + HO_2 \leftrightarrow PC_2H_4OH + H_2O_2 \quad \text{(R9)}$$

$$CH_3CHO + HO_2 \leftrightarrow CH_3CO + H_2O_2 \quad \text{(R10)}$$

The sensitivity analysis by Aramco mechanism show that the reactions that govern the ignition delay time of both ethanol and ethanol/water mixtures are similar with Frassoldati *et al.* mechanism, i.e. the hydrogen peroxide and hydroperoxyl radicals.

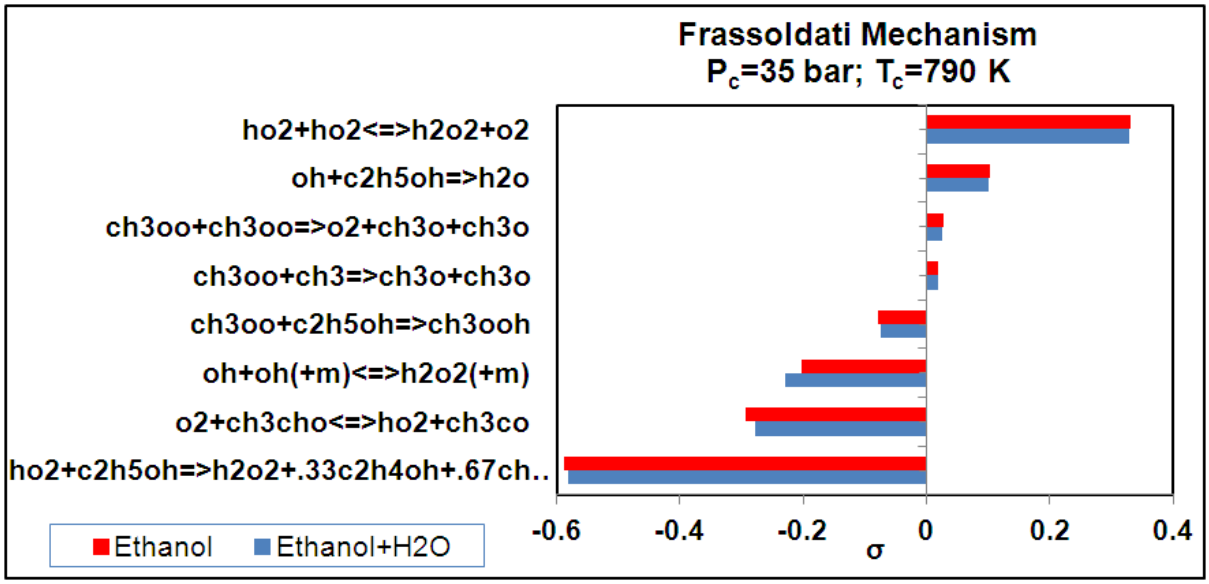

(a)

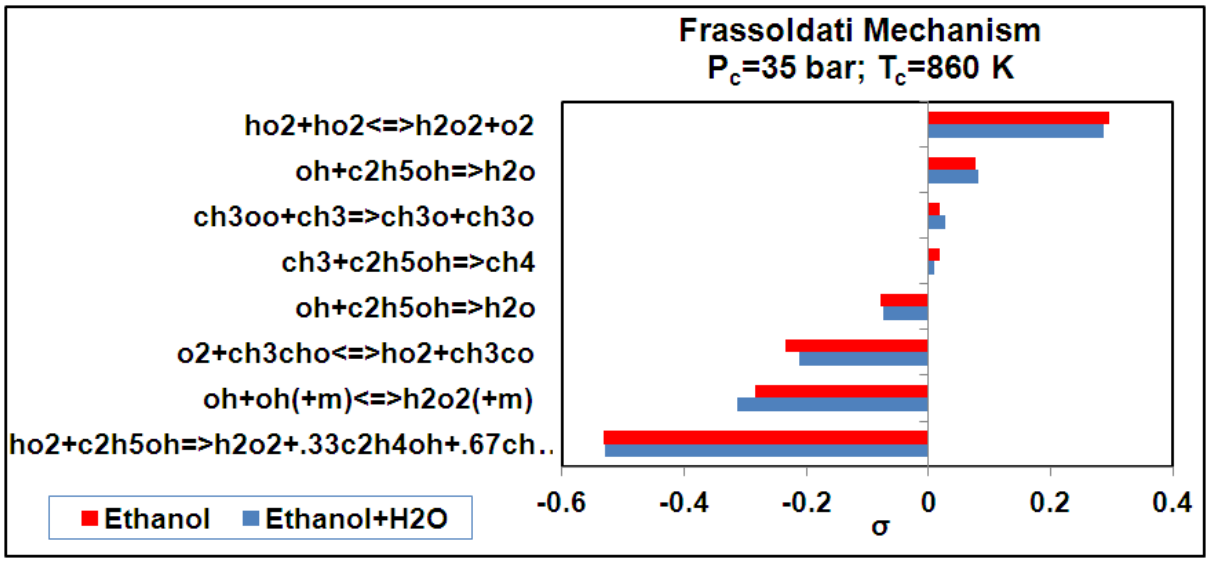

(b)

Figure 6.12: Evaluation of the most sensitive reactions with the Frassoldati mechanism of ethanol and Ethanol (70% vol)/water (30% vol) mixture at 35 bar and T_c= (a) 790 K and (b) 860 K.

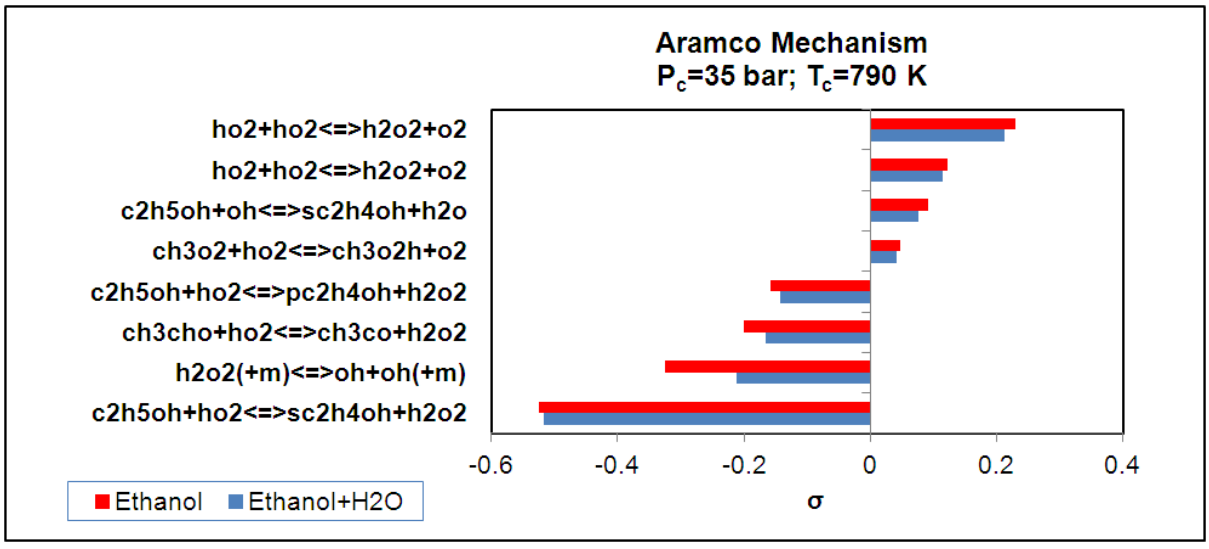

(a)

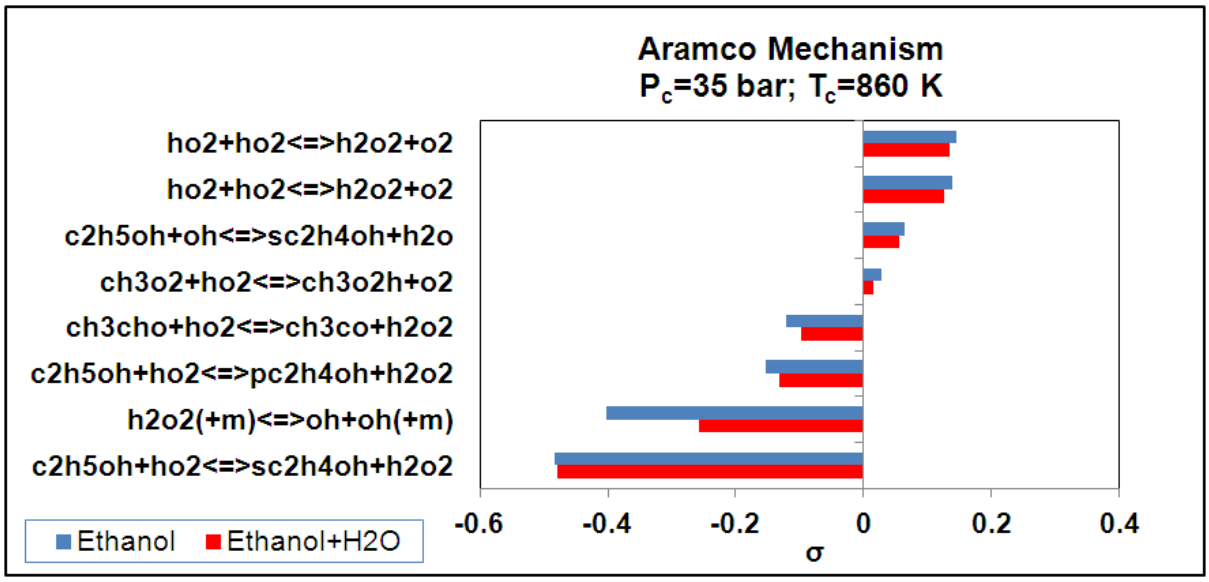

(b)

Figure 6.13: Evaluation of the most sensitive reactions with the Aramco mechanism of ethanol and Ethanol (70% vol)/water (30% vol) mixture at 35 bar and T_c= (a) 790 K and (b) 860 K.

In order to explain the effect of water addition to ethanol oxidation process, the sensitivity analysis results by Aramco mechanism have been separately plotted for both ethanol and ethanol/water mixtures. As seen previously in Figures 6.11 where the comparison between experimental and model predicted ignition delay times has been carried out, Frassoldati *et al.* mechanism do not exactly capture the effect of water addition to ethanol oxidation process. Figure 6.14 shows the most sensitive reactions at compressed temperature of 860 K for ethanol and ethanol/water respectively. As shown in previous Figure 6.13, both ethanol and ethanol/water oxidation are dominated by the similar reactions. However, the results do not definitively explain the increase of reactivity due to water addition to ethanol oxidation. As we compare between these Figures 6.14a and 6.14b, one reaction that might be the reason of increase reactivity in ethanol/water oxidation is;

$$H_2O_2(+H_2O) \leftrightarrow OH + OH(+H_2O) \quad \text{(R11)}$$

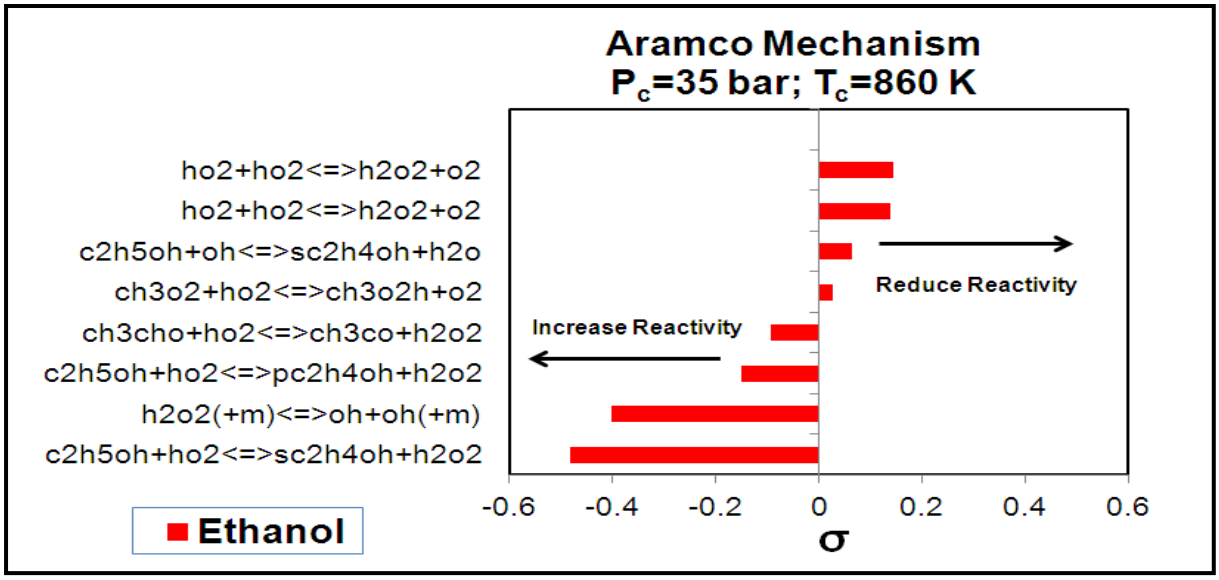

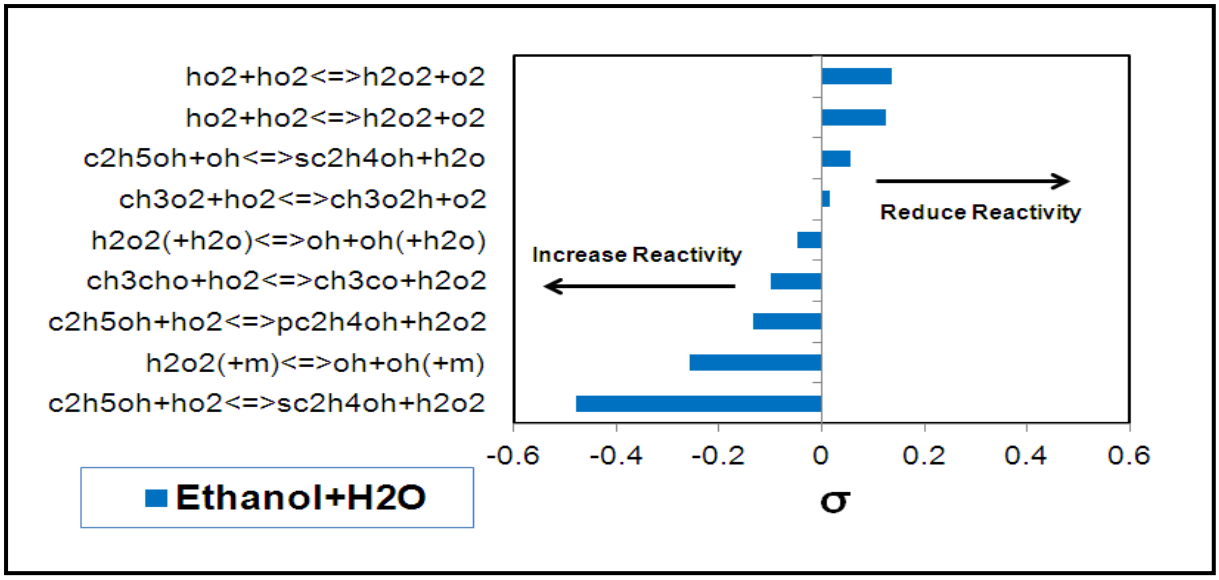

(b)

Figure 6.14: Evaluation of the most sensitive reactions with the Aramco mechanism of Ethanol and Ethanol (70% vol)/water (30% vol) mixture at P_c= 35 bar and T_c= 860 K.

These sensitivity results for 1-propanol by Johnson *et al.* mechanism indicate, as should be expected, that lower hydrocarbon and hydrogen chemistry are very important at the experimental conditions; initial fuel decomposition and a few succeeding steps are the most sensitive fuel chemistry seen here. Figure 6.15 shows the fifteen most sensitive reactions from the 860 K case, along with the sensitivity of the same reactions at 790 K, 800 K and 830 K. Key radicals such as O, H, OH, HO_2, and H_2O_2 are important in ignition processes of hydrocarbon fuels as indicated by Westbrook (2000). Therefore, it is not unexpected to see numerous reactions among those radicals in the results. The other reactions, however involve the initial decomposition of the fuel. At low temperature, the system is clearly most sensitive to reactions which involve the radicals such as methylperoxy (R12), hydroperoxyl (R13) and hydroxyl (R14):

$$nC_3H_7OH + CH_3O_2 \leftrightarrow C_3H_6OH - 1 + C_3O_2H \quad \text{(R12)}$$

$$nC_3H_7OH + HO_2 \leftrightarrow C_3H_6OH - 1 + H_2O_2 \quad \text{(R13)}$$

$$nC_3H_7OH + OH \leftrightarrow C_3H_6OH - 1 + H_2O \quad \text{(R14)}$$

These reactions are hydrogen abstraction from n-propanol by CH_3O_2, HO_2 and HO to form the α-hydroxypropylene radical corresponding to removal of α-H atom from the C—H bond which is the weakest bond due to the electron withdrawing effect of the neighbouring hydroxyl group. At low temperatures, *H*-abstraction from the fuel plays a major role in the combustion process especially on higher molecular weight alcohols such as propanol and butanol. Zhang and Boehman (2010) and Weber *et al.*, (2011) on n-butanol ignition study, showed that *H*-abstraction was also the most sensitive reaction occurred with formation of α-hydroxybutyl radical. By increasing the temperature, the sensitivity of the system to this reaction (R12) is increased. However, for reaction (R13), the sensitivity of the system to this reac-

tion decreases as the temperature increased. As Norton and Dryer (1991) discovered, the larger the alcohol the more it will behave like an alkane where hydrogenation will dominate.

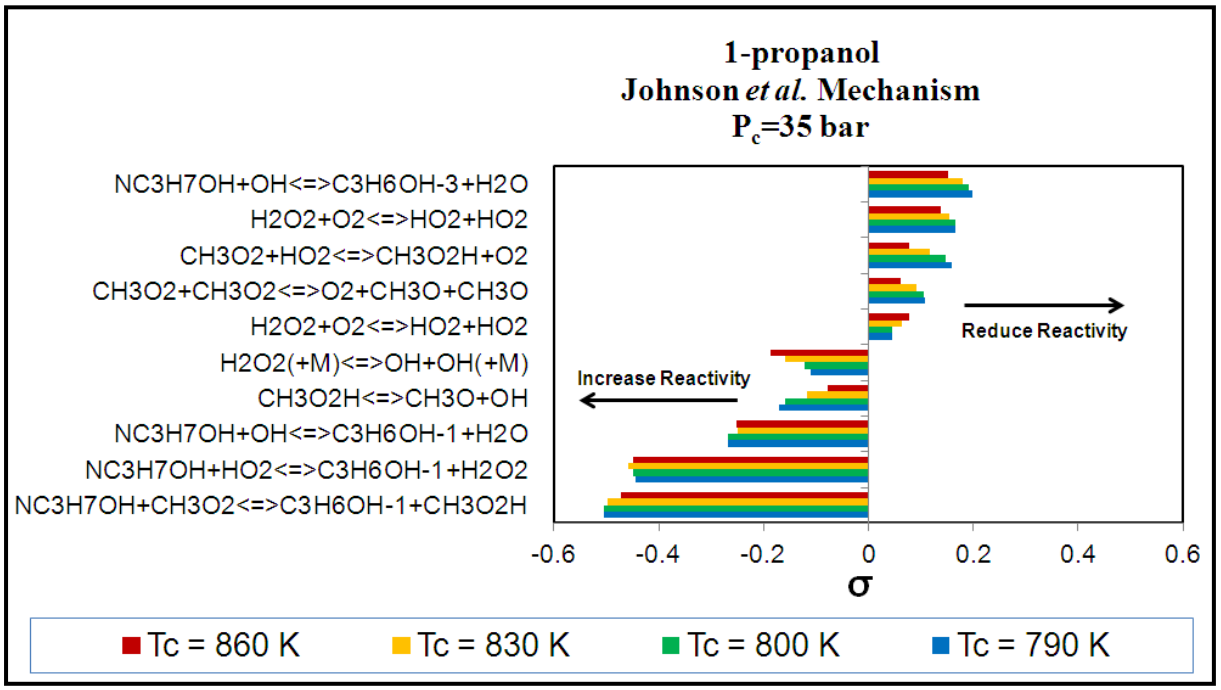

Figure 6.15: Evaluation of the most sensitive reactions with the Johnson mechanism of 1-propanol at P_c = 35 bar and at all temperatures.

6.8 Conclusions

In this rapid compression machine (RCM) study, ignition delays of ethanol, 1-propanol and ethanol/water mixture are measured at low-to-intermediate temperatures and at elevated pressure. Particularly, the compressed temperature conditions of T_c= 790 – 860 K are studied at compressed pressure of P_c= 30 bar. Results show that heavier weight alcohol, 1-propanol have shorter ignition delay time than ethanol. This result complied with their respective alkanes with the same carbon atom. Water addition to ethanol resulted in increase of reactivity of ethanol/water mixture. The ignition delay time of ethanol/water become shorter and the heat release during ignition is obviously reduced. The heat release produced during combustion process is reduced might be due to the lower ethanol concentration and energy absorp-

tion by water. Simulated ignition delay times computed using two different reaction mechanism available for ethanol (Frassoldati *et al*. and Aramco), and one reaction mechanism for 1-propanol (Johnson *et al*.) are carried out for comparison with experimental ignition delay times. For ethanol fuel, the model by Frassoldati *et al*. is observed to be in a good agreement with the experimental data. However, the model by Aramco slightly over-predicts the experimental ignition delay of ethanol. Meanwhile, there is a lack agreement with the model of Johnson *et al.* under-predicting the actual reactivity of 1-propanol fuel. For ethanol/water mixture, at the compressed temperature range studied, the increased in reactivity is captured by the Aramco mechanism as water is added to ethanol. The Frassoldati *et al.* mechanism seem to predict that the water addition to ethanol reduce the reactivity in ethanol ignition. Sensitivity analyses are carried out to determine the most important reactions that govern the overall rate of alcohols oxidation and ignition. For ethanol, both mechanisms show similarity in terms of reactions that administer the ignition delay time. The sensitivity analysis on ethanol/water by Aramco mechanism also shows that one reaction;

$$H_2O_2(+H_2O) \leftrightarrow OH + OH(+H_2O)$$

might be accountable for the reactivity increase observed in the system. For 1-propanol using Johnson *et al*. mechanism, the system is clearly most sensitive to reactions of hydrogen abstraction which involve the radicals such as metylperoxy and hydroperoxyl.

7 CONCLUSIONS

7.1 Conclusions

A detailed depiction of the vaporization of an isolated droplet has been carried out in this experimental study aimed at investigating ethanol and another aliphatic alcohol, 1-propanol. The characterization of the vaporization phenomenon is necessary for this liquid fuel to develop efficient design of injection systems for propulsion and power generation. Particularly, the vaporization rates and their dependency on temperature, important features for modeling and design, are explored for both ethanol and 1-propanol at intermediate to high temperatures. The experimental set-up consists of a pressure chamber in which the furnace, the droplet formation, the droplet support and motion devices are located. The quasi-steady theory has been employed to evaluate and to explicate the experimental results. The present work examined the vaporization characteristics and the d^2-law behaviour at high ambient temperature of 1-propanol and anhydrous ethanol droplets. The cross-fiber technique utilized has minimized the effect of heat transfer from the fiber to the droplet via conduction and it appeared to preserve the spherical shape of the droplet throughout the vaporization process, even in normal gravity. The effect of various ambient temperatures on the vaporization of 1-propanol droplets shows that at various temperatures, the d^2 law holds quite steadily and the quasi-steady behaviour is preserved. In cases of anhydrous ethanol and ethanol (95%), there are apparent deviations from the d^2 law, where two quasi-steady periods are observed through the droplet lifetime, clearly showing that the vaporization of an ethanol droplet is accompanied by the simultaneous condensation of water vapour on the droplet surface. The comparison between the calculation of both the experimental vaporization rate of anhydrous ethanol, K_i and K_f extracted from the d^2 curve, and their corresponding theoretical values permits us to verify that the first and second linear quasi-steady parts are corresponding to the vaporization of ethanol and water, respectively. The results also conclusively demonstrate that the 1-propanol vapori-

zation is not affected by the water vapour from the environment, even though it possesses a miscibility property with water. The time histories of instantaneous vaporization rate K_{inst} confirm this stationary aspect of 1-propanol droplets at various ambient temperatures. However, one can see that the volatility and miscibility properties of ethanol with water play immense roles in its vaporization process. The presence of water initially dissolved in ethanol and water gradually condensing on droplet surface changes the droplet vaporization process by modifying the diffusion transport at the droplet surface. As the temperature and concentration at the droplet surface change with time, the expected constant vaporization rate is replaced by a complex unsteady process.

An effort to associate the effect of ambient relative humidity on the behaviour of K_i and K_f has been accomplished. It clearly demonstrates that the initial vaporization rate K_i is always constant despite the change of ambient relative humidity. In contrast, the value of final vaporization rate K_f is apparently affected when the ambient relative humidity is changed. The value of K_f decreases as the ambient relative humidity increased.

The actual effect of droplet initial diameter d_0 on the ethanol vaporization remains indefinite due to the fact that ethanol is extremely affected by the ambient humidity. However, an obvious observation of d_0 impact can be made on 1-propanol vaporization. Results showed that the average vaporization rate K, increases as the droplet initial diameter d_0 increased.

In experiments of different initial water content in ethanol, as expected, a so-called 'quasi-steady' period for ethanol in all cases occurs two times throughout the droplet lifetime. The deviation of the curve from the linearity of the d^2-law becomes more prominent with the increase of initial water content and instead the values of the first linear part of all d^2-curves remain unchanged. The droplet lifetime is prolonged with increase of ambient relative humidity.

The study of chemical kinetics through autoignition experiments of ethanol, 1-propanol and blends of ethanol and water in a rapid compression machine (RCM) have been carried out. The thermodynamic conditions are set to those relevant in internal combustion engines and the experiments have been performed in the twin piston at NUIG RCM. The ignition delay times recorded show a strong temperature dependence and decrease with increase temperature. 1-propanol is more reactive than ethanol which results in shorter ignition delay times. Nonetheless, water addition to ethanol increases the reactivity of the mixture and results in a shorter ignition delay times than 1-propanol. Ethanol and 1-propanol autoignition process results in the same level of peak pressure but water addition to ethanol reduces the peak pressure to less than half due to the absorption by water of the part of the heat released.

Simulated ignition delay times computed using two different mechanisms available, Frassoldati *et al.* and Aramco show an agreement with ethanol experimental ignition delays. However, the increase of reactivity due to water addition to ethanol is only captured by Aramco mechanism. Sensitivity analyses by both mechanisms demonstrate a similarity in terms of reactions that administer the experimental ignition delay time of ethanol and ethanol/water blend. The sensitivity analysis on ethanol/water by Aramco mechanism also shows that one reaction $H_2O_2(+H_2O) \leftrightarrow OH + OH(+H_2O)$ might be liable for the reactivity increase observed in the system. For 1-propanol using Johnson *et al*. mechanism, the system is clearly most sensitive to reactions of hydrogen abstraction which involve the radicals such as metylperoxy and hydroperoxyl.

7.2 Perspective and future works

As mentioned, there is still much to be investigated before biofuels especially isolated alcohols droplet vaporization are fully understood. Future research should focus on a more de-

tailed determination of the data which could only be estimated at this time. Improvements could be made in the experimental design and the experimental scope by including broadening the test temperature, pressure and fluid mixture range. Improvements and modification could also be carried out on the design of the droplet injector nozzle to adapt to that higher density fuels such as biodiesel, and heavier molecular weight alcohol such as n-butanol. Furthering the study by including other alcohols and/or alcohols mixtures would lead to an increased generality in the vaporization characterization. Improvement of theoretical modeling and calculation can be adapted by incorporating the effect of water fraction in alcohols vaporization rate calculation. Some measurements by Infrared (IR) camera will enhance and verify the important factors such as temperature gradient and internal flow of droplets during vaporization process. For better understanding and comparison purposes of the possible behaviour of alcohols vaporization, modeling aspect need to be established.

In this present study, the kinetic impact of water on ethanol ignition process has been carried out only at single percentage of water addition, i.e. 30 %. For better assessment on the actual behaviour and to raise the confidence level of existing findings, a wider experimental scope of water percentage is required as more data are needed as to improve the existing kinetic mechanisms.

REFERENCES

1. Affleck, W.S. and Thomas, A., (1968) An opposed piston rapid compression machine for preflame reaction studies, *Proc. Inst. Mech Eng*., 183, pp.365–385.

2. Agarwal A. K., (2007), Biofuels (Alcohols and Biodiesel) Applications as Fuels for Internal Combustion Engines, *Prog. in Energy and Combustion Science*, 33(3), pp. 233-271.

3. Al-Farayedhi A.A., Al-Dawood A.M. and Gandhidasan P. (2004) Experimental investigation of SI engine performance using oxygenated fuel. *J. Eng. Gas Turbine Power*, 126, pp.178–191.

4. Al-Hasan M. (2003) Effect of ethanol–unleaded gasoline blends on engine performance and exhaust emission, *Energy Convers Manage* 44, pp.1547–1561.

5. Anderson J. E., Kramer U., Mueller S. A. and Wallington T. J., (2010) Octane numbers of ethanol- and methanol-gasoline blends estimated from molar concentrations, *Energy and Fuels*, 24, pp. 6576-6585.

6. Assessing Biofuels, 2008. UNEP

7. Atsumi S. and Liao J.C., (2008) Directed evolution of *Methanococcus jannaschii* citramalate synthase for biosynthesis of 1-propanol and 1-butanol by *Escherichia coli*., *Appl. Environ. Microbiol.*, 4(24), pp. 7802-7808.

8. Aul C. J. and Petersen E. L., (2009) Early ignition phenomena in low-temperature, high-pressure shock-tube experiments for non-diluted alkane blends in air, *6th U.S. National Combustion Meeting*, May 17-20, Ann Arbor, MI.

9. Avedisian, C.T. and Jackson, G.S., (2000) Soot patterns around suspended n-heptane droplets in a convection free environment, *J. of Propulsion and Power*, 16**(**4), pp. 974-979

10. Balakrishnan B., Sundararajan T., Natarajan R., (2001) Combustion of a fuel droplet in a mixed convective environment, *Combustion Science and Tehnology*, 163 (1), pp. 77-106.

11. Barata, J., (2008) Modelling of biofuel droplets dispersion and evaporation, Renewable Energy, 33 (4), pp. 769-779.

12. Beerer D. J. and McDonell V. G., (2011) An experimental and kinetic study of alkane autoignition at high pressures and intermediate temperatures, *Proceedings of the Combustion Institute*, 33, pp. 301–307.

13. Botero M. L., Huang Y., Zhu D. L., Molina A. and Law C. K., (2012) Synergistic combustion of droplets of ethanol, diesel and biodiesel mixtures, Fuel, 94, pp. 342-347.

14. Brett L., (2001) Simulation of methane autoignition in a rapid compression machine with creviced pistons, *Combustion and Flame*, 124 (1-2), pp. 326-329.

15. Canada G. S. and Faeth G. M., (1973) Fuel droplet burning rates at high pressures, *Symposium (Int.) on Combustion*, 14 (1), pp. 1345-1354.

16. Castanet, G., and Lemoine, F., 2007, Heat transfer within combusting droplets, *Proceedings of the Combustion Institute*, 31 (2), pp. 2141-2148.

17. Chauveau C, Birouk M. and Gökalp I., (2007) Why d^2-law does not hold during droplet vaporization in microgravity conditions?, *21st Annual Conference on Liq-*

uid Atomization and Spray Systems,(ILASS Europe 2007), Mugla, Turkey, September 10-12.

18. Chauveau C., Halter F., Lalonde A. and Gökalp I. (2008) An Experimental Study on the Droplet Vaporization: Effects of Heat Conduction through the Support Fiber, *Proc. of 22nd Annual Conference on Liquid Atomization and Spray Systems (ILASS Europe 2008).*

19. Chauveau, C., 2009, "Vaporization rate of distillated water at high temperature," Personal communication. CNRS - ICARE, France.

20. Chauveau C., Birouk M. and Gökalp I., (2011) An Analysis of the d^2-Law Departure during Droplet Evaporation in Microgravity, *Int. Journal of Multiphase Flow*, 37(3), pp. 252-259.

21. Chesneau X., (1994) Vaporisation et combustion de gouttes isolée de combustibles liquides-Influence de la pression, *Thése de doctorat, Université d'Orléans*.

22. Chin J. S. and Lefebvre A. H., (1983) Steady-state evaporation charateristics of hydrocarbon fuel drops, *AIAA J.*, 21, pp. 1437-1443.

23. Cho S. Y., Choi M. and Dryer F. L., (1991) Extinction of a Free Methanol Droplet in Microgravity, *Proc. of the 23rd Int. Combustion Symposium*, pp. 1611-1617.

24. Choi M. Y., Dryer F. L., Haggard J. B. Jr. and Brace M. H. , (1988) The Burning Behaviour of Methanol Droplets in Humid Air, *Fall Technical Meeting of the Eastern Section*, Combustion Institute.

25. Coelho R. M. L. and Telles A. S., (2002) Extended Graetz problem accompanied by Dufour and Soret effects, *International Journal of Heat and Mass Transfer*, 45, pp. 3101–3110.

26. Cooke D. F., (1971), Dodson M. G. and Williams A., (1971) A Shock-Tube Study of Tthe Ignition of Methanol and Ethanol with Oxygen, (1971) *Combustion and Flame*, 16(3), pp. 233– 236.

27. Costa, R. C., and Sodré, J. R., (2010) Hydrous ethanol vs. gasoline-ethanol blend: Engine performance and emissions, *Fuel*, 89 (2), pp. 287-293.

28. Crossley R. W., Dorko E. A. Scheller K. and Burcat A., (1972) The effect of higher alkanes on the ignition of methane-oxygen-argon mixtures in shock waves, *Combustion and Flame*, 19 (3), pp. 373-378.

29. Daho T., Vaitilingom G., Sanogo O., Ouiminga S. K., Segda B. G., Valette J., Higelin P. and Koulidiati J., (2012) Study of droplet vaporization of various vegetable oils and blends of domestic fuel oil-cottonseed oil under different ambient temperature conditions, *Biomass and Bioenergy*, 46, pp. 653-663.

30. Daif A., Buoaziz M., Chesneau X. and Ali A., (1999) Comparison of multicomponent fuel droplet vaporization experiments in forced convection with the Sirignano model, *Exp. Therm. Fluid Sci*., 18 (4), pp. 282-290.

31. Dakka S.M. and Shaw B.D., (2006) Influences of Pressure on Reduced-Gravity Combustion of 1-Propanol Droplets, *Microgravity Science and Technology*, 18(2), pp. 5-13.

32. Delgado R. C. O. B., Araujo A. S. and Fernandes Jr. V. J., (2006) Properties of Brazilian gasoline mixed with hydrated ethanol for flex-fuel technology, *Fuel Processing Technology*, 88, pp. 365–368.

33. Desantes J. M., Pastor J. V. and Molina S. A., (1999) Analysis of the combustion process in a heavy duty D.I. diesel engine through in-cylinder visualization, *ICE*, pp. 105-113.

34. Desante J. M., Pastor J. V., Payri R. M. and Pastor J. M., (2005) Experimental characterization of internal nozzle flow and diesel spray behaviour, Part II: Evaporative condition, *Atomization and Sprays*, 15 (5), pp. 517-544.

35. Dunphy M. P. and Simmie J. M. (1991), High-temperature oxidation of ethanol, *Journal of Chemical Society - Faraday Transactions*, 87 (11), pp. 1691–1696.

36. Dunphy M. P., Patterson P. M., and Simmie J. M., (1991) High-temperature oxidation of ethanol: Part 2-Kinetic Modelling, *Journal of Chemical Society - Faraday Transactions*, 87, pp. 2549–2559.

37. Ebrahimian V. and Habchi C., (2011) Towards A Predictive Evaporation Model For Multi-Component Hydrocarbon Droplets at All Pressure Condition, Int. Journal of Heat and Mass Transfer, 54, pp. 3552-3565.

38. Faeth, G. M., (1977), Current status of droplet and liquid combustion, *Progress in Energy and Combustion Science*, 3 (4), pp. 191-224.

39. Founti M., Kolaitis D., Zannis G., Kastner O. and Trimis D., (2002) Experimental determination of fuel evaporation rates using IR-thermography, In: *Proceedings of*

the 6th Int. Conference on Quantitative Infrared Thermography, Dubrovnik, Croatia

40. Frassoldati A., Cuoci A., Faravelli T., Niemann U., Ranzi E., Seiser R. and Seshadri K., (2010) An Experimental and Kinetic Modeling Study of n-Propanol and iso-Propanol Combustion, *Combustion and Flame*, 157(1), pp. 2-16.

41. Ghasemmi H., Baek S. W. and Khan Q. S., (2006) Experimental study of evaporation of kerosene droplet at elevated pressures and temperatures, *Combust. Sci. And Tech*., 178, pp. 1669-1684.

42. Godsave G. A. E., (1953) Studies of the Combustion of Drops in a Fuel Spray, the Burning of Single Drops of Fuel, *4th Symposium (Int.) on Combustion*, 4(1), pp. 818-830.

43. Gokulakrishnan P., Gaines G., Currano J., Klassen M. S. and Roby R. J., (2007) Experimental and kinetic modelling of kerosene-type fuels at gas turbine operating conditions, Journal of Engineering for Gas Turbines and Power, 129 (3), pp. 655-663.

44. Gökalp I., Chauveau C., Berrekam H. and Ramos-Arroyo N., (1994) Vaporization of miscible binary fuel droplets under laminar and turbulent convective conditions, *Atomization and Sprays*, 4. pp. 661-676.

45. Gopalakrishnan V. and Abraham J., (2004) Effects of multicomponent diffusion on predicted ignition characteristics of an n-heptane diffusion flame, *Combustion and Flame*, 136, pp. 557-566.

46. Ha V. M. And Lai C. L., (2001) The onset of stationary Marangoni instability of an evaporating droplet, Proceedings of the Royal Society of London Series A 457, pp. 885-909.

47. Hallett W. L. H., (2000) A simple model for the vaporization of droplets with large numbers of components. *Combustion and Flame* ,121(1), pp. 334–344.

48. Hara H. and Kumagai S., (1994) The effect of initial diameter on free droplet combustion with spherical flame, *25th Symposium (Int.) on Combustion*, pp. 423–430.

49. Hartfield J. P. and Farrell P. V., (1993) Droplet vaporization in a high pressure gas, *Journal of Heat Transfer*, 115 (3), pp. 699-706.

50. Healy D., Curran H., Simmie J. M., Kalitan D. M., Zinner D. M., Barret A. B., Petersen E. L. and Bourque G., (2008) Methane/ethane/propane mixture oxidation at high pressures and at high intermediate and low temperatures, *Combustion and Flame*, 155, pp. 441-448.

51. Healy D., Donato N.S., Aul C.J., Petersen E.L., Zinner C.M., Bourque G. and Curran H.J., (2010) Isobutane ignition delay time measurements at high pressure and detailed chemical kinetic simulations, *Combustion and Flame*, 157, pp. 1540-1551.

52. Hegseth J. J., Rashidnia N. and Chai A., (1996) Natural convection in droplet evaporation, *Phys. Rev. E*, 54 (2), pp. 1640–1644.

53. Heufer K., Fernandes R., Olivier H., Beeckmann J., Rhl O. and Peters N., (2011) Shock tube investigations of ignition delays of n-butanol at elevated pressures be-

tween 770 and 1250K, *Proceedings of the Combustion Institute*, 33(1), pp. 359 – 366,.

54. Hiroyasu, H. and Kadota, T., (1974) Fuel droplet size distribution in diesel combustion chamber, *SAE Paper 740715*.

55. Hiroyasu H. and Arai M., (1990) Structure of fuel sprays in diesel engines, *SAE Paper 900475.*

56. Hirschfelder, J.O., Curtiss, C.F. and Bird, R.B., (1954) Molecular Theory of Gases and Liquids, John Wiley & Sons.

57. Hopkins R. J. and Reid J. P., (2005) Evaporation of Ethanol/Water droplets: Examining the temporal evolution of droplet size, composition and temperature, *Journal of Physical Chemistry A*, 109, pp. 7923-7931

58. Hopkins, R. J., and Reid, J. P., (2006), A comparative study of the mass and heat transfer dynamics of evaporating ethanol/water, methanol/water, and 1-propanol/water aerosol droplets, *Journal of Physical Chemistry B*, 110 (7), pp. 3239-3249.

59. Hsieh W. D., Chen R. H., Wu T. L. and Lin T. H., (2002) Engine performance and pollutant emission of SI engine using Ethanol-Gasoline blended fuels, *Atmospheric Environment*, 36(3), pp. 403-410.

60. Hubbard G. L., Denny V. E. and Mills A. F., (1975) Droplet evaporation: effects of transient and variable properties, *Int. J. Heat Mass Transfer*, 18, pp. 1003-1008.

61. Jeuland, N., Montagne, X. and Gautrot, X., (2004), Potentiality of ethanol as a fuel for dedicated engine, *Oil & Gas Science and Technology*-Revue De L Institut Francais Du Petrole, 59 (6), pp. 559-570

62. Johnson, M. V., Goldsborough, S. S., Serinyel, Z., O'Toole, P., Larkin, E., O'Malley, G. and Curran, H. J., (2009) A shock tube study of n- and iso-propanol ignition, *Energy and Fuels*, 23 (12), pp. 5886-5898.

63. Kadota and Hiroyasu (1976) Evaporation of a single droplet at elevated pressures and temperatures. *Bull. JSME*, 19(138), pp.1515.

64. Kazakov, A., Conley, J. and Dryer, F. L., (2003) Detailed modeling of an isolated, ethanol droplet combustion under microgravity conditions, *Combustion and Flame*, 134 (4), pp. 301-314.

65. Khan Q. S., Baek S. W. And Lee S. Y., (2007) Effect of droplet initial diameter on droplet vaporization regimes for kerosene fuel droplet, *45th AIAA Aerospace Sciences Meeting and Exhibit, Nevada.*

66. Kong S. C., Senecal P. K. and Reitz R. D., (1999) Developments in spray modeling in diesel and direct-injection gasoline engines, *Oil and Gas Science and Technology Rev. IFP*, 54 (2), pp. 197-204.

67. Koshland C. P, (1996) Impacts and Control of Air Toxics from Combustion, *26th Symposium (Int.) on Combustion*, 26(2), pp. 2049-2065.

68. Kumagai S. Sakai T. and Okajima S., (1971) Combustion of free fuel droplets in a freely falling chamber, *13th Symposium (Int.) on Combustion*, 13(1), pp 779 .) .

69. Law C. K. and Binark M., (1979), Fuel spray vaporization in humid environment, *Int. Journal of Heat and Mass Transfer,* 22 (7), pp. 1009-1020.

70. Law C. K., (1982) Recent Advances in Droplet Vaporization and Combustion, *Prog. Energy Combust. Sci*., 8, pp. 171-201.

71. Law C. K., Xiong T. Y. and Wang C., (1987) Alcohol Droplet Vaporization in Humid Air, *Int. Journal of Heat and Mass Transfer,* 30(7), pp. 1435-1443.

72. Lee A. and Law C. K., (1992) An Experimental Investigation on the Vaporization and Combustion of Methanol and Ethanol Droplets, *Combustion Science and Technology*, 86(1-6), pp. 253-265.

73. Lee D., Hochgreb S. and Keck J. C., (1993) Autoignition of alcohols and ethers in a rapid compression machine, *SAE Paper 932755*.

74. Lefebvre A. H., (1989) Atomization and Sprays. New York: Hemisphere Pub. Co.

75. Li J., Kazakov A., Chaos M. and Dryer F., (2007) Chemical Kinetics of Ethanol Oxidation, *5th US Combustion Meeting,* US Combustion Institute, March 2007. Paper C26.

76. Lifshitz A., Ignition delay times, in: Ben-Dor G., Igra O., Elperin T. (Eds.), Handbook Shock Waves, in: Chemical Reactions in Shock Waves and Detonations, vol. 3, Academic Press, New York, 2001, chap. 16.5.

77. Lu X., Hou Y., Ji L., Zu L. and Huang Z., (2006) Heat Release Analysis on Combustion and Parametric Study on Emissions of HCCI Engines Fueled with 2-Propanol/n-Heptane Blend Fuels, *Energy and Fuels*, 20(5), pp. 1870-1878.

78. Mack J. H., Aceves S. M. and Dibble R. W., (2009) Demonstrating direct use of wet ethanol in a homogeneous charge compression ignition (HCCI) engine, *Energy*, 34, pp. 782-787.

79. Mandal D. K. and Bakshi S. (2011) Measurement of surface concentration of an evaporating multicomponent droplet under different ambient conditions, *24th European Conference on Liquid Atomization and Spray Systems*, (*ILASS Europe 2011)*.

80. Marchese A. J. and Dryer F. L. (1996) The Effect of Liquid Mass Transport on the Combustion and Extinction of Bicomponent Droplets of Methanol and Water, *Combustion and Flame*, 105(1-2), pp. 104-122.

81. Marin, M. C., Jost, C. A., Irwin, M. S., DeCaprio, J. A., Caput, D. and Kaelin, W. G. Jr (1998). Viral oncoproteins discriminate between p53 and the p53 homolog p73. *Mol. Cell. Biol.* 18, pp. 6316-6324.

82. Marinov N., (1999) A Detailed Chemical Kinetic Model for High Temperature Ethanol Oxidation, *International Journal of Chemical Kinetics*, 31(3) pp. 183–220.

83. Meiring P., Hansen A.C., Vosloo A.P. and Lyne P.W.L., (1983) High concentration ethanol–diesel blends for compression–ignition engines, *SAE paper no. 831360*.

84. Mikami M., Oyagi H., Kojima N., Kikuchi M., Wakashima Y. and Yoda S., (2005) Microgravity experiments on flame speed along fuel-droplet arrays using a new droplet-generation technique, *Combustion and Flame*, 141 (3), pp. 241-252.

85. Minetti R., Ribaucour M., Carlier M., Fittschen C. and Sochet L. R., (1994) Experimental and modeling study of oxidation and autoignition of butane at high pressure, *Combustion and Flame*, 96 (3), pp. 201-211.

86. Morin, C., Chauveau, C. and Gokalp, I., (2000) Droplet vaporisation characteristics of vegetable oil derived biofuels at high temperatures, *Exp. Thermal and Fluid Science*, 21 (1-3), pp. 41-50.

87. Moss J. T., Berkowitz A. M., Oehlschlaeger M. A., Biet J., Warth V., Glaude P. A. and Battin-Leclerc F., (2008) An experimental and kinetic modeling study of the oxidation of the four isomers of butanol, *Journal of Physical Chemistry*, 112(43), pp. 10843–10855.

88. Mouloungui Z., Vaitilingom G., Berge J.C. and Caro P.S., (2001) Interest of combining an additive with diesel ethanol blends for use in diesel engines. *Fuel*, 80(4), pp.565–574.

89. Mukhopadhyay A. and Sanyal D. (2001) A theoretical study of quasisteady sphericosymmetric combustion of alcohol droplets, *Int. Comm. in Heat and Mass Trans*., 28(5), pp. 713-721.

90. Natarajan K. and Bhaskaran K. A., (1981) An Experimental and Analytical Study of Methanol Ignition Behind Shock Waves," *Combustion and Flame*, 43, pp. 35–49.

91. Nigam P. S. and Singh A., (2011) Production of liquid biofuels from renewable resources, *Progress in Energy and Combustion Science*, 37, pp. 52-68.

92. Nomura, H., Ujiie, Y., Rath, H.J., Sato, J. and Kono, M. (1996) Experimental study on high-pressure droplet evaporation using microgravity conditions. *Proc. Combust. Instit.*, 26, pp. 1267.

93. Nomura H., Hirai H. and Ujiie Y., (2003) Effects of suspender diameter and natural convection on measured evaporation constant of a fuel droplet, *Proc. of 9th International Conference on Liquid Atomization and Spray Systems (ICLASS 2003).*

94. Noorani K. M.,, Akih-Kumgeh B. and Bergthorson J. M., (2011) Comparative High Temperature Shock Tube Ignition of C1-C4 Primary Alcohols, *Energy and Fuel*, 24, pp. 5834–5843.

95. Norton T. S. and Dryer F. L., (1991) The flow reactor oxidation of C1-C4 alcohols and MTBE, *Proceedings of the Combustion Institute*, 23, pp. 179–185.

96. Okajima S. and Kumagai S., (1975) Further investigations of combustion of free droplets in a freely falling chamber including moving drplets, *15th Symposium (Int.) on Combustion*, , pp. 401-407,

97. Okajima S. and Kumagai S., (1982) Experimental studies on combustion of fuel droplets in flowing air under zero- and high-gravity conditions, *19th Symposium (Int.) on Combustion*, pp. 1021.

98. Parag S. and Raghavan V., (2009) Experimental investigation of burning rates of pure ethanol and ethanol blended fuels, *Combustion and Flame*, 156, (5), pp. 997-1005.

99. Park C., Choi Y., Kim C., Oh S., Lim G. and Moriyoshi Y., (2010) Performance and Exhaust Emission Characteristics of a Spark Ignition Engine using Ethanol and Ethanol-Reformed Gas, *Fuel*, 89(8), pp. 2118-2125.

100. Park, P. and Keck, J., (1990) Rapid compression machine measurements of ignition delay times for PRD Mixtures, *SAE paper 900027, SAE International Congress & Exposition, Detroit, MI, Feb. 26 - Mar. 2, SAE Trans*., 99, pp. 11-23.

101. Park, S. H., Choi, S. C., Choi, M. Y. and Yozgatligil, A., 2008, New observations of isolated ethanol droplet flames in microgravity conditions, *Combustion Science and Technology*, 180 (4), pp. 631-651.

102. Payri R., Garcia J. M., Salvador F.J. and Gimeno J., (2005) Using spray momentum flux measurements to understand the influence of diesel nozzle geometry on spray characteristics, *Fuel*, 84 (5), pp. 551-561.

103. Postelnicu A., (2004) Influence of a magnetic field on heat and mass transfer by natural convection from vertical surfaces in porous media considering Soret and Dufour effects *International Journal of Heat and Mass Transfer*, 47, pp. 1467–1472.

104. Raj M. D., Mandal D. K., Navaneethakrishnan S. and Bakshi S., (2010) Measurement of the surface concentration (liquid) of an evaporating multicomponent droplet using pendant droplet method, Experiment in Fluids, 48 (4), pp. 715-719.

105. Raghavan V., Rajesh S., Shintre P. and Avinash V., (2009) Investigation of combustion characteristics of bio-diesels and its blends, *Combustion Sci. Technology*, 181(6), pp. 877-891.

106. Rasskazchikova T.V., Kapustin V.M. and Karpov S.A., (2004) Ethanol as high-octane additive to automotive gasolines. Production and use in Russia and abroad, *Chem Technol Fuels Oils*, 40(4), pp. 203–210.

107. Reid, R.C., Prausnitz, J.M. and Poling, B.E., (1987) The Properties of Gases and Liquids, Fourth edition, McGraw – Hill Book Company.

108. Renaud, F., Chauveau, C. and Gokalp, I., (2004) "On the effects of supporting fibers and natural convection on fuel droplet vaporization," *Proc. 19th Annual Conference on Liquid Atomization and Spray Systems* (ILASS-Europe'04), Nottingham, pp. 475-480.

109. Rice R. W., Sanyal A. K., Elrod A. C. and Bata R. M. (1991) Exhaust Gas Emissions of Butanol, Ethanol, and Methanol-Gasoline Blends, *J. of Engineering for Gas Turbines and Power*, 113(3), pp. 377-381.

110. Ristau R., Nagel U., Iglseder H., Konig J., Rath H. J., Nomura H., Kono M., Tanabe M. and Sato J., (1993**)** Theoretical and experimental investigations on droplet evaporation and droplet ignition at high pressures, *Microgravity Sci. Technol*, VI/4, pp. 223-228.

111. Ruff G. A., Liu S. and Ciobanescu I., (2003) Droplet vaporization in a levitating acoustic field, *NASA*.

112. Runge T., Teske M. and Polymeropoulos C. E., (1998) Low temperature vaporization of JP-4 and JP-8 fuel droplets, *Atomization and Sprays*, 8, pp. 25-44.

113. Saha A., Kumar R. and Basu S. (2010) Infrared Thermography and Numerical Study of Vaporization Characteristics of Pure and Blended Bio-Fuel Droplets, *Int. J. of Heat and Mass Transfer*, 53(19-20), pp. 3862-3873.

114. Saharin S., Lefort B., Morin C., Chauveau C. and Le Moyne L., Kafafy R., (2012) Vaporization characteristics of ethanol and 1-propanol droplets at high temperatures, *Atomization and Sprays*, 22 (3), pp. 207–226.

115. Sato J., (1993) Studies on droplet evaporation and combustion in high pressures, *AIAA Paper 93-0813, 31st Aerospace Sciences Meeting and Exhibit*, Reno, Nevada.

116. Sayin C., (2010) Engine Performance and Exhaust Gas Emissions of Methanol and Ethanol-Diesel Blends, *Fuel*, 89(11), pp. 3410-3415.

117. Sazhin S., Abdeghaffar W. A., Sazhina E. M. and Heikal M. R., (2005) Models for droplet transient heating: effects on droplet evaporation, ignition and break-up, *Int. J. Thermal Sci.*, 44 (7), pp. 610-622.

118. Shen C. R. and Liao J. C., (2008) E.*coli* for 1-butanol and 21-propanol production via keto-acid pathway, *Metabolic Engineering*, 10, pp. 213–320.

119. Shih A. T. and Megaridis C. M., (1995) Suspended droplet evaporation modeling in a laminar convective environment, *Combustion and Flame*, 102 (3), pp. 256-270.

120. Silke, E. J., Curran H. J. and Simmie, J. M., (2005) The influence of fuel structure on combustion as demonstrated by the isomers of heptane: a rapid compression machine study, Proc. Combust. Inst., 30, pp. 2639–2647.

121. Silke E.J., Würmel J. O'Conaire M.S., Simmie J.M. and Curran H.J., (2007) The effect of diluent gases in the shock tube and rapid compression machine, *5th US Combustion Meeting*, Paper No. P42.

122. Spalding D. B., (1953) The combustion of liquid fuels, *4th Symposium (Int.) on Combustion*, 4(1), pp. 847-864.

123. Spadaccini L. J. and TeVelde J. A., (1982) Autoignition characteristics of aircraft-type fuels, *Combustion and Flame*, 46. pp. 283.

124. Sparrow, E.M. and Gregg, J.L., (1958) The variable fluid property problem in free convection, *Trans. ASME*, 80, pp. 879–886.

125. Stengele J., Prommersberger K., Willmann M. and Wittig S.,(1999) Experimental and theoretical study of one- and two-component droplet vaporization in a high pressure environment, *Int. J. Heat and ,Mass Transfer*, 42 (14), pp. 2683-2694.

126. Surisetty V. R., Dalai A. K. and Kozinski J., (2011) Alcohols as alternative fuels: An overview, *Applied Catalysis A: General*, 404, pp. 1-11.

127. Tanaka S., Ayala F. and Keck J. C., (2003) A reduced chemical kinetic model for HCCI combustion of primary reference fuels in a rapid compression machine, *Combustion and Flame*, 133, pp. 467-481.

128. Taşkiran Ö. O. and Ergeneman M., (2011) Experimental Study on Diesel Spray Characteristics and Autoignition Process, *Journal of Combustion*, Article ID 528126.

129. Togbé C., Dagaut P., Halter F. and Foucher F., (2011) 2-Propanol Oxidation in a Pressurized Jet-Stirred Reactor (JSR) and Combustion Bomb: Experimental and Detailed Kinetic Modeling Study, *Energy and Fuels*, 25(2), pp. 676-683.

130. Tran L. S., Sirjean B., Glaude P. A., Fournet R. and Battin-Leclerc F., (2012) Progress in Detailed Kinetic Modeling of the Combustion of Oxygenated Components of Biofuels, *Energy*, 43, pp. 4-18.

131. Veloo P. S. and, Egolfopoulos F. N., (2011) Studies of n-Propanol, iso-Propanol and Propane Flames, *Combustion and Flame,* 158(3), pp. 501-510.

132. Wang C. H., Liu X. Q. and Law C. K., (1984) Combustion and micro-explosion of freely-falling multicomponent droplet, *Combustion and Flame,* 56, pp. 175-197.

133. Weber B. W., Kumar K., Zhang Y. and Sung C. J., (2011) Autoignition of n-butanol at Elevated Pressure and Low-to-Intermediate Temperature, *Combustion and Flame,* 158, pp. 809-819.

134. Westbrook C. K., (2000) Chemical Kinetics of Hydrocarbon ignition in Practical Combustion Systems, *Proc. Combust. Inst.*, 28, pp. 1563–1577.

135. Williams A., (1973) Combustion on droplets of liquid fuels: A review, *Combustion and Flame*, 21, pp. 1-31.

136. Wilson S. K., (1994) The onset of steady Marangoni convection, Journal of Engineering Mathematics, 28, pp. 427-445.

137. Würmel J. and Simmie J. M., (2005) CFD studies of a twin-piston rapid compression machine, *Combustion and. Flame*, 141(4), pp. 417–430.

138. Würmel J. and Silke E.J., Curran H. J., O Conaire M. S., Simmie J. M., (2007) The Effect of Diluent Gases on Ignition Delay Times in The Shock Tube and in The Rapid Compression Machine, *Combustion and Flame*, 151, pp. 289-302.

139. Yang J. R. and Wong S. C., (2002) On the discrepancies between theoretical and experimental results for microgravity droplet evaporation, *Int. J. Heat and Mass Transfer*, 44, pp. 4433-4443.

140. Yarin A. L., Brenn G., Kastner O., Rensink O. And Tropea C., (1999) Evaporation of acoustically levitated droplets, *J. Fluid Mech*. (399), pp. 151-204.

141. Yarin A. L., Brenn G., Kastner O., Rensink D., Tropea C., (1999) Evaporation of acoustically levitated droplets, *J. Fluid Mech*., 399, pp. 151-204.

142. Yozgatligil, A., Choi, M. Y., Kazakov, A., Dryer, F. L., Manzello, S. L. and Dobashi, R., (2003) Ethanol Droplet Combustion at Elevated Pressures and Enhanced Oxygen Concentrations, *41st . Proc. AIAA, Aerospace Sciences Meeting and Exhibit, Nevada*, pp. 1-7.

143. Zhang, B. L. and Williams, F. A., (1996) Alcohol droplet combustion, *Acta Astronautica*, 39 (8), pp. 599-603.

144. Zhang Y. and, Boehman A. L., (2 010) Oxidation of 1-butanol and a Mixture of n-heptane/1- butanol in a Motored Engine, *Combustion and Flame*, 157, pp. 1816–1824.

145. Zhao F., Yoo J. H., Liu Y., Lai M. C. Zhang L. and Yoshida Y., (1997) Characteristics of gasoline direct-injection sprays, *Proceedings of ILASS-America*.

146. Zhao F., Lai M. C. and Harrington D. L., (1999) Automotive spark-ignited direct-injection gasoline engines, *Progress in Energy and Combustion Science*, 25, pp. 437-562.

APPENDIX

A. Experimental apparatus and procedures

A-1 MUCC (Multi User Combustion Chamber)

1. Description of the under-pressure chamber (Figure A.1)

   The main chamber is consists of high–temperature furnace, three dimensional motorized displacement system of piezo-electric injector, movable frame and other various related equipment. The cylindrical chamber is made from aluminium alloy with the furnace made from stainless steel. The furnace is a cylinder with an inner diameter of 68 mm and 100 mm height. The heating system is by Joule effect. The furnace is capable of generating temperatures up to 1200 K by the Joule effect and it is placed in a steel chamber that could be pressurized if required.

2. Programmable Logic Controller (PLC) and temperature operation panel

   The panel consists of adjustment and display of the resistance intensity controller, visualisation of actual temperature in the furnace, visualization of pressure, furnace ignition controller, selection of thermocouple and lights controller.

3. Droplet injector data acquisition Microdrop™ (Figure A.2)

   The main command of the control unit, Microdrop™ is the mode of operation button. It offers a number of modes;

   Continuous operation- allows adjustment of the injector. Simultaneously use with the driver voltage button.

External trigger- position is engaged when the program is pilot mode. Simultaneously used with the driver voltage button.

External block trigger- does not utilized in current experimental works.

Manual trigger- allows the adjustment of point (in case of disturbance of the position).

4. Information Management

The information management consists of four main elements:

Motors management that leads to the moving frame (Software utilized is Smart Move PM™).

High speed camera (Software utilized is Phantom™) and acquisitions (Software utilized is Version 544™).

Real-time temperature display and chronogram evolutions.

Data recovery.

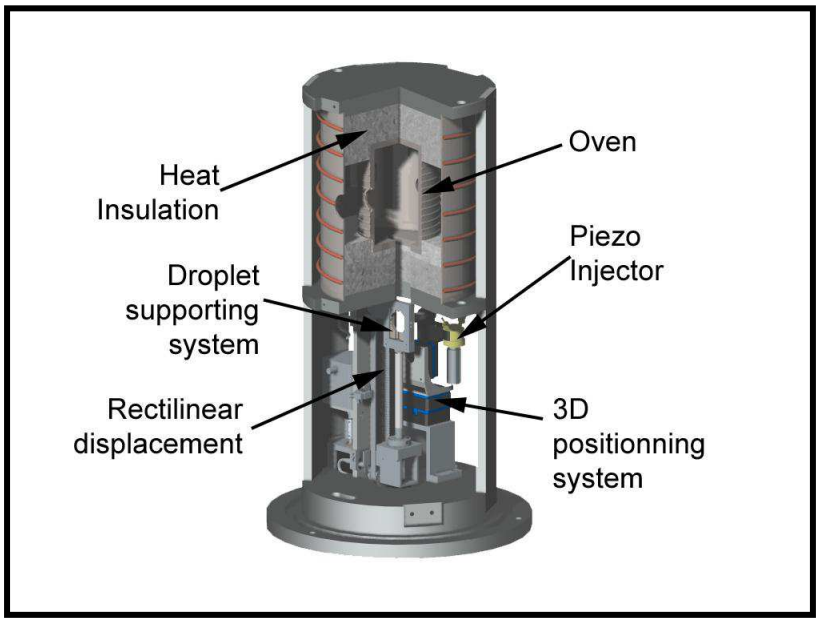

Figure A.1: A 3D image of main elements of under-pressure chamber

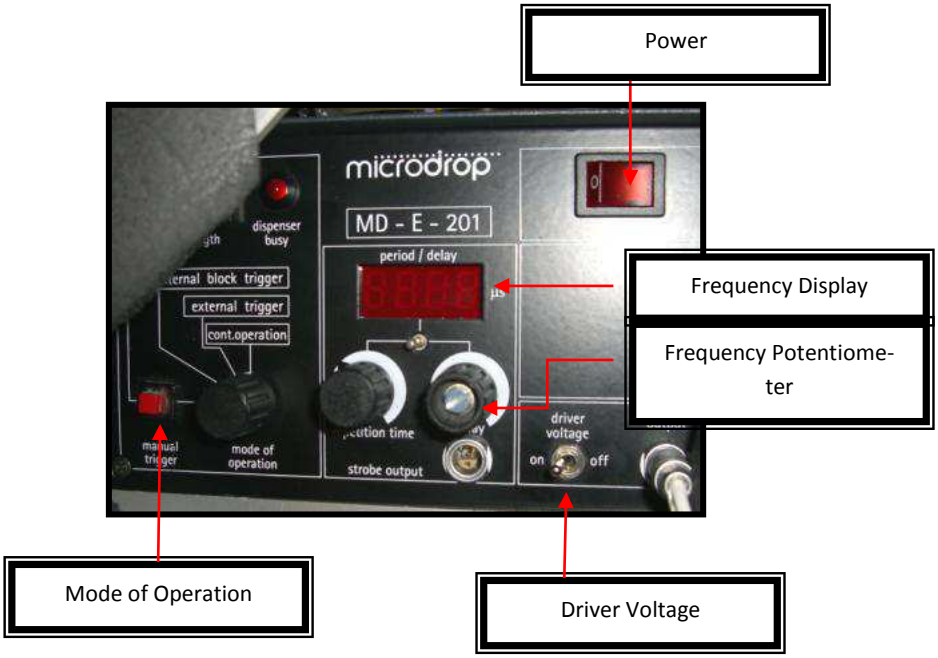

Figure A.2: Droplet injector data acquisition Microdrop™

A-2 Rapid compression machine experimental procedures

Figure A.3: The RCM operation manifold

Figure A.4: Schematic diagram of NUIG RCM.

RCM pre-firing procedure

1. Turn air extractor fan on.
2. Turn pump on, close tap 1 (to atmosphere).
3. Turn oscilloscope, reaction chamber assembly thermometer and charge amplifier on.
4. Confirm vacuum and pressure gauges are on and that the reaction chamber assembly is at good vacuum ($\approx 10^{-2}$ Torr).
5. Prepare oscilloscope for acquisition by, “File” _ “Recall” _ “Recall Setup Only”.

RCM firing procedure

1. Following a compression valve 4 should be closed, valves 1, 2, 3 and 5, as well as the air admittance tap should be open: confirm this is the case.
2. Open the solenoid valve to allow the depressurised hydraulic fluid to equilibrate around the entire hydraulic system by depressing the fire button for five seconds.

3. To withdraw the pistons to the pre-fired position:
    a. Close valves 1, 3 and 5 and the air admittance tap.
    b. Close pump to manifold by closing tap 4.
    c. Evacuate drive chambers by first opening tap 3, then slowly opening valve 1, confirm pistons are withdrawn (visually).
4. To charge hydraulic lock:
    a. Close pump to drive chamber by closing tap 3 and apply vacuum to manifold and reaction chamber assembly by opening taps 4, 5 and 6.
    b. Close valves 1 and 2, open air admittance tap.
    c. Charge hydraulic pressure slowly to 100 psi (6.9 bar), test seals by opening valve 4 and continue charging to 450-500 psi (31-34.5 bar).
    d. Close hydraulic pressure compressed air cylinder.
5. To apply drive pressure:
    a. Open valve 2 and then open valve 1 to bring drive chamber to atmospheric pressure.
    b. With ear defenders on, close valve 2 and open air compressor to fill drive chamber to drive pressure of 170 psi (11.7 bar).
    c. Close air compressor.
6. Close valve 1 and open valve 2, observe discharge.
7. Adjust hydraulic lock pressure to 400 psi (27.6 bar) by very slowly opening and then closing valve 3.

8. Close tap 4 and fill reaction chamber assembly with test gas to desired *Pi* by opening and then closing tap 7 (or tap 10 or tap 11).
9. Close tap 6 to (reaction chamber assembly), close tap 5.
10. Prime oscilloscope by depressing the “Run” button.
11. Record the initial pressure, *Pi*, initial temperature, *Ti*, and then open path to hydraulic fluid dump tank by opening valve 5.
12. Fire RCM by depressing the “Fire” button.

RCM post-compression procedure

1. Depress the “Stop” button to place the oscilloscope on standby.
2. Open valve 1 to vent drive pressure.
3. Open tap 4 to evacuate reaction chamber assembly.
4. Determine experimental measurements (compressed pressure, *Pc*, ignition delay time, τ etc.) and save oscilloscope data.
5. Open tap 5 to evacuate manifold.
6. Open valve 3 to vent residual hydraulic pressure.

B. Property data for theoretical calculations.

Table B-1: Physical properties of all compounds used in this study.

Name	Formula	Molecular Weight (g/mol)	T_b (K)	T_c (K)	P_c (bar)	V_c (cm^3/mol)
Nitrogen	N_2	28.013	77.4	126.2	33.9	89.8
Ethanol	C_2H_5OH	46.069	351.4	513.9	61.4	167.1
1-propanol	C_3H_7OH	60.096	370.3	536.8	51.7	219.0
Water	H_2O	18.015	373.2	647.3	221.2	57.1

T_b = normal boiling point

T_c = critical temperature

P_c = critical pressure

V_c = critical volume

Table B-2: Constants to calculate the saturated vapour pressure by using equation of Wagner (Equation 4-8).

Name	Formula	A	B	C	D
Ethanol	C_2H_5OH	-8.51838	0.34163	-5.73683	8.32581
1-propanol	C_3H_7OH	-8.05594	0.04.25183	-7.51296	6.89004
Water	H_2O	-7.76451	1.45838	-2.77580	-1.23303

Table B-3: Constants to calculate the isobaric heat capacity of the ideal gas by method of Joback (Equation 4-11) and Lennard-Jones potentials of all compounds used in this study.

Name	Formula	A	B	C	D	σ (Å)	ε/k (K)
Nitrogen	N_2	3.115E+1	-1.357E-2	2.680E-5	-1.168E-8	3.798	71.4
Ethanol	C_2H_5OH	9.014E+0	2.141E-1	-8.390E-5	1.373E-9	4.530	362.6
1-propanol	C_3H_7OH	2.470E+0	3.325E-1	-1.855E-4	4.296E-8	4.549	576.7
Water	H_2O	3.224E+1	1.924E-3	1.055E-5	-3.596E-9	2.641	809.1

A, B, C and D = constants to calculate isobaric heat capacity of the ideal gas

σ = characteristic length of Lennard-Jones (Å)

ε/k = characteristic energy of Lennard-Jones, (K)

C. Supporting figures for the effects of initial droplet diameter and ambient relative humidity to average vaporization rate.

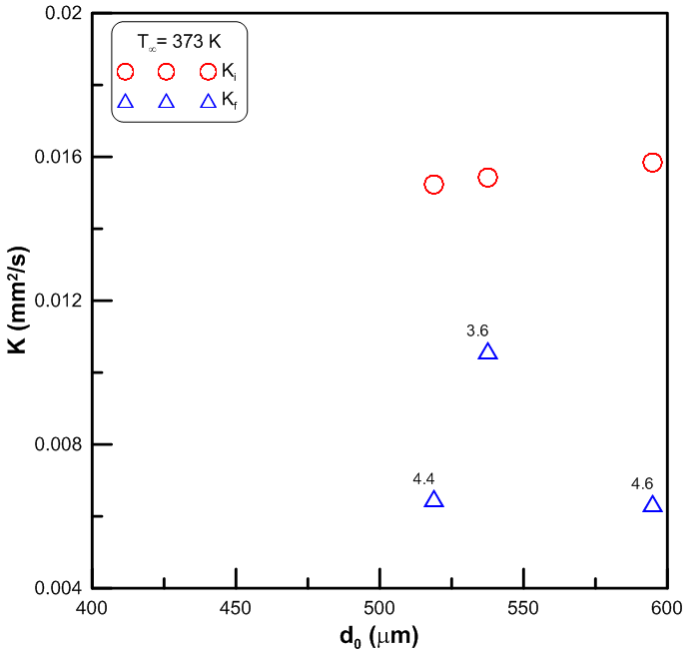

(a)

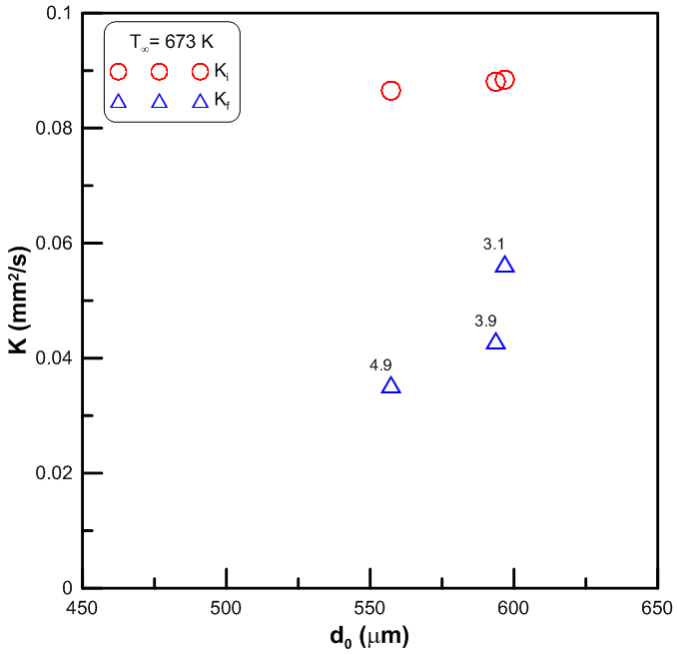

(b)

Figure C.1: The disparity of initial vaporization rate K_i and final vaporization rate K_f of ethanol droplets at different values of ambient relative humidity and various initial droplet diameters; T_∞ = (a) 373 K and (b) 673 K. The values of ambient relative humidity (in %) are shown at each K_f value.

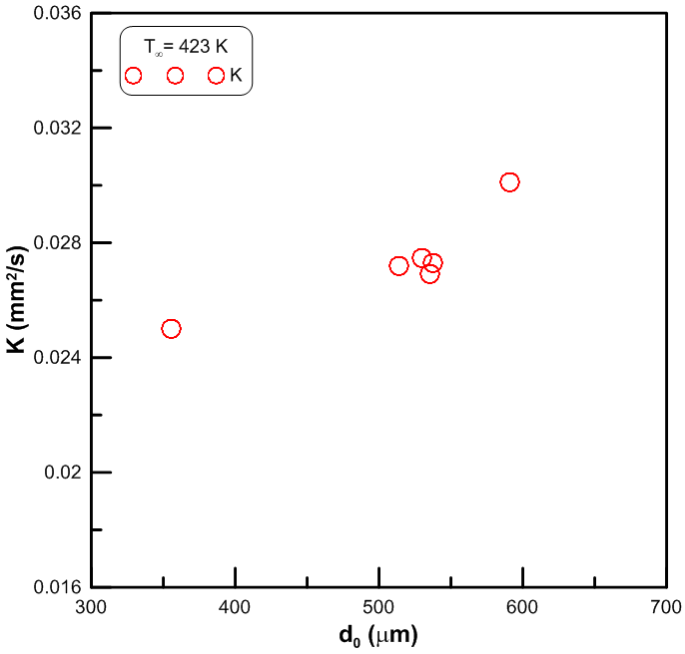

(a)

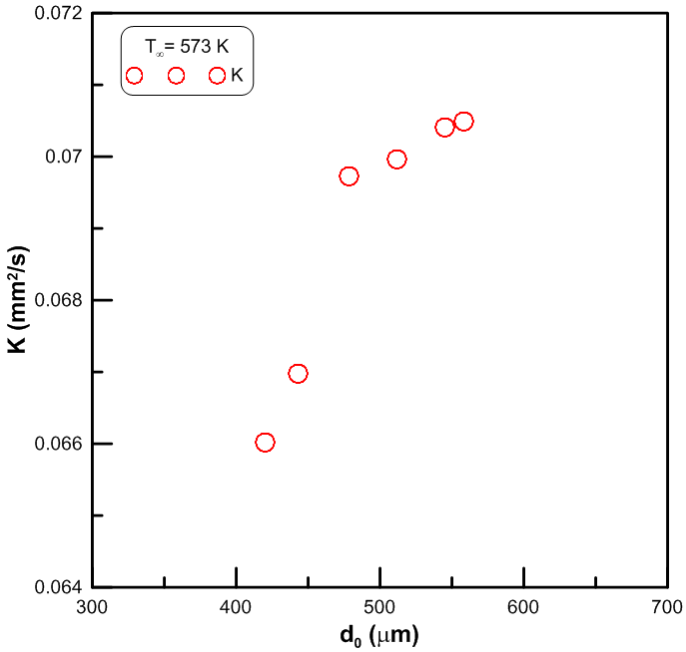

(b)

Figure C.2: The disparity of average vaporization rate of 1-propanol droplets at various initial droplet diameters; T_∞ = (a) 423 K and (b) 573 K.

D. Supporting figures for experimental and simulated pressure profile.

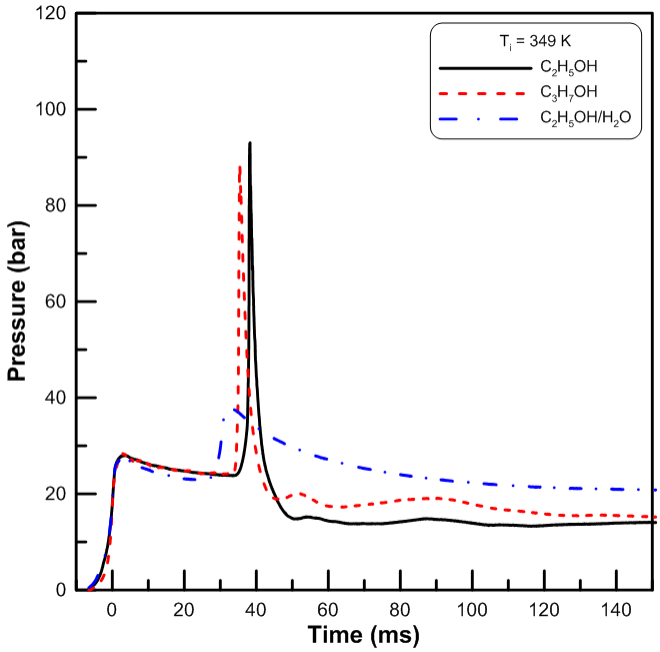

(a)

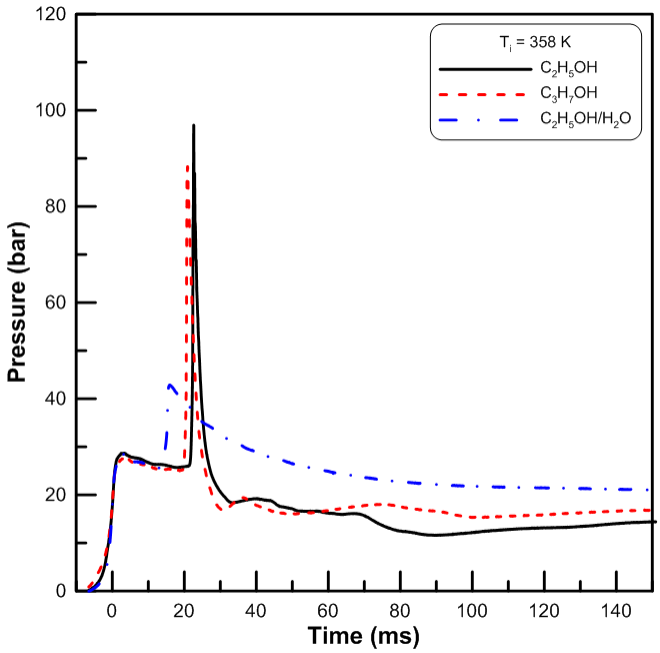

(b)

Figure D.1: Comparison of experimental pressure profile measured in RCM of Ethanol and 1-propanol and Ethanol (70% vol)/water (30% vol) mixture at temperatures T_i= (a) 349 K and (b) 358 K; P_i=1.0 bar, φ=1.0.

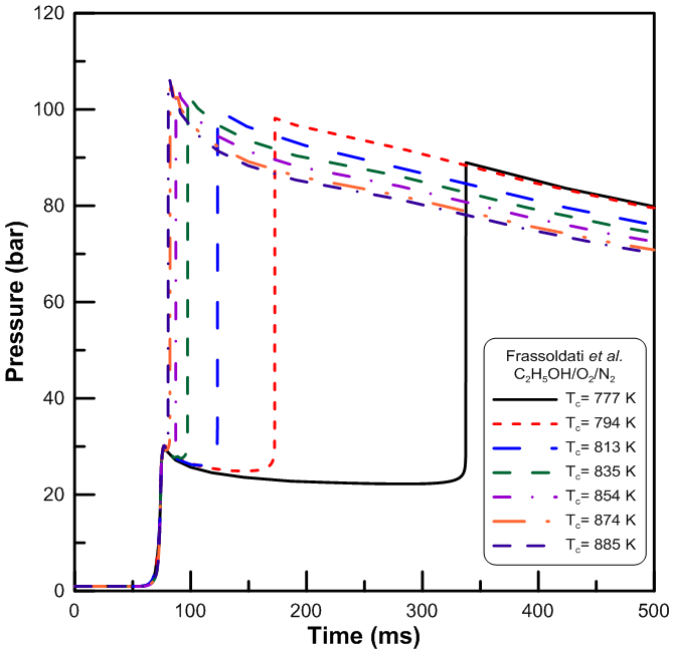

(a)

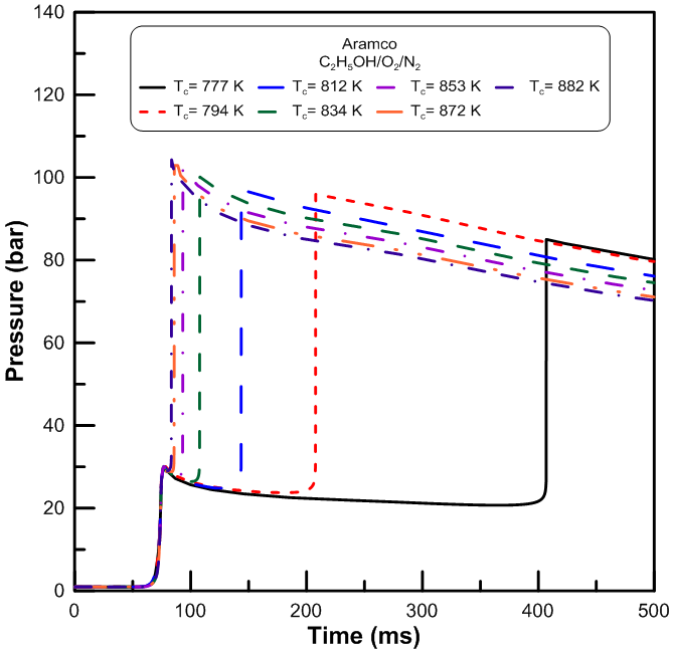

Figure D.2: Pressure profile of Ethanol at all temperatures using the mechanism of (a) Frassoldati *et al.* (b) Aramco; P_c=30.0 bar, φ=1.0.

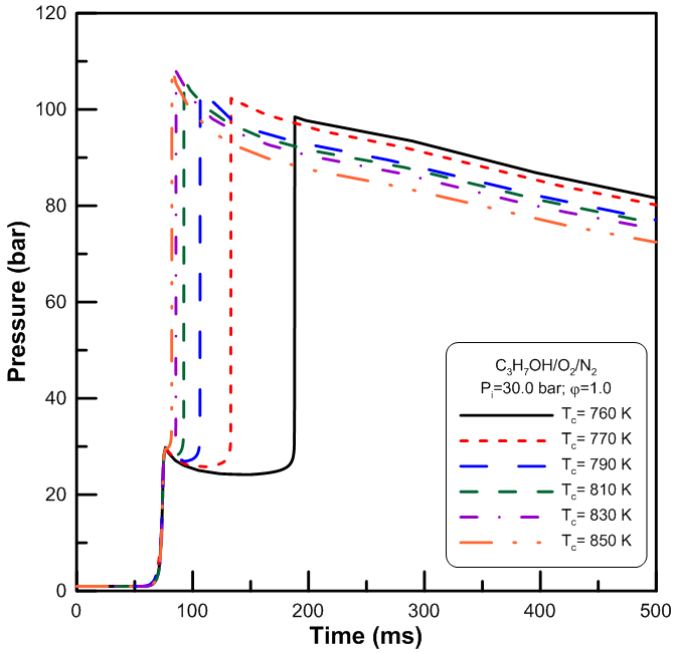

Figure D.3: Pressure profile of 1-Propanol at all temperatures using the mechanism of Johnson *et al.*; P_c=30.0 bar, φ=1.0.

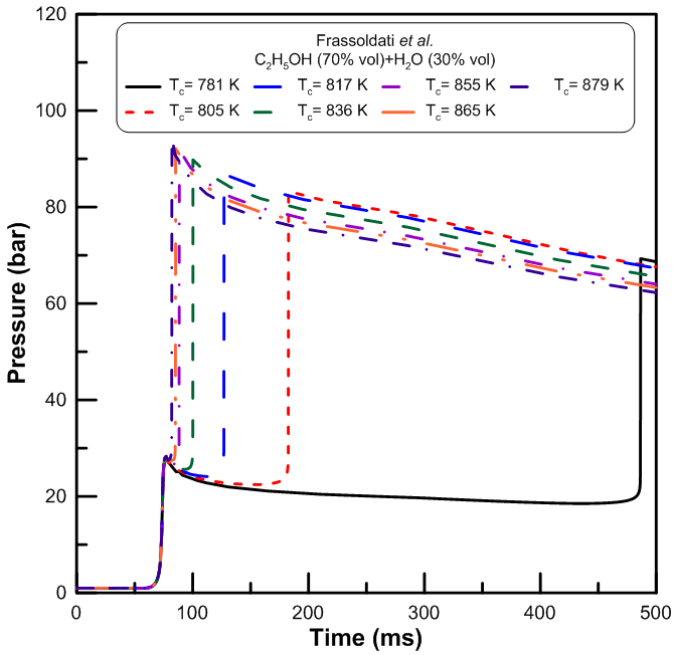

(a)

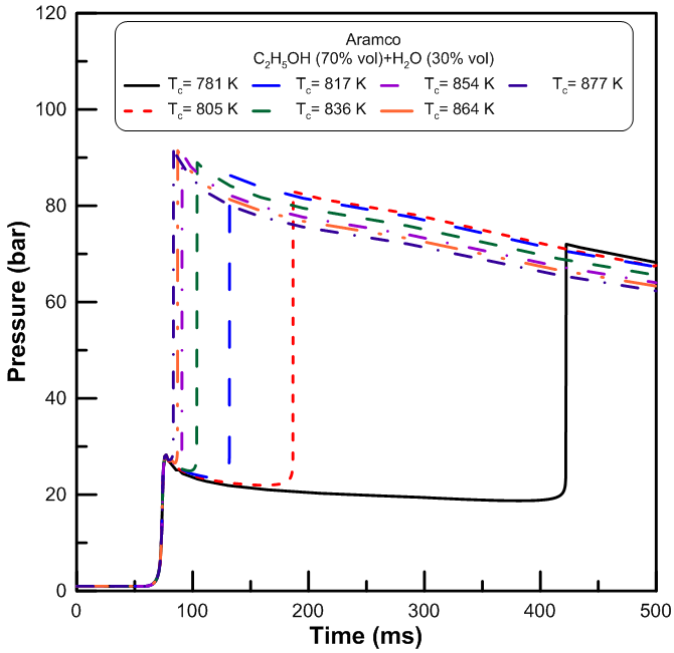

(b)

Figure D.4: Pressure profile of Ethanol (70% vol)/water (30% vol) mixture at all temperatures using the mechanism of (a) Frassoldati *et al.* and (b) Aramco; P_c=28.0 bar, φ=1.0.

E. Tabulated ignition delay times

Table E-1: Experimental ignition delay times of ethanol at various compressed temperature T_c; P_c= 34-35 bar; φ= 1.0.

P_i (mbar)	T_i (K)	P_c (bar)	T_c (K)	10000/T_c (K^{-1})	τ, (dP/dt) max (ms)
1000	347.82	35.44	815	12.27	24.6
979	348.77	34.70	817	12.24	35.2
957	348.96	34.19	818	12.22	30.7
980	348.71	34.90			Non Reactive
953	340.00	33.74	799	12.52	92.5
952	339.74	34.74	804	12.44	82.3
969	339.35	34.64	799	12.52	79.8
959	339.46	34.52			Non Reactive
970	358.36	34.64	837	11.95	16.6
969	358.64	34.60	837	11.95	18.6
968	358.36	34.66	837	11.95	17.6
967	358.26	34.75			Non Reactive
980	367.32	35.19	855	11.70	9.0
959	367.66	34.22	855	11.70	9.0
958	367.70	34.94			Non Reactive
955	377.68	34.28	875	11.43	4.6
954	377.74	34.40	876	11.42	5.2
957	377.75	34.45			Non Reactive

Table E-2: Experimental ignition delay times of 1-Propanol at various compressed temperature T_c; P_c= 34-35 bar; φ= 1.0.

P_i (mbar)	T_i (K)	P_c (bar)	T_c (K)	10000/Tc (K^{-1})	τ, (dP/dt) max (ms)
963	339.41	34.79	798	12.53	61
956	339.44	33.65	794	12.59	64.5
978	339.42	34.90	796	12.56	59
968	339.24	34.12			Non Reactive
971	329.80	34.44	776	12.89	153
972	329.08	33.71	771	12.97	174
977	328.01	35.28	775	12.90	150.4
959	332.01	34.74			Non Reactive
973	349.61	34.44	815	12.27	30
960	349.06	34.29	813	12.30	30.4
974	348.95	34.30	813	12.30	30
968	348.73	34.05			Non Reactive
971	358.54	34.69	834	11.99	15.2
963	358.58	33.84	831	12.03	15.6
976	358.54	34.92	834	11.99	15.4
960	358.60	34.38			Non Reactive
963	368.29	33.68	849	11.78	8.6
965	368.15	34.07	851	11.75	8.2
964	368.07	33.84	849	11.78	8.2
967	368.17	35.07			Non Reactive
973	378.02	34.53	871	11.48	4.2
962	377.89	34.04	870	11.49	4.2
961	377.91	34.04	870	11.49	3.9
964	377.85	34.36			Non Reactive

Table E-3: Experimental ignition delay times of Ethanol/water at various compressed temperature T_c; P_c= 34-35 bar; φ= 1.0.

P_i (mbar)	T_i (K)	P_c (bar)	T_c (K)	10000/T_c (K^{-1})	τ, (dP/dt) max (ms)
970	349.17	34.44	816	12.25	21.7
952	349.12	33.49	814	12.29	23.2
975	349.07	35.52	821	12.18	21.4
968	349.05	32.84			Non Reactive
969	358.52	34.68	836	11.96	9.6
978	358.60	34.67	834	11.99	9.9
966	357.20	34.57	833	12.00	10.4
980	360.31	33.24			Non Reactive
969	368.18	35.18	858	11.66	4.4
968	368.16	34.95	856	11.68	4.6
950	368.19	33.73	853	11.72	4.65
984	368.28	33.34			Non Reactive

Table E-4: Simulated ignition delay times of ethanol by Frassoldati *et al.* mechanism at various compressed temperature T_c; P_c= 30 bar; φ= 1.0.

P_i (mbar)	T_i (K)	P_c (bar)	T_c (K)	10000/Tc (K^{-1})	τ, (dP/dt) max (ms)
959	340	29.60	776.9	12.87	260.2
980	349	30.10	794.1	12.59	94.6
967	358	29.90	812.6	12.31	45.4
958	368	30.10	834.9	11.98	20.6
958	378	30.10	854.2	11.71	10.4
958	388	30.10	874.1	11.44	5.4
958	393	30.20	884.6	11.30	3.8

Table E-5: Simulated ignition delay times of ethanol by Aramco mechanism at various compressed temperature Tc; Pc= 30 bar; φ= 1.0.

P_i (mbar)	T_i (K)	P_c (bar)	T_c (K)	10000/T_c (K^{-1})	τ, (dP/dt) max (ms)
959	340	29.60	776.7	12.87	329.6
980	349	30.10	793.8	12.6	129.8
967	358	29.90	812	12.32	65.8
958	368	30.10	834.2	11.99	31.0
958	378	30.10	853.1	11.72	16.4
958	388	30.10	872	11.47	9.0
958	393	30.10	881.5	11.34	6.6

Table E-6: Simulated ignition delay times of ethanol/water by Frassoldati *et al.* mechanism at various compressed temperature T_c; P_c= 28 bar; φ= 1.0.

P_i (mbar)	T_i (K)	P_c (bar)	T_c (K)	10000/T_c (K^{-1})	τ, (dP/dt)max (ms)
968	349	27.9	781.4	12.8	410.6
980	360	28.6	804.8	12.43	106.2
984	368	28.2	817.4	12.23	50.2
984	378	28.2	836.3	11.96	23.4
984	388	28.2	855.3	11.69	11.6
984	393	28.3	864.9	11.56	8.4
984	400	28.3	878.8	11.38	5.2

Table E-7: Simulated ignition delay times of ethanol/water by Aramco mechanism at various compressed temperature T_c; P_c= 28 bar; φ= 1.0.

P_i (mbar)	T_i (K)	P_c (bar)	T_c (K)	10000/T_c (K^{-1})	τ, (dP/dt) max (ms)
968	349	27.9	781.2	12.8	346.4
980	360	28.6	804.5	12.43	110.2
984	368	28.2	817	12.24	55.0
984	378	28.2	835.7	11.97	26.8
984	388	28.2	854.3	11.71	14.0
984	393	28.2	863.5	11.58	10.2
984	400	28.2	876.5	11.41	6.6

Table E-8: Simulated ignition delay times of 1-propanol by Johnson *et al.* mechanism at various compressed temperature T_c; P_c= 30 bar; φ= 1.0.

P_i (mbar)	T_i (K)	P_c (bar)	T_c (K)	10000/T_c (K^{-1})	τ, (dP/dt) max (ms)
959	332	29.8	760.3	13.15	111.6
968	340	29.4	771.3	12.97	55.8
968	349	29.3	789.1	12.67	29.2
960	358	29.6	810	12.35	15.6
967	368	30.2	830.6	12.04	9.0
964	378	29.6	848.1	11.79	5.2

F. Supporting figures for sensitivity analysis.

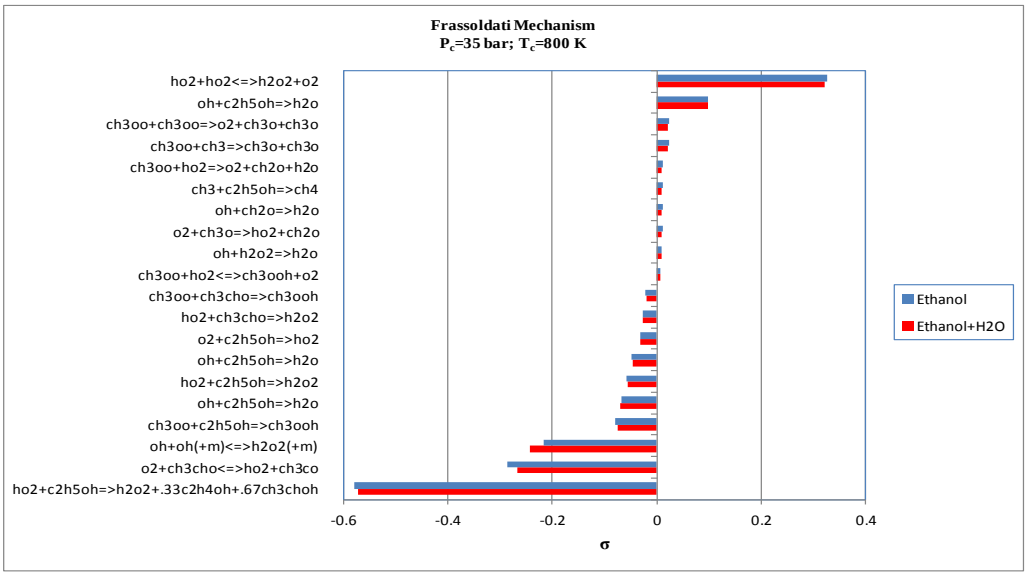

(a)

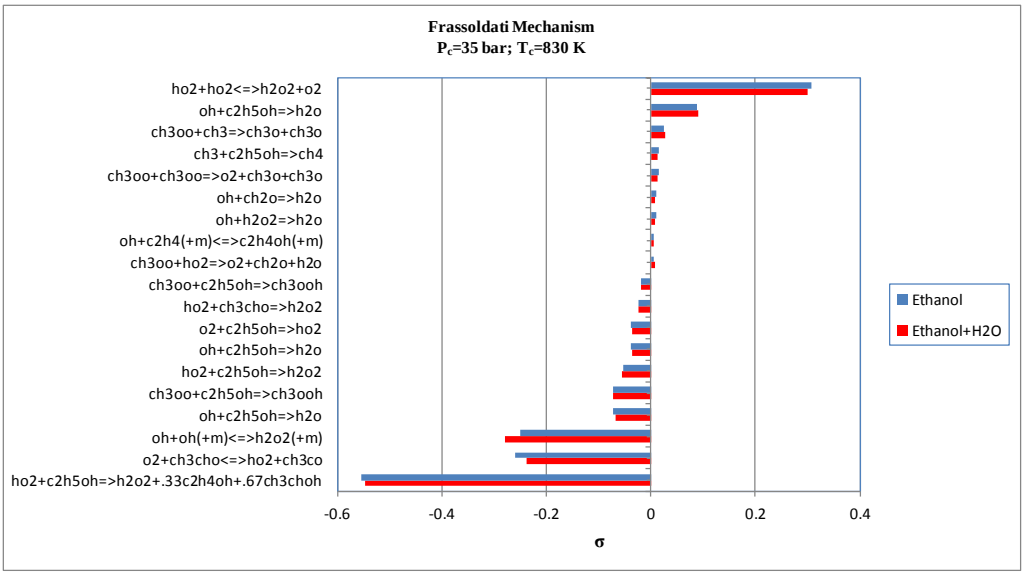

(b)

Figure F.1: Evaluation of the most sensitive reactions with the Frassoldati *et al.* mechanism of ethanol and Ethanol (70% vol)/water (30% vol) mixture at 35 bar and T_c= (a) 800 K and (b) 830 K.

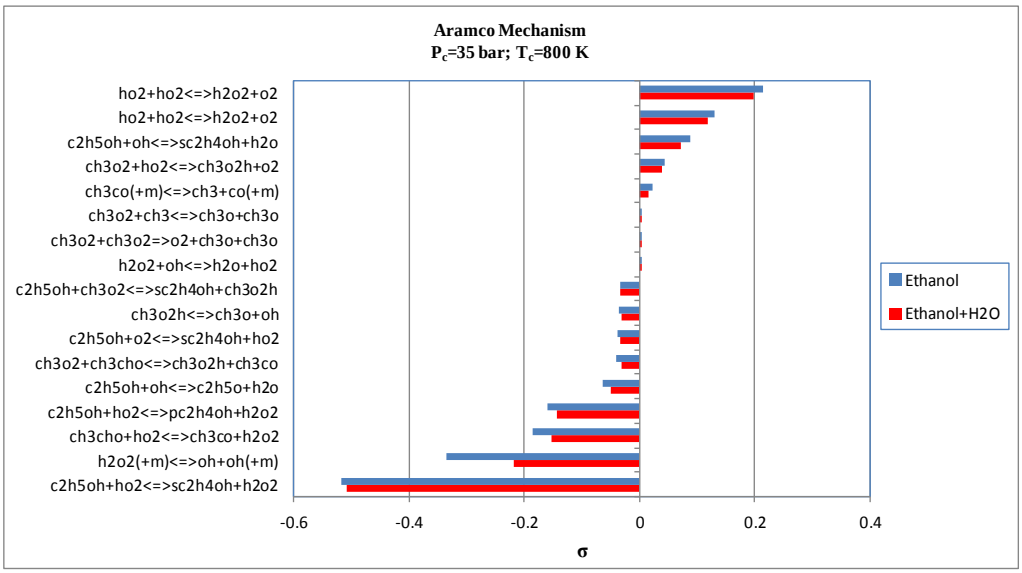

(a)

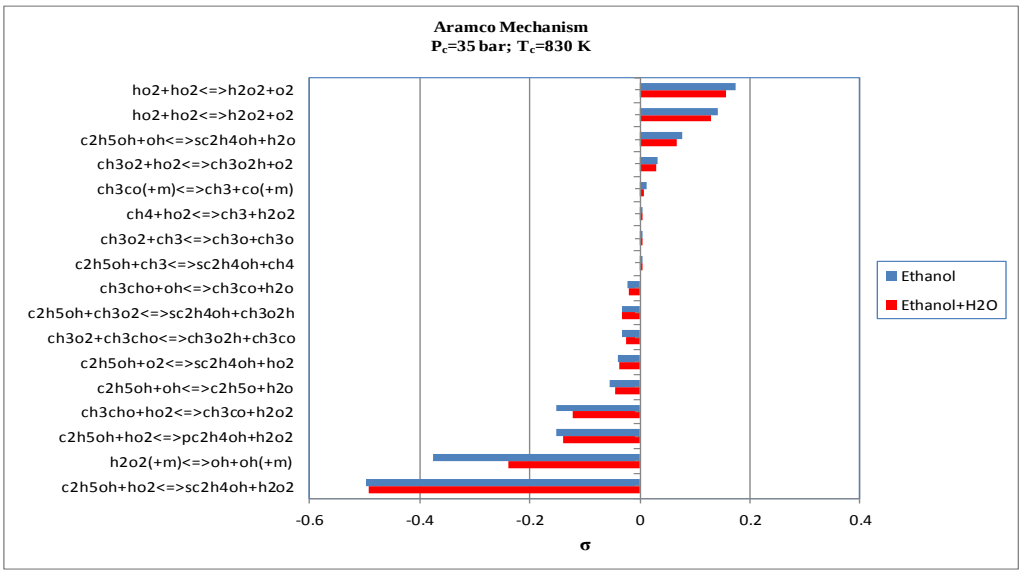

(b)

Figure F.2: Evaluation of the most sensitive reactions with the Aramco mechanism of ethanol and Ethanol (70% vol)/water (30% vol) mixture at 35 bar and T_c= (a) 800 K and (b) 830 K.